

MASARYKOVA UNIVERZITA  
Přírodovědecká fakulta  
Ústav teoretické fyziky a astrofyziky



## DIPLOMOVÁ PRÁCE

**Simulace extraterestrického prostředí a jeho vliv na  
modelový organismus**

Magdalena Špoková

Vedoucí diplomové práce: Mgr. Michaela Musilová, Ph.D.

2018



# Bibliografický záznam

- Autor:** Magdalena Špoková  
Přírodovědecká fakulta, Masarykova univerzita  
Ústav teoretické fyziky a astrofyziky
- Název práce:** Simulace extraterestrického prostředí a jeho vliv na modelový organismus
- Studijní program:** Fyzika
- Studijní obor:** Teoretická fyzika a astrofyzika
- Vedoucí práce:** Mgr. Michaela Musilová, Ph.D.
- Akademický rok:** 2017/18
- Počet stran:** xiv + 103
- Klíčová slova:** Astrobiologie, mikroskopie atomárních sil, sinice, meziplanetární prostředí, fotosyntetická aktivita, sluneční vítr, *Nostoc commune*



# Bibliographic entry

**Author:** Magdalena Špoková  
Faculty of Science, Masaryk University  
Department of Theoretical Physics and Astrophysics

**Title of thesis:** Simulation of extraterrestrial environments and their impact on the survival of specially-selected organisms

**Degree Programme:** Physics

**Field of Study:** Theoretical physics and astrophysics

**Supervisor:** Mgr. Michaela Musilová, Ph.D.

**Academic Year:** 2017/18

**Number of Pages:** xiv + 103

**Keywords:** Astrobiology, atomic force microscopy, cyanobacteria, interplanetary environment, photosynthetic activity, solar wind, *Nostoc commune*



Děkuji řediteli ústavu astrofyziky a teoretické fyziky prof. Rikardovi von Ungemu, Ph.D., že mi toto téma povolil, a proto zde nyní můžu vyjádřit vděčnost všem, co s touto prací měli co do činění (jak přímo, tak nepřímo).

Chtěla bych poděkovat vedoucí této práce Mgr. Michaele Musilové, Ph.D. za vedení a všechny poskytnuté rady. Dále bych chtěla poděkovat všem svým konzultantům. Mgr. Barboře Chattové, Ph.D., nejprve za její inspirativní hodiny Fylogeneze a diverzity řas a hub a za to, že jí nápad psaní astrobiologické práce nepřipadal příliš šílený. Také za její ochotu, rady, poskytnutí prostoru a vybavení pro práci a hlavně za úhradu provozu AFM. Prof. Mgr. Vítovi Kudrle, Ph.D. velmi děkuji, že souhlasil se spoluúčastí na této práci, za poskytnutý prostor k práci, za veškerou pomoc a trpělivost při vymýšlení aparatury a při měření. Stejně jako děkuji za mnoho hodin strávených při procházení textu práce. Mgr. Peteru Váczimu, Ph.D. děkuji za veškeré poskytnuté vybavení, vzorky a prostor pro práci s nimi, stejně jako za jeho pomoc a konzultace při zpracovávání výsledků.

Také bych chtěla poděkovat Mgr. Janu Příbylovi, Ph.D. za čas se mnou strávený u přípravy a skenování vzorků, stejně jako za jejich zpracování.

Poděkování také patří Mgr. Pavlu Dvořákovi, Ph.D. za jeho pomoc při odhadu parametrů výboje. M. Šnírerovi za pořízení a zpracování fotek. I. Dadákové bych chtěla poděkovat za radu, kde hledat *Nostoc* a za to, že mě nechala na zkoušku pracovat se svými vzorky. Děkuji M. Růžičkové za ochotu a pomoc se zprovozněním autoklávu, stejně jako poskytnutí misek a rukavic.

Děkuji všem svým spolužákům, za jejich spolužákování. Hlavně děkuji M. Pieckovi za studijní pátky a za jeho postřehy a poznámky (nejen) k této práci. Děkuji také všem svým přátelům, obzvláště pak Karle, Ketce, Magdě, Ondrovi, Terce a Veučí, že mi zpříjemňovali celou dobu mého studia kvalitní konverzací a oslavami na úrovni. Děkuji své spolubydlící Marušce, že tolerovala moje výkyvy nálad při psaní. Velké díky i Jirkovi za odstranění mých prohřešků proti angličtině.

Také děkuji svým rodičům Radmile a Markovi, že mě po celou dobu studia podporovali jak svými financemi, tak tím, že jsou prostě skvělí rodiče. Taky děkuji svojí nejlepší přítelkyni a sestře Markétě, za všechno, jako např. studijní pobyty v Českém Brodě.

The author would also like to thank to the scientific infrastructure of the *J.G. Mendel Czech Antarctic Station* (as a part of the Czech Polar Research Infrastructure, CzechPolar2) and its crew for their support.



Prohlašuji, že jsem svou diplomovou práci napsala samostatně a výhradně s použitím citovaných pramenů. Souhlasím se zapůjčováním práce a jejím zveřejněním.

V Brně dne:

Magdalena Špoková

.....

.....



Abstrakt:

Práce se zabývá schopností sinice *Nostoc commune*, nasbírané ve dvou různých lokalitách (Antarktida a Brno), přežít v podmínkách podobných meziplanetárnímu prostředí. Také se zabývá morfologií a mechanickými vlastnostmi povrchu vzorků prostřednictvím dvou různých módů mikroskopie atomárních sil. Jsou zjišťovány rozdíly ve fotosyntetické aktivitě vzorků po různé době jejich vystavení nízkému tlaku a prostředí podobnému slunečnímu větru. Stejně tak jsou zjišťovány rozdíly mezi vzorky z obou oblastí sběru.

Klíčová slova: Astrobiologie, mikroskopie atomárních sil, sinice, meziplanetární prostředí, fotosyntetická aktivita, sluneční vítr, *Nostoc commune*

Abstract:

The aim of this thesis is to analyze the ability of cyanobacteria *Nostoc commune* to survive in an interplanetary-like environment. Samples of cyanobacteria specie *Nostoc commune* were gathered on two geographic locations (Antarctica and Brno). Their morphological and mechanical properties were studied, with the use of two different modes of atomic force microscopy. Photosynthetic activity of samples was measured after their exposure to low pressure and to solar wind-like conditions. Certain patterns were found in the results of the measurement as well as some significant differences between the samples from Brno and Antarctica.

Keywords: Astrobiology, atomic force microscopy, cyanobacteria, interplanetary environment, photosynthetic activity, solar wind, *Nostoc commune*





MASARYKOVA UNIVERZITA  
Přírodovědecká fakulta

## ZADÁNÍ DIPLOMOVÉ PRÁCE

Akademický rok: 2016/2017

**Ústav:** Ústav teoretické fyziky a astrofyziky

**Studentka:** Bc. Magdalena Špoková

**Program:** Fyzika

**Obor:** Teoretická fyzika a astrofyzika

**Směr:** Astrofyzika

Ředitel Ústavu teoretické fyziky a astrofyziky PřF MU Vám ve smyslu Studijního a zkušebního řádu MU určuje diplomovou práci s názvem:

**Název práce:** Simulace extraterestrického prostředí a jeho vliv na modelový organismus

**Název práce anglicky:** Simulation of extraterrestrial environments and their impact on the survival of specially-selected organisms

### Oficiální zadání:

V poslední době stoupá význam vědního oboru astrobiologie, ať už na poli zkoumání původu života na Zemi, jeho šíření, či možnosti využití jednoduchých organismů pro eventuální kolonizaci jiných vesmírných těles lidmi.

V rámci této práce se student pokusí vhodně nasimulovat meziplanetární či jiné extraterestrické prostředí a ověřit viabilitu a vybrané vlastnosti modelového organismu (např. vysoce odolné sinice *Nostoc* spp.) po pobytu v tomto prostředí pomocí vhodných dostupných přístrojů a provede diskusi nasimulovaných podmínek s již existujícími údaji. Pro účel práce student sestaví aparaturu tak, aby bylo možné experiment realizovat.

**Jazyk závěrečné práce:** angličtina

**Vedoucí práce:** Mgr. Michaela Musilová, Ph.D.

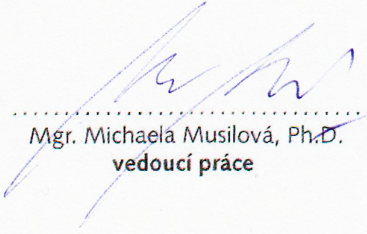
**Konzultant:** doc. Mgr. Vít Kudrle, Ph.D.

**Datum zadání práce:** 27. 6. 2016

**V Brně dne:** 21. 3. 2017

Souhlasím se zadáním (podpis, datum):

  
Bc. Magdalena Špoková  
studentka

  
Mgr. Michaela Musilová, Ph.D.  
vedoucí práce

  
prof. Rikard von Unge, Ph.D.  
ředitel Ústavu teoretické fyziky a  
astrofyziky



# Contents

<b>List of Abbreviations</b>	<b>4</b>
<b>Introduction</b>	<b>5</b>
<b>1 Interplanetary Environment</b>	<b>7</b>
1.1 Estimating Surface Temperature . . . . .	7
1.1.1 Maximum Temperature . . . . .	9
1.1.2 Minimum Temperature . . . . .	12
1.2 Radiation . . . . .	16
1.2.1 Shortly About the Sun . . . . .	16
1.2.2 Radiation Profile . . . . .	19
1.3 Interplanetary Medium . . . . .	20
1.3.1 Near the Solar Surface . . . . .	20
1.3.2 Solar Wind . . . . .	21
1.3.2.1 Shortly About Plasma . . . . .	24
<b>2 Selected Organism</b>	<b>27</b>
2.1 <i>Nostoc commune</i> and Its Viability . . . . .	30
2.2 Photosynthesis and Cyanobacterial Cell . . . . .	32
2.3 Mechanisms of Stress Response . . . . .	36
2.4 Damage Expected Due to Experiment . . . . .	37
<b>3 Experimental Methodology</b>	<b>38</b>
3.1 Experimental Apparatus . . . . .	38
3.2 Measuring Equipment . . . . .	40
3.2.1 Fluorometer . . . . .	40
3.2.2 Atomic Force Microscope . . . . .	43
3.2.2.1 Sample attachment . . . . .	44
3.3 Sample Preparation and Storage . . . . .	45

3.3.1	Visual Characterisation of Samples . . . . .	46
3.4	Measuring Protocols . . . . .	48
3.4.1	Measuring with the Fluorometer . . . . .	48
3.4.2	Experiments in Apparatus . . . . .	48
3.4.2.1	Low pressure . . . . .	49
3.4.2.2	Plasma . . . . .	49
3.4.3	AFM . . . . .	50
<b>4</b>	<b>Results</b>	<b>52</b>
4.1	AFM Surface Mapping . . . . .	52
4.1.1	Force mapping . . . . .	52
4.1.1.1	Antarctic Samples . . . . .	52
4.1.1.2	Brno Samples . . . . .	54
4.1.2	Quantitative imaging . . . . .	57
4.1.2.1	Antarctic Samples . . . . .	57
4.1.2.2	Brno Samples . . . . .	60
4.2	Low Pressure Tolerance . . . . .	64
4.2.1	20 Pa . . . . .	64
4.2.2	100 Pa . . . . .	66
4.3	Plasma Tolerance . . . . .	67
4.3.1	150 W . . . . .	68
4.3.1.1	Antarctic Samples . . . . .	68
4.3.1.2	Brno Samples . . . . .	72
4.3.2	250 W . . . . .	76
4.3.2.1	Antarctic Samples . . . . .	76
4.3.2.2	Brno Samples . . . . .	79
<b>5</b>	<b>Discussion</b>	<b>82</b>
5.1	AFM . . . . .	82
5.2	Low Pressure . . . . .	83
5.3	Plasma . . . . .	83
<b>6</b>	<b>Conclusions</b>	<b>86</b>
6.1	Synthesis . . . . .	86
6.2	Future Work . . . . .	87
	<b>Bibliography</b>	<b>88</b>

<b>Appendices</b>	<b>98</b>
A Data for Antarctic samples plasma treatment . . . . .	98
B Data for Brno samples plasma treatment . . . . .	101

# List of Abbreviations

AFM	Atomic force microscopy
CCP	Capacitively coupled plasma
EPS	Extracellular polysaccharides
PS	Photosystem
PSI	Photosystem I
PSII	Photosystem II
RF	Radio frequency
sp.	Species
UV	Ultraviolet

# Introduction

Is there life somewhere else in the universe? If yes, how evolved is it? And how alien is it? Could any organisms we know from the Earth live there? These are some of the questions, a curious mind might ask. A scientific field, which studies life's origin, evolution and distribution in our universe is astrobiology. Throughout human history a lot of different theories were made about life's origin and evolution. Was life created? Did it come from somewhere else? No one can say which is true, but we can build up theories and test them. The theory of panspermia might be considered. This theory according to (Gargaud et al., 2011) states that life rose somewhere else and was transported by asteroids, comets, impact mass ejecta (see Worth et al., 2013) or even by free floating ("rogue") planet, entering some planetary system, contaminating it by collisions with its planets. Until we find life outside the Earth and estimate amount of interplanetary objects biologically active (or rather whether if any object is biologically active), we cannot decidewhether is this hypothesis reasonable (Lin & Loeb, 2015). This theory is commonly associated with microorganisms like viruses or bacterial spores, because of their resistance (Sharov & Gordon, 2013). For example, cyanobacteria are still quite simple organisms, even though they can form macroscopic colonies. So it might be possible for them to arise in suitable conditions and then propagate using some celestial body. In this work, so-called lithopanspermia, the transfer of life forms by solid objects, is considered. Another theory also suggests radiopanspermia, small life forms propagating in space by radiation pressure. Another suggested hypothesis is a direct panspermia, supposing the life seeded and was distributed by some intelligent life forms (Secker et al., 1996).

The existence and distribution of life in our universe is an actual question, since we are finding more and more exoplanets orbiting stars in our Galaxy (exoplanet catalogue e.g. at ("NASA Exoplanet Archive", 2017)). And there are not only these far objects where we might be looking for an alien life, in our Solar system there are objects of interest, too, like moons of Jupiter or Saturn or there is a popular question of life on Mars. These objects have the advantage of being relatively near, so it is

possible for us to look closely at them. Although it is not possible to explore these worlds in person yet, we are able to study them with the use of probe pictures and rovers. Unfortunately, with this type of research a problem occurs, an organism from Earth might be delivered on the object of our interest, although all missions to space have to deal with planetary protection policy, created by the Committee on Space Research (COSPAR). The thing is, that in principle it is not possible to fully sterilize equipment, just to minimize the potential contamination threat to acceptable level (DeVincenzi et al., 1998). The limits are different for different missions (see COSPAR policy), for example for Mars mission for life detection, the density of spores has to be less than 0.03 spores per square meter (see Frick et al., 2014). The question is, could an organism from Earth survive exposition to alien conditions?

In this work, it is assumed an organism is delivered to some body by humans deliberately, as the purpose of an experiment or accidentally. Our main goal is to test the organism's ability to survive in extraterrestrial conditions. The extraterrestrial conditions we want to simulate in this work are solar wind-like environment and low pressure. These conditions will try to be established in a laboratory apparatus, which will be built specifically for this series of experiments. The test organism, selected because of its well known endurance to stress conditions, is the terrestrial cyanobacterium *Nostoc commune*. In this work *Nostoc commune* from two different locations is used, one from Brno, the other one from Antarctica. One of the goals of this project is to compare the survival of the cyanobacteria from different locations. Another goal is to establish mechanical properties of these cyanobacteria using atomic force microscopy.

In the first chapter of the thesis, temperature, radiation, solar wind and vacuum as properties of extraterrestrial environment will be considered. The analysis of temperature, solar wind etc. will not be done in detail, as it is not the aim of this thesis to do detailed analysis of it but to outline the basics and discuss the parts important for this work.

In the second chapter the cyanobacteria in general and also the selected one, *Nostoc commune*, will be described in more detail. A basic description of photosynthetic processes will be given and expected influence of extraterrestrial environment to the test organism will be considered.

In the section Experimental Methodology the procedure of collecting organisms will be described, as well as the protocol of treatment and storage. In addition, the used equipment and testing procedure will be described.

Results will be shown in chapter Results and discussed in the chapter Discussion. Conclusions will be summarized in the last chapter.

# Chapter 1

## Interplanetary Environment

Since one of the aims of this work is to simulate extraterrestrial environment, it is necessary to consider how it looks outside our planet's atmosphere. This means considering the radiation, the solar wind particle density, what the temperature is and how these parameters change with heliocentric distance and how these parameters might influence an organism. This chapter is dealing with environment specifications and associated problems.

### 1.1 Estimating Surface Temperature

Let's look at estimations of temperatures across the Solar System. Temperature (as well as solar wind particle density and solar radiation intensity) is expected to drop with distance from the Sun. In the following subsections the estimations of maximum and minimum temperatures will be done. It is important to think about how these expectations correlate with reality, either for minor bodies (asteroids or near earth objects) or terrestrial planets and their moons. For simplicity the analysis will be done for idealized, atmosphere-less, Vesta sized, radius is considered  $r = 500$  km, rocky body in the Solar System. This way ice and gas giants are excluded, for their disputable surface existence. Also the comets and centaurs (objects behaving both like asteroids and comets) are not considered, because of ongoing changes through their orbit. The bodies with insufficient gravitational effect are excluded too.

So what influences the surface temperature? Besides the distance, other parameters might be important, whether the axial tilt (obliquity) or rotation period. The distance of objects is changing as it orbits the Sun. Ever since Kepler it has been known, that the trajectories of bodies in the Solar System have different shapes, from nearly circular to highly eccentric ellipses. This means the objects is orbiting the Sun

from the furthest point, aphelion, to the nearest point, perihelion (in general cause from apocenter to pericenter). For orbit illustration see Figure 1.1. Dealing with small bodies like meteoroids or small asteroids (less than about 40 km in diameter), one should consider Yarkovsky effect, altering semi-major axis,  $a$ , of asteroid (Bottke et al., 2006).

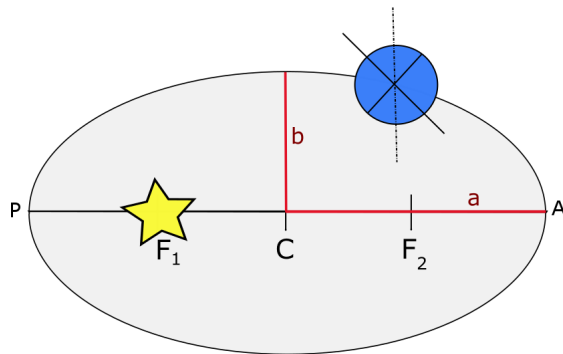


Figure 1.1: Object's circulation around the Sun.

The Sun is situated at focus  $F_1$  of ellipse with center  $C$  and semi-major axis  $a$  and semi-minor axis  $b$ , orbit's apocentre is  $A$  and pericenter  $P$ . Object has some axial tilt (axis is dotted line).

Another thing is the axial tilt, the Earth's axial tilt is  $23.5^\circ$  and this inclination causes changing of seasons. The most extreme case are polar nights and days, causing long terms of darkness and light on the southernmost and the northernmost places.

Rotation period has its extreme case of tidal locking. For tidal locked object, time to revolve around its axis and orbital period are the same. This form of rotation can be seen at the Moon, orbiting the Earth facing it only one side. It has large consequences for temperature of an object leading to high differences in temperature on both sides. Again, for small bodies like meteoroids or small asteroids, should be considered YORP (Yarkovsky-O'Keefe-Radzievskii-Paddack) effect. This effect can alter the rotation period and obliquity (Bottke et al., 2006).

Global shape of the object, surface roughness and surface composition are influencing the temperature, too. Among asteroids and moons myriad of different, hardly spherical, shapes can be found. And there is no absolutely smooth surface in the Solar system. There are always some higher spots bathing in sunlight while shadowing near valley and some craters in which temperature might be completely different than on surrounding surface. For example on Mercury's hot surface there is a permanently shadowed crater where water ice was found (Slade et al., 1992).

Compositon of object's surface needs to be taken into account, because materials differ in their ability to conduct and accept heat (more in subsection 1.1.2).

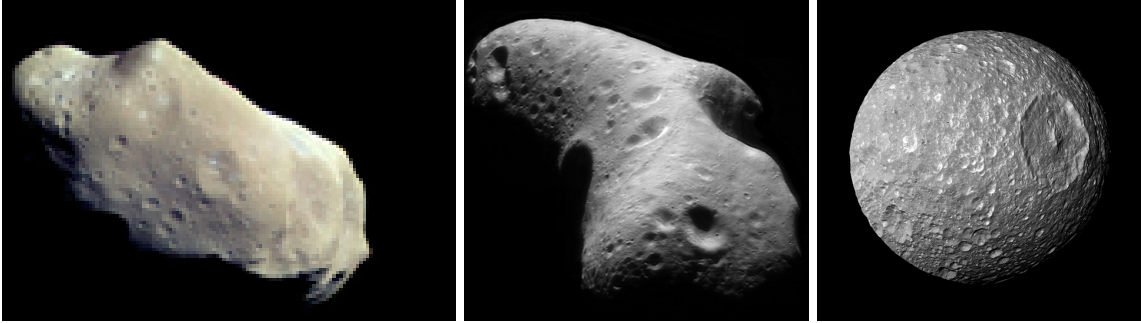


Figure 1.2: Irregular shapes of asteroids Ida and Eros and spherical shape of Saturn's moon Mimas. Credit: NASA.

Many other things can affect the surface temperature; as it was said if an object has some atmosphere there might be the greenhouse effect rising surface temperature thanks to gases transparent to light, but opaque to infrared radiation (like  $\text{CO}_2$  and  $\text{H}_2\text{O}$  on Earth, Venus or Mars). Or anti-greenhouse effect, lowering it thanks to atmosphere opacity. Both these effects might occur simultaneously, this is a case of Titan, where  $\text{N}_2$ ,  $\text{H}_2$ ,  $\text{CH}_4$  are causing the greenhouse effect, but a higher layer of organic haze causes anti-effect (McKay et al. 1999). An interesting phenomenon similar to the greenhouse one is the so-called solid state greenhouse effect. In the same way as atmosphere layers can be transparent for some kinds of radiation but not for infrared, some surface layers like ice and snow can do the same, so it is possible that under the icy cold surface, the ice is melted (Gargaud et al., 2011).

It is very difficult and complex science to determine temperature in some general way for all bodies in Solar System. Therefore in our calculations we simply take into account atmosphere-less spherical smooth rocky body on circular orbit in the plane of the Solar System, without internal source of energy.

### 1.1.1 Maximum Temperature

In this subsection the maximum temperature will be estimated. But first let's estimate equilibrium temperature  $T_{\text{eq}}$ . If it is assumed the body is heated only by Sun's radiation, amount of energy received by the body,  $P_{\text{in}}$ , can be written as

$$P_{\text{in}} = \pi R^2(1 - A) \frac{L_{\odot}}{4\pi r^2}, \quad (1.1)$$

where  $\pi R^2$  is illuminated area of body of radius  $R$ ,  $A$  is Bond albedo (ratio of reflected or scattered flux over incoming flux, values from 0 to 1, (Mueller, 2007),  $L_\odot$  is solar luminosity and  $r$  is distance from the Sun. Since it is assumed the body is in thermal equilibrium, the amount of energy received, must be equal to the amount of energy radiated by the whole surface of the body,  $P_{\text{out}}$ , therefore we use Stefan–Boltzmann law

$$P_{\text{out}} = 4\pi R^2 \epsilon \sigma T^4, \quad (1.2)$$

where  $\epsilon$  is emissivity of the body (infrared emissivity is commonly used for asteroids, with value 0.9 according to (De Pater & Lissauer, 2015), because the maximum of asteroid’s thermal radiation is in infrared part of spectra, see section 1.2 ),  $\sigma$  is Stefan-Boltzmann constant and  $T$  is temperature. With these two formulas the equilibrium temperature can be found

$$T_{\text{eq}} = \sqrt[4]{\frac{L_\odot(1 - A)}{16\pi r^2 \sigma \epsilon}}. \quad (1.3)$$

This simple formula is widely used across studies of planetary habitability, thermal studies of asteroids etc. as the first guess of temperature. It can be expressed or modified in many ways. There might be factor  $S$ , Solar constant,  $S = \frac{L_\odot}{4\pi(1AU)^2}$ , so  $r^2$  can be in astronomical units, AU. The factor  $\beta$  might be included:

$$T_{\text{eq}} = \sqrt[4]{\frac{L_\odot(1 - A)}{16\beta\pi r^2 \sigma \epsilon}}. \quad (1.4)$$

If  $\beta$  equals 0.5 this is case of a tidal locked planet or a moon if it equals to one, it is a fast rotator, as it is Earth for example (Méndez & Rivera-Valentín, 2017). In works dealing with eccentricity,  $e$ , effects (Williams & Pollard, 2002; Kaltenecker & Sasselov, 2011) it is

$$T_{\text{eq}} = \sqrt[4]{\frac{L_\odot(1 - A)}{16\beta\pi r^2 \sigma \epsilon(1 - e^2)^{1/2}}}. \quad (1.5)$$

Or modification with redistribution factor  $f$ , describing energy distribution

$$T_{\text{eq}} = \sqrt[4]{\frac{S(1 - A)}{f\sigma}} \quad (1.6)$$

(Selsis et al., 2007) and many other versions can be found.

Let us find the estimation of maximum temperature. For this estimation the sub-solar temperature  $T_{ss}$ , will be used e.g. surface temperature in sub-solar point, point when the Sun is in zenith (overhead). If global areas in equations 1.1 and 1.2 are replaced with unit areas temperature can be calculate from formula

$$T_{ss} = \sqrt[4]{\frac{L_{\odot}(1 - A)}{4\pi r^2 \sigma \epsilon}} = \sqrt{2}T_{eq}. \quad (1.7)$$

In Figure 1.3 the values of  $T_{eq}$  and  $T_{ss}$  were plotted, farther from the Sun differences between these values diminish.

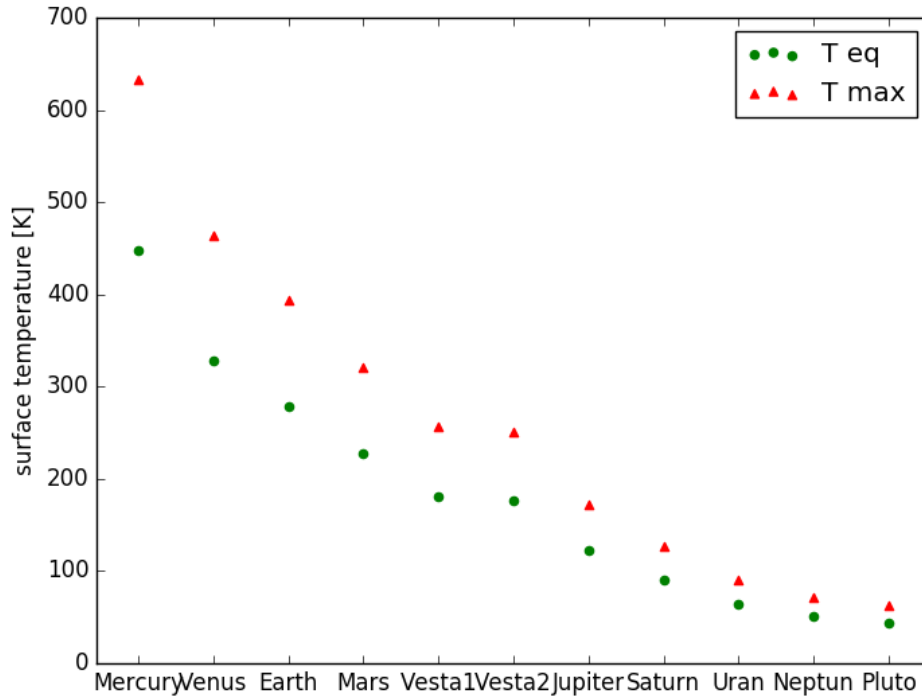


Figure 1.3:  $T_{eq}$  and  $T_{ss}$  computed for idealized object with Bond albedo  $A = 1$  at the distance of planets, Pluto and Vesta. To illustrate how albedo affects temperature Vesta1 is plot for idealized object with  $A = 1$ , Vesta2 with Vesta's Bond albedo  $A = 0.18$  (actual value from (Li et al., 2013)).

Atmospheric effect can be included in the following form. Atmosphere (optically

thick for IR) absorbs solar radiation, due to this absorption and the absorption of radiation from the surface it gains a temperature  $T_{\text{atm}}$  and radiate itself (and heats the surface).and radiates itself (and heats the surface). Put in equations according to (Brož & Šolc, 2013):

$$(1 - A)k_{\text{trans}}\frac{L}{4\pi r^2} + 4(1 - A_{\text{ir}})\varepsilon\sigma T_{\text{atm}}^4 = 4\varepsilon\sigma T_{\text{eq}}^4, \quad (1.8)$$

$$k_{\text{abs}}\frac{L}{4\pi r^2} + k_{\text{abs,ir}}4\varepsilon\sigma T_{\text{eq}}^4 = 8\varepsilon\sigma T_{\text{atm}}^4, \quad (1.9)$$

The first equation is the conservation of energy for surface, the second one for atmosphere, where  $k$  with appropriate index is either transition or absorption or infrared absorption coefficient of atmosphere and  $A_{\text{ir}}$  is albedo for IR radiation. Here are two equations for two unknowns, so if  $k$  parameters and  $A_{\text{ir}}$  are known, equations are easy to solve. For other ways to include greenhouse effect see e.g. (Méndez A. & Rivera-Valentín, 2017) or (Barcza, 2016).

### 1.1.2 Minimum Temperature

When maximum temperature  $T_{\text{ss}}$  is estimated, temperature distribution on the body might be written in form

$$T(\varphi) = T_{\text{ss}} \cos^{1/4}(\varphi), \quad (1.10)$$

$\varphi$  is angular distance from the subsolar point, for  $\varphi > 90^\circ$ ,  $T = 0$  K. This simple approach is called Standard Thermal Model (STM, Lebofsky et al., 1986). The STM and other simple models might be used for albedos and radii estimations from observational data. To fit the data better STM was modified with beaming parameter, considering enhanced thermal emission towards the Sun (Deblo & Harris, 2002). But still the temperature of non illuminated side is 0 K and this model was not good for all data (near Earth objects). Another model was used for the estimation of object temperature distribution

$$T(\theta) = T_{\text{ss}} \cos^{1/4}(\theta), \quad (1.11)$$

formula looks the same, the difference is the  $\theta$  is geographic latitude. This is the Fast Rotating Model (FRM, Lebofsky and Spencer, 1989), expecting the same temperature for all point with given latitude. These two simple models were several times modified (Near-Earth Asteroid Thermal Model (NEATM, Harris, 1998), Night Emission Simulated Thermal Model (Wolters & Green, 2009) NESTM, more on models also in Deblo, 2004 or Mueller, 2007; Rozitis & Green, 2011 and many others).

These modifications brought nothing new to estimations of the dark side temperature. Nowadays the best information about the temperatures on a body gives thermophysical modeling (Deblo et al., 2015).

In this work  $T_{\min}$  will be estimated in a simple way, but not  $T_{\min} = 0$ . For our estimations is, again, considered Vesta-like, smooth body, with the rotation period  $P = 5.5$  hours, i.e. close to real value for Vesta from NASA fact sheet ("Asteroid Fact Sheet", 2017),  $P = 5.342$  hours. To see the correlation between the rotation period and the asteroid diameter see Figure 1.4 or look at (Pravec et al., 2002) or (Pravec et al., 2006). Our's body thermal inertia, property of material causing the

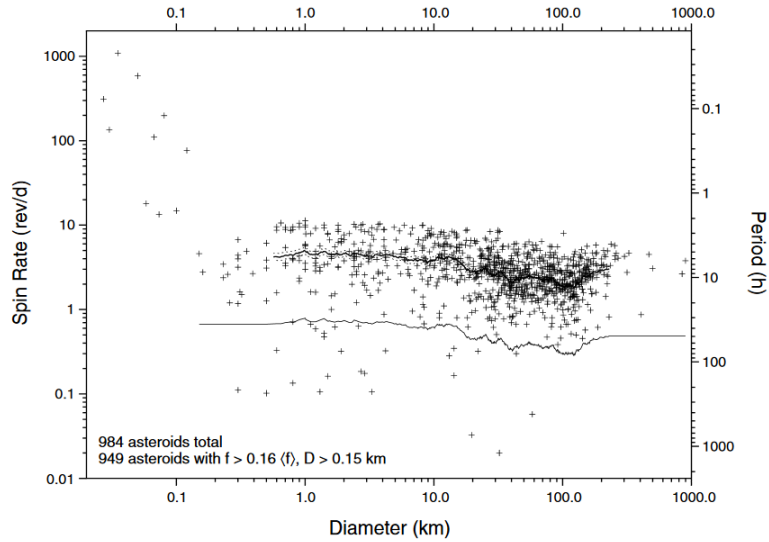


Figure 1.4: Rotational period of asteroids depending on the diameter.  
Credit Pravec et al. (2002).

fact it takes some time to cool it and heat it, has to be considered (Rozitis & Green, 2011). Well known consequence of this property is that the hottest part of the day on Earth is not when the Sun is highest in zenith, but some hours later. And a hot road and rocks, warmed by sunlight during a day remain warm for part of night, so snakes, etc. go there to get warm.

$$\Gamma = \sqrt{\kappa\rho C}, \quad (1.12)$$

where  $\kappa$  is thermal conductivity,  $\rho$  is material density and  $C$  specific heat capacity. While strictly speaking  $\Gamma$  is not a constant, because thermal conductivity is temperature dependent (Gundlach and Blum, 2013), in this work it is considered a

constant. So brought into context with models: STM model object is assumed to have no thermal inertia, in FRM infinitely large thermal inertia, but without lateral heat conduction (Mueller, 2007). Value for lunar regolith is  $\Gamma = 51 \text{ J s}^{-1/2} \text{ K}^{-1} \text{ m}^{-2}$  (Winter and Krupp, 1971). For Vesta is average thermal inertia  $\Gamma = 30 \text{ J s}^{-1/2} \text{ K}^{-1} \text{ m}^{-2}$ , differing in regions from 10 to 50 (Leyrat et al., 2012; Capria, 2014). For comparison, values of  $\Gamma$  for metals are much larger, iron (Mueller, 2007) has  $\Gamma = 17 \cdot 10^3 \text{ J s}^{-1/2} \text{ K}^{-1} \text{ m}^{-2}$ . Table of thermal inertia of celestial objects alongside with diameter, distance and taxonomy is in Figure 1.5.

Number	Name	$D$ (km)	$\Delta_D$ (km)	$\Gamma$ (SI)	$\Delta_\Gamma$ (SI)	Tax	$r$ (au)
1	Ceres	923	20	10	10	C	2.767
2	Pallas	544	43	10	10	B	2.772
3	Juno	234	11	5	5	S	2.671
4	Vesta	525	1	20	15	V	2.3
16	Psyche	244	25	125	40	M	2.7
21	Lutetia	96	1	5	5	M	2.8
22	Kalliope	167	17	125	125	M	2.3
32	Pomona	85	1	70	50	S	2.8
41	Daphne	202	7	25	25	Ch	2.1
44	Nysa	81	1	120	40	E	2.5
45	Eugenia	198	20	45	45	C	2.6
87	Sylvia	300	30	70	60	P	2.7
107	Camilla	245	25	25	10	P	3.2
110	Lydia	93.5	3.5	135	65	M	2.9
115	Thyra	92	2	62	38	S	2.5
121	Hermione	220	22	30	25	Ch	2.9
130	Elektra	197	20	30	30	Ch	2.9
277	Elvira	38	2	250	150	S	2.6
283	Emma	135	14	105	100	P	2.6
306	Unitas	56	1	180	80	S	2.2
382	Dodona	75	1	80	65	M	2.6
433	Eros	17.8	1	150	50	S	1.6
532	Herculina	203	14	10	10	S	2.772
617	Patroclus	106	11	20	15	P	5.9
694	Ekard	109.5	1.5	120	20	-	1.8
720	Bohlinia	41	1	135	65	S	2.9
956	Elisa	10.4	0.8	90	60	-	1.8
1173	Anchises	136	15	50	20	P	5.0
1580	Betulia	4.57	0.46	180	50	C	1.1

Figure 1.5: Sample of table from work of (Deblo et al., 2015).

If it is known how temperature changes through time it is possible to estimate minimum temperature  $T_{min}$ . Procedure in accordance with (Brož & Šolc, 2013) will be used for it. The day/night changes in 1D approximation will be computed. The basis is to solve heat conduction equation. In one dimension, neglecting lateral heat

flow and considering  $\kappa$  is independent of depth, it is

$$\frac{\partial T}{\partial t} = \frac{\kappa}{\rho C} \frac{\partial^2 T}{\partial x^2}. \quad (1.13)$$

The boundary condition is needed to solve the equation, in this case it must be said, the energy radiated by surface and heat conducted inwards is equal to incoming irradiance

$$\epsilon\sigma T^4 - \kappa \frac{\partial T}{\partial x} = (1 - A)\Phi(t). \quad (1.14)$$

Diurnal changes are simulated by variable light source of irradiance ( $\Phi = \frac{L}{4\pi r^2}$ , in literature can be signed as  $F$ ). It consists of constant and variable part

$$\Phi(t) = \Phi_0 + \Phi_1 e^{i2\pi ft}. \quad (1.15)$$

Note only real part is physically significant. The form of solution can be guessed since irradiance is harmonic, the solution will have the same form

$$T(x, t) = T_0 + T_1(x) e^{i2\pi ft}. \quad (1.16)$$

So let's try to put this solution back in the initial equation (1.13). The  $T_0$  is in fact  $T_{eq}$ , but the form of  $T_1(x)$  it is not known. The calculation results in to equation

$$i2\pi f T_1(x) = \frac{\kappa}{\rho C} \frac{d^2 T_1(x)}{dx^2}. \quad (1.17)$$

Its solution is

$$T_1(x) = T_1(0) e^{-\sqrt{2i\pi f \rho C / \kappa} x}. \quad (1.18)$$

Applying the boundary condition, (1.14), assuming  $x = 0$  (changes on the surface) and using identity  $2i = (1 + i)^2$ , quite complicated equation to find coefficient  $T_1(0)$  is obtained

$$\epsilon\sigma(T_0 + T_1(0)e^{i2\pi ft})^4 + \kappa(1+i)\sqrt{\pi f \rho C / \kappa} T_1(0) e^{i2\pi ft} = (1 - A)(\Phi_0 + \Phi_1 e^{i2\pi ft}). \quad (1.19)$$

If  $T_1(0) \ll T_0$ , then the approximation leads to  $(T_0 + T_1)^4 \approx T_0^4 + 4T_0^3 T_1$ . And combined with equations (1.1), (1.2), it results to equation

$$4T_{eq}^3 T_1(0) \epsilon\sigma + (1 + i)\sqrt{\pi f \kappa \rho C} T_1(0) = (1 - A)\Phi_1. \quad (1.20)$$

$T_1(0)$  can now be expressed and put in equation (1.16). Solution has to be multiplied with its complex conjugate to eliminate complex number in denominator. Thermal

parameter  $\Theta = \Gamma\sqrt{\pi f}/4\pi\epsilon\sigma T_{\text{eq}}^3$ , where  $f = 1/P$ , and a thermal delay parameter,  $\phi_{\text{th}} = \arctan\left(-\frac{\Theta}{\Theta+1}\right)$  are used. Results of this treatment are shown in following equation

$$T(0, t) = T_{\text{eq}} + \frac{(1-A)\Phi_1}{4\pi\epsilon\sigma T_{\text{eq}}^4} \frac{1}{\sqrt{1+2\Theta+2\Theta^2}} e^{i(2\pi ft + \phi_{\text{th}})}. \quad (1.21)$$

Here is the surface temperature as a function of time ( $T_{\text{eq}}$  is known from (1.3)). The minimum  $T_{\text{min}}$  and maximum  $T_{\text{max}}$  can be found in time values

$$\begin{aligned} t_{\text{max}} &= -\phi_{\text{th}}/2\pi f, \\ t_{\text{min}} &= (\pi - \phi_{\text{th}})/2\pi f. \end{aligned} \quad (1.22)$$

Amplitude of irradiance  $\Phi_1$  was chosen so that  $T_{\text{max}}$  in time (1.22) is the same as the  $T_{\text{ss}}$  (1.7). To see results in dependence of distance from the Sun see following Figure 1.6.

What if the real data for Vesta and data obtained by this procedure (for idealized Vesta) are compared? In the work of (Tosi et al., 2014) might be found the maximum temperature derived from measurement is 260 K, minimum is not estimated because of instrument limitations. In the work of (Leyrat et al., 2012) temperature seems to be in interval (40, 248) K. Larger difference in minimum temperature is expected since real shape was not assumed and was considered as an infinite plane.

The temperature in dependence of depth could be calculated if the  $x \neq 0$ . The distance (depth) to which day/night changes of temperature can penetrate (in this depth variations in temperature have dropped by factor  $e^{-1}$ , (Rozitis & Green, 2011)). It is given by equation (De Pater & Lissauer, 2015)

$$l_s = \sqrt{\kappa P / \pi \rho C}. \quad (1.23)$$

Typical values of skin depth of asteroids are in centimeters (Harris & Lagerros, 2002).

## 1.2 Radiation

To see what radiation can be expected it is necessary to take a look at our star's radiation profile. In the first subsection basic information about the Sun will be given, in the second solar radiation profile will be shown.

### 1.2.1 Shortly About the Sun

If anyone was asked what the Sun is, the answer would probably be: The Sun is a giant burning ball/sphere in the centre of our Solar System. More precisely the

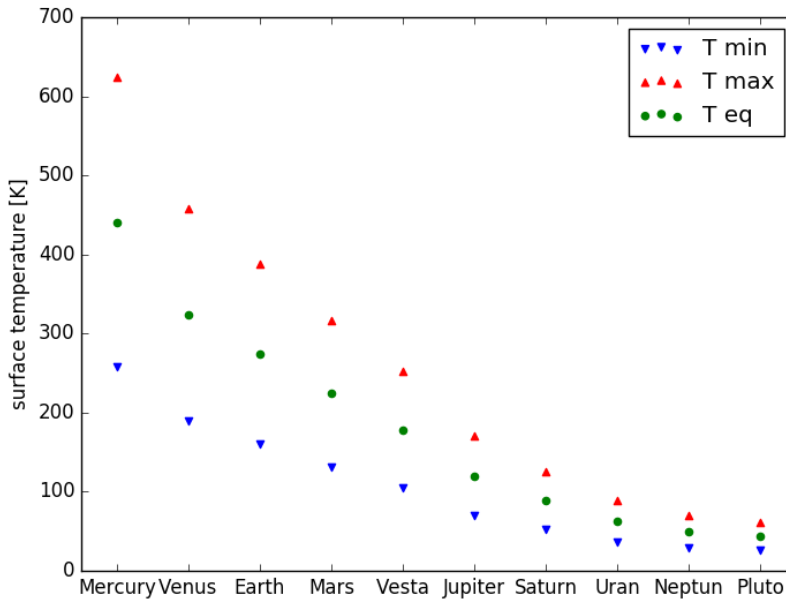


Figure 1.6: Surface temperature of idealized body at various orbits.  $T_{max}$  is maximum and  $T_{min}$  minimum temperatures obtained from (1.21).  $T_{eq}$  is equilibrium temperature from (1.3). Distances for computing were taken from NASA fact sheets ("Asteroid Fact Sheet", 2017).

Sun is 4,6 Ga old main sequence star, with total mass  $M = 2 \cdot 10^{30}$  kg, radius  $R = 7 \cdot 10^8$  m, effective temperature  $T_{eff} = 5800$  K (see subsection 1.2.2) and luminosity  $L = 3.86 \cdot 10^{36}$  W, data from NASA fact sheet ("Sun Fact Sheet", 2017) and (Carroll & Ostlie, 2014). The Sun can be classified as G spectral type star or yellow dwarf. It is also known that our star does not have a partner star, considerable number of stars lives in the multiple star systems, but not the Sun (Carroll & Ostlie, 2014).

Sun is composed mainly of hydrogen H, helium He and a small amount of other elements like oxygen, carbon, iron etc. usually referred to as metals (i.e. in astrophysics every element which is not hydrogen or helium is called metal). Abundance, relative mass fraction of given element, in the Sun is  $X = 0,738$  for hydrogen,  $Y = 0,248$  for helium and  $Z = 0,013$  for metals (values from (Asplund et al., 2009)). Abundances are estimated more and more precisely, so nowadays values are different than those estimated 20 years ago, but they do not differ significantly,

just in the third decimal place. Changes in chemical composition are taking place in the star as it ages. Future evolution of the Sun and its current position in HR (Hertzsprung–Russell) in Figure 1.7.

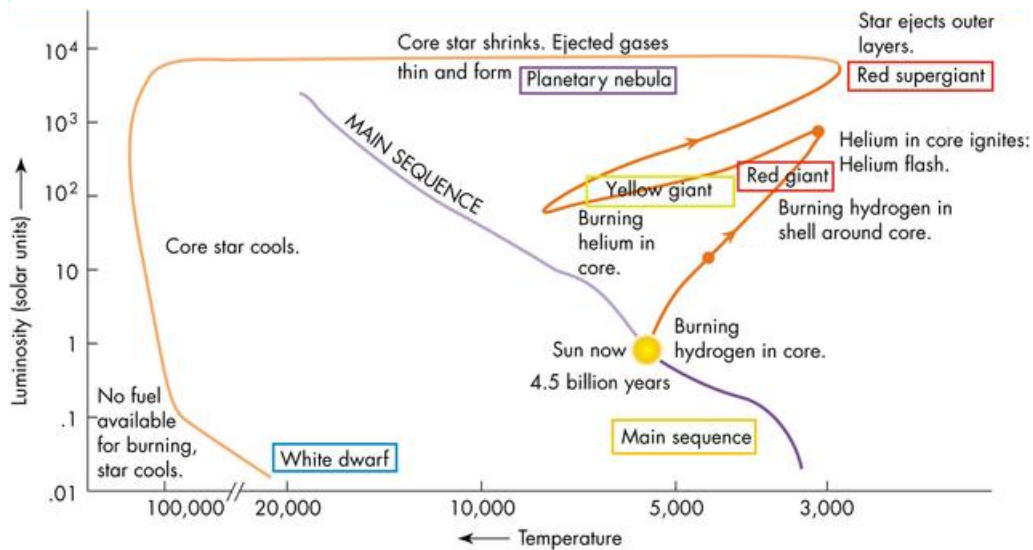
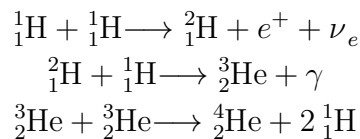


Figure 1.7: Evolutionary scheme of the Sun in HR diagram.

Dependence of luminosity on temperature as our star ages is shown. Evolution from main sequence star fusing hydrogen to cooling white dwarf. During its way through the diagram, the Sun will fuse nearly all hydrogen to helium, then the helium will fuse to heavier element, etc. Modified from ("Stars and Nebulae", 2017).

The Sun shines thanks to hydrogen fusion occurring in the core maintaining it hot. The proton-proton chain (pp chain) is dominant



As these photons try to get out of the star's interior, they are losing energy due to interactions with matter. The energy from core (hydrogen burning) region might be transferred at first radiatively (zone of radiative transfer), because opacity is low, in upper layers (due to higher opacity) it is more effective to transfer energy by convection (convection zone) to surface. (Carroll & Ostlie, 2014).

## 1.2.2 Radiation Profile

Good approximation of the solar spectrum can be obtained if the Sun is considered as a black body radiator. This means that the amount of emitted energy depends only on the surface temperature of the Sun, it is isotropic and homogenous and can be described by Planck's law of black-body radiation:

$$B_{\lambda}(\lambda, T) = \frac{2hc^2}{\lambda^5} \frac{1}{e^{\frac{hc}{\lambda kT}} - 1}, \quad (1.24)$$

where  $B_{\lambda}$  is spectral flux density of a body,  $h$  is Planck's constant,  $c$  is speed of light,  $\lambda$  wavelength,  $k$  Boltzmann constant and  $T$  is temperature.

This approach gives a continuous curve (emission and absorption lines are absent). But it is good enough to see where the maximum of the function is. For the Sun with effective temperature,  $T_{\text{eff}}$ , around 5 800 K (effective temperature is the temperature of black body that emits the same radiation as an object, which in reality is not a black body) the maximum,  $\lambda_{\text{max}}$ , is in visible wavelengths, see Figure 1.8. If the Sun would be hotter the maximum would be shifted to shorter wavelengths. This describes Wien's displacement law:

$$\lambda_{\text{max}} = \frac{b}{T}, \quad (1.25)$$

$b$  is Wien's displacement constant.

Radiation profile does not change with the distance, but the energy from the Sun is spread out to a larger area, so the object on the orbit of Mercury gets more energy per area than the one on the orbit of Jupiter.

Object	Irradiance [ $\text{W m}^{-2}$ ]
Mercury	9040
Earth	1366
Jupiter	50
Uranus	3.7

Beside the photon flow from the Sun are bodies in Solar system exposed to the Sun particle flow, solar wind. Sources of particles from outside of the Solar system are galactic cosmic rays - composed mostly of nuclei of atoms from cataclysmic processes in our galaxy (Gargaud et al., 2011).

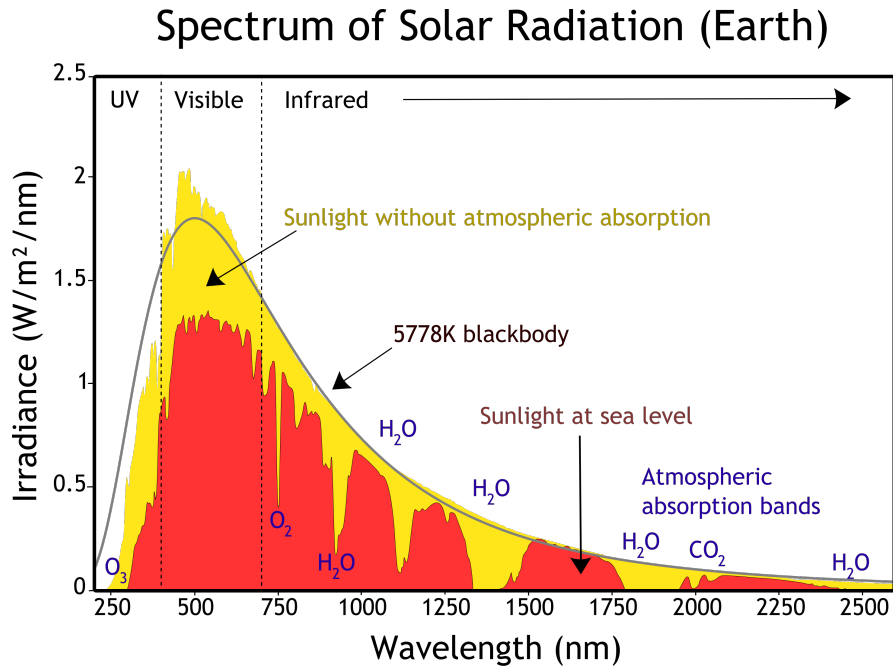


Figure 1.8: Solar spectral irradiance of Earth.

The graph shows the difference between incoming spectral irradiance and the one at the sea level (caused by atmosphere). The idealized black body curve for 5778 K is also shown. From: ("Solar spectrum", 2017).

## 1.3 Interplanetary Medium

### 1.3.1 Near the Solar Surface

Sunspots, flares or for example prominences can be seen, if one looks to the Sun. The sunspot is a phenomenon on the Sun's surface (photosphere) but the flare and prominences are not, so the area above the photosphere might be referred to as the solar atmosphere. The outermost and the hottest part of the solar atmosphere extending to interplanetary space is called the corona. The region above the photosphere, but below the corona, is called the chromosphere. One might observe the inner part of the corona during solar eclipse, see Figure 1.9, otherwise it can not be seen because of the much brighter photosphere. Another way to see the corona is by using a telescope/satellite with coronagraph (e.g. current shots of the Sun made by SOHO satellite's LASCO coronagraphs at mission website ("The Very Latest SOHO Images", 2017)), or observation in X-ray wavelengths.



Figure 1.9: Solar corona during the Solar eclipse. On the left we can see corona around the period of solar maximum in 2016, on the right side the Figure captured around the solar minimum in 2005. Credit: 2016 Mirek Dočekal, Miloslav Druckmüller, 2005 Miloslav Druckmüller, Fred Espenak.

As was mentioned in Figure 1.9, the Sun goes through periodic changes. In these cycles the magnetic field reverses and the maximum and minimum of solar activity (number of sunspots, flares etc.) is recorded.

The matter inside the Sun and in its atmosphere is in the form of plasma. This means atoms are ionized, electrons are no longer bounded to nuclei. If the Sun is watched in X-ray, see Figure 1.10 there can be seen some bright and the dark areas. ones referred to as active regions, are made up of tightly closed magnetic field lines. The processes of magnetic field lines reconnection and reconfiguration leads to processes like plasma heating and coronal loops, flares, coronal mass ejections (CME). The dark regions are marked as coronal holes. In this case the magnetic lines are "open" to space and particles are free to escape forming the solar wind. (Aschwanden, 2005).

### 1.3.2 Solar Wind

The Solar wind is coronal wind, i.e. it is caused by particle flow from the hot corona. Its major compound is hydrogen, then there is helium and the small amounts of other elements (Bochsler, 2001). The Solar wind can be divided into two groups - a fast wind and a slow wind. The fast wind, with velocity around  $800 \text{ km s}^{-1}$ , is produced in regions with open magnetic field lines and the slow wind, with velocity around  $400 \text{ km s}^{-1}$ , in regions with closed field lines. (Aschwanden, 2005).

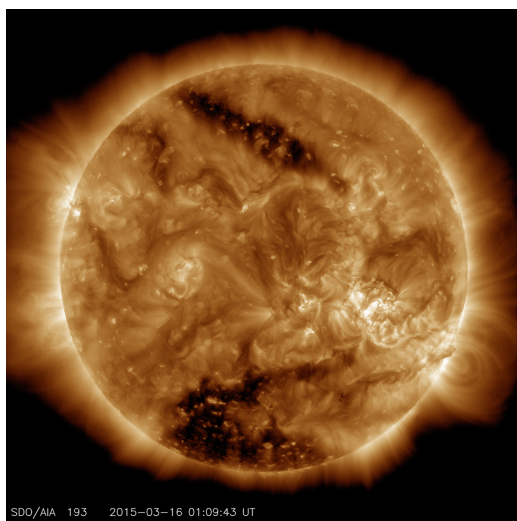


Figure 1.10: Solar X-ray image  
Credit: NASA/SDO

Another particulate contribution to interplanetary space are the coronal mass ejections. This phenomenon according to textbooks (de Pater & Lissauer, 2015) and (Carroll & Ostlie, 2014), might occur while prominence or filament erupts, or is associated with flares, probably triggered by magnetic reconnection, during which the energy is released accelerating particles. CME may occur a few times a day during the solar maximum and once in five days during the solar minimum (Carroll & Ostlie, 2014) releasing mass of  $10^{11} - 10^8$  kg per event (Aschwanden, 2005). CME, flares, other solar activity phenomena and the solar wind modelling is an interesting and yet not fully understood problem. It is intensively studied, mostly using magnetohydrodynamic (MHD) equations (see for example (Aschwanden, 2005) or any other work or textbook dealing with solar wind). The region where solar wind meets interstellar medium is called heliopause.

While the models are successful (for a simple solar wind model see Parker model in (De Pater & Lissauer, 2015); (Kirk et al., 1994); (Priest, 2000)), we can now get real time data from probe observations e.g. from ACE (Advanced Composition Explorer), placed near Earth in L1 Lagrange point (about Lagrange points see (Carroll & Ostrlie, 2014) or any other astrophysical textbook). On the Mars orbit is MAVEN (Mars Atmosphere and Volatile Evolution mission) measuring solar wind characteristic with instrument SWIA (Solar Wind Ion Analyzer) and there are measurements from New Horizons SWAP (Solar Wind Around Pluto) or of course from Voyager,

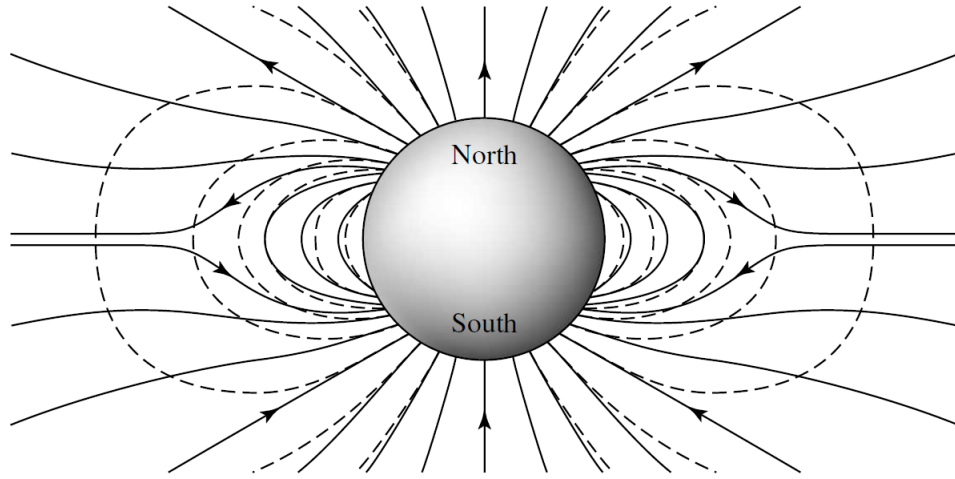


Figure 1.11: The simple visualisation of solar magnetic field. Dashed line depict idealized dipole field, the full line idealized solar magnetic field. From (Carroll & Ostlie, 2014).

Ulysses and others mission.

Parameters of solar wind for Earth and Pluto are in following table:

	Earth	Pluto
$n_p$	$6.6 \text{ cm}^{-3}$	$0.025 \text{ cm}^{-3}$
$n_e$	$7.1 \text{ cm}^{-3}$	
$T_p$	$1.2 \cdot 10^5 \text{ K}$	$7.7 \cdot 10^3 \text{ K}$
$T_e$	$1.4 \cdot 10^5 \text{ K}$	

$n_p$  is proton density,  $n_e$  electron density,  $T_p$ ,  $T_e$  proton and electron temperatures. SWAP data for Pluto was taken from (Bagenal, et al., 2016), averaged data for Earth taken from (Schwartz et al., 2004). Note that for electron temperature there is a larger interval of values, see (Newbury et al., 1998). For further comments of measured data from SWAP see besides the mentioned work e.g. (Bagenal, et al., 2015) or (Elliott, 2016). Solar wind properties around Earth are explored better. Values in the table are averaged, to see table for fast and slow wind separately, see e.g. (Gargaud, 2011).

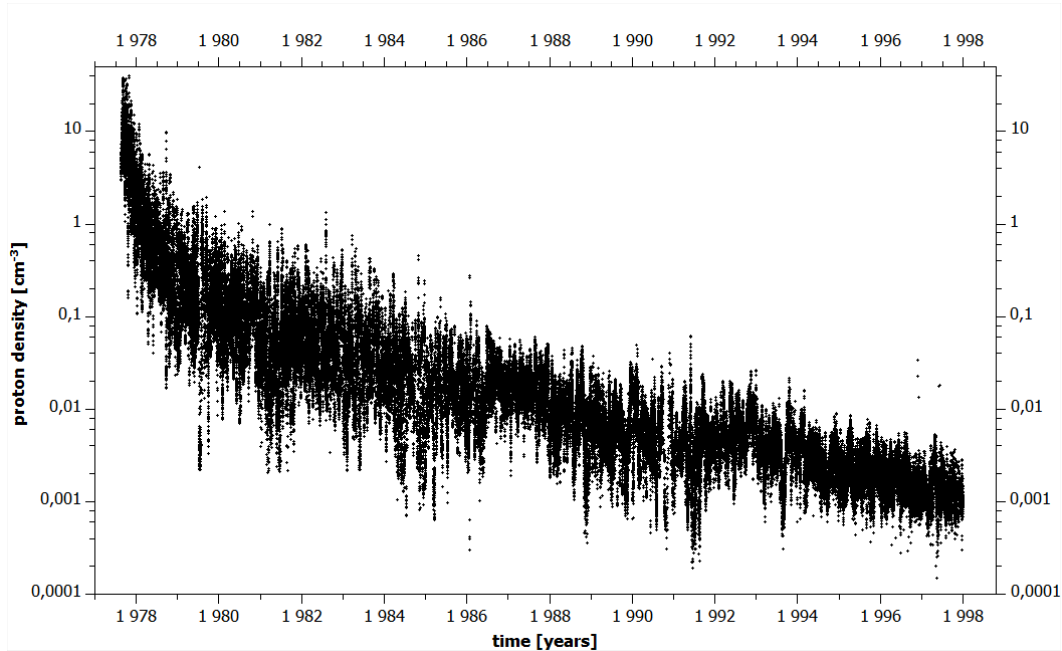


Figure 1.12: Proton density as measured by Voyager 2.

This time scale covers distance approximately up to 50 AU (for the time-distance dependence see e.g. (Richardson et al., 1995) or (Kim et al., 2016)). Data from <ftp://space.mit.edu/pub/plasma/vgr/v2/ha/key/>.

### 1.3.2.1 Shortly About Plasma

As was mentioned above the matter in the Sun (and stars) exists in form of plasma. Also the stellar atmosphere material is plasma. In fact vast majority of observed matter in our universe exists in form of plasma, from the stars through nebulae, interplanetary or interstellar medium, etc. Plasma is ionized gas, usually referred to as the fourth state of matter. To be labeled as plasma it has to meet certain criteria like the macroscopical neutrality and collective behavior (mediated by long range coulomb forces). (Bittencourt, 2004).

If the energy of particles is considered, plasma can be classified as hot, plasma found in space (astrophysical plasma), and cold plasma. Hot plasma is considered as plasma with temperature higher than  $1 \cdot 10^6$  K, i.e. material found in the stars is a hot plasma, on the other hand the laboratory produced plasma is a cold plasma (except e.g. nuclear fusion). In plasma physics the temperature is commonly given in eV,

electronvolt, the relation between temperature in eV and Kelvin is:  $1 \text{ eV} = 11\,600 \text{ K}$  (Chen, 1984). The degree of ionization can be considered, then the plasma is weakly, strongly or fully ionized. The plasma found in outer space is usually fully ionized but with low density. To see typical values of the electron number density and temperature, look at Figure 1.13.

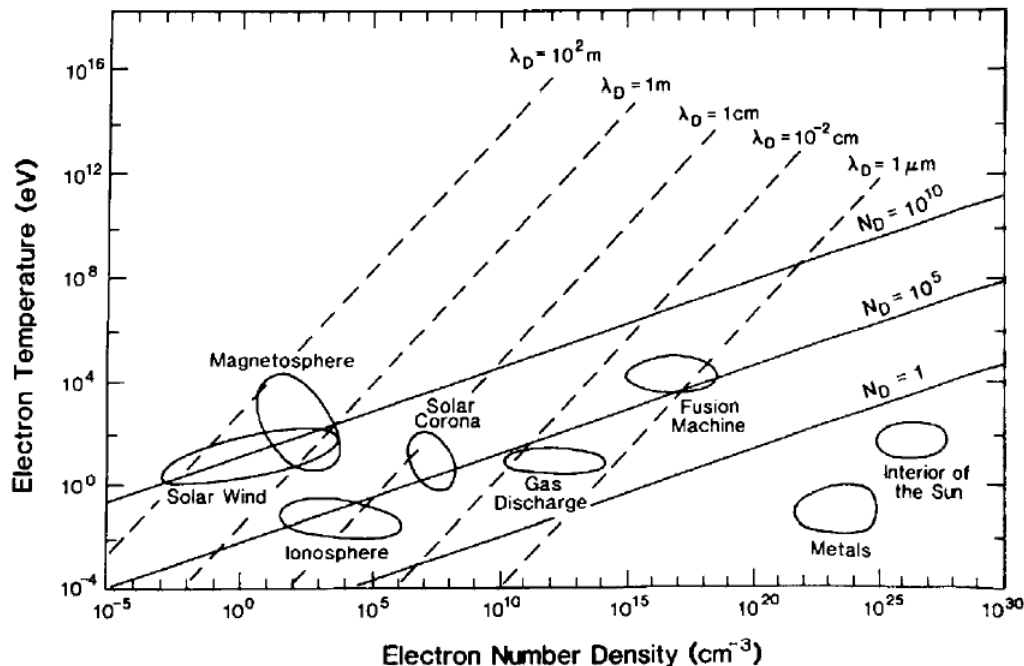


Figure 1.13: Plasmas overview.

Overview of different types of plasma and their wide range of electron densities and temperatures.  $\lambda_D$  is Debye length,  $N_D$  is number of electrons. Taken from (Schwartz et al., 2004).

Although plasma is macroscopically neutral ( $n_i = n_e$ ,  $n_i$  is ion density), this neutrality might be violated on small scale, this scale is called Debye length,  $\lambda_D$ , (and has to be much less than macroscopic scale of plasma). The disruption is restored again by the plasma electrons movement, their oscillations with certain eigen frequency - plasma frequency.

Plasma can be formed from a gas by different means e.g. by increasing the temperature or placing it to electric field. In this work the plasma is formed be-

tween two planar electrodes and excited by radio frequency (RF) generator, forming capacitively coupled plasma. Apparatus description is in section 3.1.

To ionize the gas between electrodes the free electrons are important, when electric field is applied these free electrons are accelerated and by collision with neutral particles they ionize the gas. Around electrodes, there are regions of plasma not in equilibrium, with dimension of  $\lambda_D$  called plasma sheaths. The electrons with higher energy arrive to the electrode first creating a negative layer. Above the negative layer there is a higher concentration of ions. (Lieberman & Lichtenberg, 1994).

Parameters of our plasma discharge are estimated in section 3.1.

# Chapter 2

## Selected Organism

For the purpose of our testing the cyanobacteria, prokaryotic phylum of the Domain Bacteria has been chosen. The word "cyanobacteria" consist of two parts: the first - cyano, hints to its greenish-blue color, the second part - bacteria, refers to the domain. They are gram-negative bacteria (i.e. if the Gram staining method of bacterial differentiation is used, they turn pink and not violet as gram-positive ones, this is caused by diverse cell wall structure).

The cyanobacteria are one of the oldest organisms on the Earth, probably evolved from some older photosynthetic bacteria. The oldest cyanobacteria found is at least 3.2 Ga old (Kalina & Vána, 2005); such old samples can be found in stromatolites, rocky structures made of layers of carbonate sediment and mainly cyanobacterial sediment. Nowadays the phylum covers unicellular species forming, or not forming, colonies, as well as the multicellular filaments. Filament is row of cells (or trichome) surrounded by slime sheath (Kehr & Dittmann, 2015). The phylum is worldwide spread with individual representatives able to live in the most extreme conditions including Antarctica or Atacama Desert. The representatives are often pioneer organisms able to live in mats cooperating with other organisms and can be found in symbiotic relationships for example with lichens (Paerl, 2000), while in hostile conditions, it might form akinetes, thick-walled dormant cells (Kalina & Vána, 2005). They reproduce asexually by cell division. Among public, the freshwater cyanobacteria are the best-known, for their ability to pollute ponds and other water surfaces in algal bloom, see the left of Figure 2.1. The terrestrial cyanobacteria are usually unnoticed, for their small dimensions, they might look inconspicuous, see the right of Figure 2.1.

The cyanobacteria perform oxygenic photosynthesis. And they also have some specific abilities, like forming heterocyst, a specialized cell containing nitrogenase



Figure 2.1: Cyanobacterial bloom on a lake and the terrestrial cyanobacterium *Nostoc commune* (dimensions approximately 5x3 cm) on the soil.

Left photograph from

(<http://ns.umich.edu/Releases/2013/Mar13/algae.html>)

enzyme for nitrogen fixation. Cyanobacteria living in water have a specialized vacuole permeable for gases dissolved in the water (gas vesicle/aerotop), which permits to change its depth in the water (Kalina & Váňa, 2005). A cyanobacterium exhibits chromatic adaptation, i.e. it can adapt itself for the best "gain of photons" by adjusting ratios of pigments in phycobilisomes (see section 2.2), so it can thrive under different light conditions like low light intensity, monochromatic light, etc (Tandeau de Marsac, 1977). Besides well known chlorophylls (mainly *a*, in small amounts also *b* or *d*), it contains other pigments as carotenoids, xanthophylls and it uses phycobiliproteins (phycocyanin, allophycocyanin, phycoerythrin). Absorption curves are in Figure 2.2.

The phylum is divided into several orders: *Nostocales*, the most numerous order of phylum, containing filamentous cyanobacteria with heterocytes, akinetes, *Chroococciopsidales*, order of primitive coccoid (unicellular, spherical) extremophilic cyanobacteria, *Spirulinales*, order of coiled trichomes cyanobacteria, *Pleurocapsales*, order of unicellular or filamentous cyanobacteria, reproducing by baeocytes (cell is fissioning binary but daughter cells are formed inside the mother cell, until the cell is "full" and ruptures), *Chroococcales*, order of coccoid cyanobacteria with specified thylakoid (see section 2.2) arrangement, *Oscillatoriales*, filamentous cyanobacteria without akinetes and heterocytes, *Synechococcales*, simple coccoid or filamentous cyanobacteria, *Gloeobacterales*, coccoid cyanobacteria lacking thylakoids (Komárek

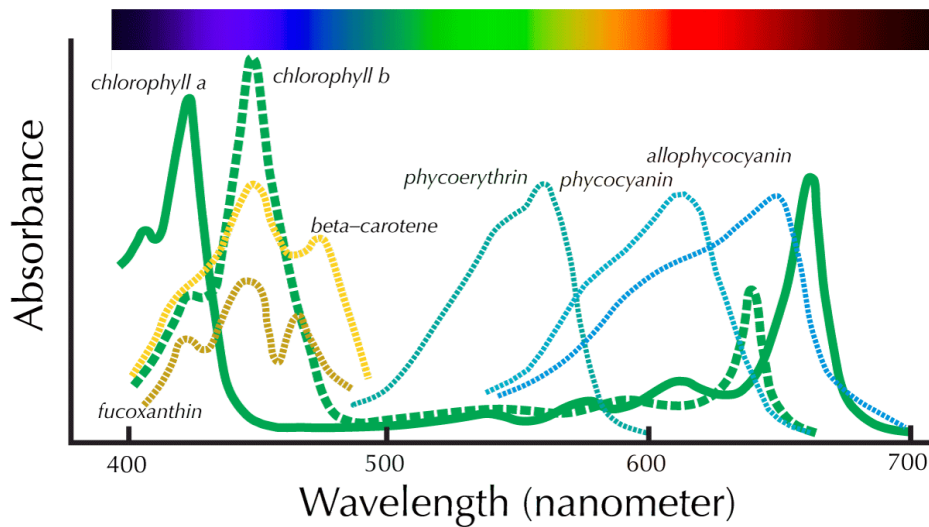


Figure 2.2: Absorption of pigments.

Spectral dependence of relative absorbance of different pigments. The ability of phyco-pigments to complement the chlorophyll absorption permits survival of cyanobacteria in various habitats including dark spaces (deep water, inside stones,...). (Taiz & Zeiger, 2002). From: ("Photosynthesis Lab Manual", 2014).

et al., 2014).

With plenty of remarkable abilities various cyanobacteria have been used for many experiments to test their ability to survive. For instance, *Chroococcidiopsis* for its ability to survive Martian conditions (Billi et al., 2008). *Anabaena* sp., *Synechocystis* sp. PCC 6803, *Synechococcus* sp. PCC 7942, and *Plectonema boryanum* sp. UTEX 485 were cultured in high CO<sub>2</sub> concentration air (Thomas et al., 2005). *Nostoc flagelliforme* was tested for its sensitivity to the UV radiation during desiccation or rehydration (Gao & Ye, 2007). The UVC radiation was successfully used for cleaning algal and cyanobacterial (*Anabaena variabilis* and *Lyngbya birgei*) cultures from bacteria to obtain axenic cultures (Mehta & Hawxby, 2017). *Nostoc* sp. HK-01 was proven to be able to survive at least three years in a vacuum in tests of (Kimura et al., 2014, 2016). In the work of (Arai et al., 2008) it is stated that cyanobacteria lumps, collected in nature consisting of cyanobacteria and some other microorganisms, survived one year in vacuum (10<sup>-5</sup> Pa), this suggest extreme endurance of cyanobacteria in a vacuum. In the same paper the growth of *Nostoc* sp. HK-01 on Mars Regolith Simulant in special container was successful. *Nostoc commune* and most of the cyanobacteria mentioned above are in (Verseux et al.,

2015) considered as usable for Mars life support. Also selected cyanobacteria were exposed to ionizing radiation and e.g. *Nostoc commune* sp. UTEX 584 survived radiation dose of  $8 \cdot 10^3$  Gy (Potts, 1999). These various experiments show great potential of the cyanobacteria and in particular the genus *Nostoc*. On the other hand if freshwater cyanobacteria *Microcystis aeruginosa*, forming algal bloom, are exposed to e.g. pulsed streamer-like discharge, it causes death to them (Sakugawa et al., 2014).

## 2.1 *Nostoc commune* and Its Viability

For our research one species of the genus *Nostoc*, the *Nostoc commune*, was chosen. This organism was collected in two different locations, one in Antarctica in February 2017, thanks to people in Masaryk University Antarctica station situated on James Ross Island (63.8067S, 57.8433W), the other one collected near Masaryk University Campus in Brno-Bohunice in November 2016, Czech Republic by author (49.1791N, 16.5680E).



Figure 2.3: The Czech Antarctic Station on James Ross Island and the path in Brno-Bohunice.

This terrestrial cyanobacterium, spread world wide, usually can be noticed after rain, when it absorbs considerable amount of water and turns from an unnoticeable small form to what looks like a jelly mass, which in the past was thought to have fallen from the sky, hence people named it the Star Jelly, Witch butter, etc. For the name "*Nostoc*" is probably responsible Paracelsus (Potts, 1997).

The typical habitat would probably be around routes, in the grass, on the soil. Like all cyanobacteria it is a relatively simple prokaryotic (does not have advanced organelles nor nucleus) photoautotrophic organism performing photosynthesis thanks to phycobilisomes containing phycobiliproteins and thylakoids containing chlorophyll. Like all cyanobacteria it reproduces asexually, forming hormogonia. It is a colonial species; a large number of fibers are enveloped by mucilaginous sheath i.e. by extracellular polymeric substance (Di Pippo et al., 2013; Pereyra & Ferrari, 2016; Kehr & Dittmann, 2015). The substance is mainly composed of polysaccharides along with some lipids (Pippo et al., 2013, Borowitzka et al., 2016), these polysaccharides are called extracellular polysaccharides, EPS in short (but be careful as EPS in literature is also an abbreviation for exopolymeric substances). This forms a natural shield against harmful effects (Borowitzka et al., 2016). For *Nostoc commune* (as for nearly all members of *Nostoc* genus) the dominant sugar in EPS should be glucose, other sugars as galactose, ribose or uronic acids are found there, too (more in table on pages 568 to 571 in (Borowitzka et al., 2016)).

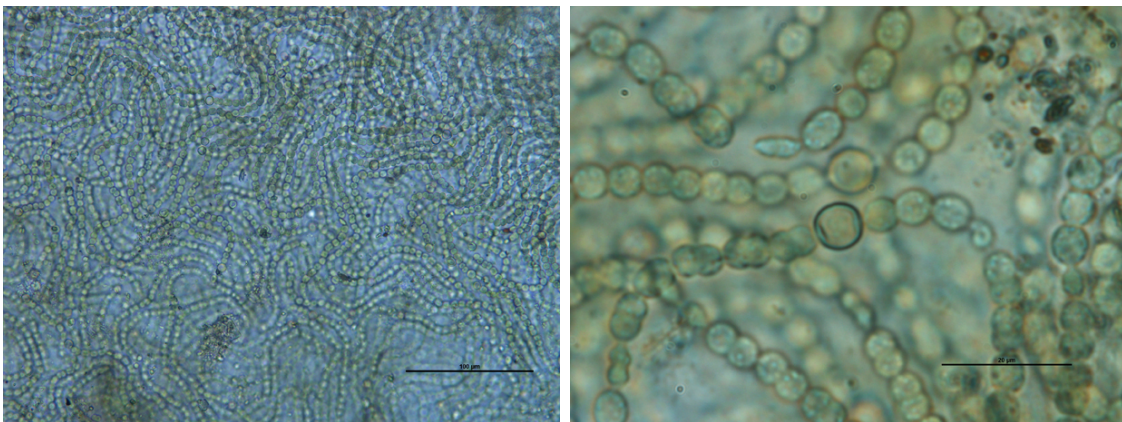


Figure 2.4: *Nostoc commune*.

Picture of Brno sample, taken by Nikon DS-Fi1 camera on Olympus BX50 microscope by UPlanFl 20x and UPlanFl 100x oil immersion objective. Scale bar on the left Figure represents 100  $\mu\text{m}$ , on the right Figure 20  $\mu\text{m}$ .

As stated in the previous section, *Nostoc commune* should have high tolerance to desiccation, a colony usually goes through the cycle of desiccation and rehydration (Tamaru et al., 2005). In that work it was studied, whether the EPS has any effect on the desiccation tolerance, comparing samples with and without EPS. It showed that samples with EPS survived better, so the role of EPS is not negligible. The

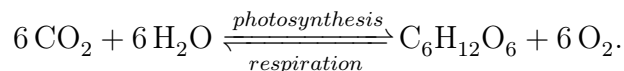
tolerance of *Nostoc commune* to the desiccation-rehydration cycle was further tested - in four cycles there were nearly identical levels of O<sub>2</sub> photosynthetic production soon after rewetting (around 10 minutes - but full photosynthetic recovery takes hours, nitrogen fixation recovery a days). The desiccated colony of *Nostoc commune* was heat-tolerant, survived temperature of 80°C for an hour, here again the samples with EPS survived much better.

Another remarkable property of this cyanobacterium is the tolerance to low temperatures. In work of (Sand-Jensen & Jespersen, 2012), both wet and dried colonies of *Nostoc commune* was exposed to temperature variation in range of -269 to 105 °C for 36 hours. Samples exposed to temperature range -269 to 70 °C after rewetting at room temperature showed only small changes in its metabolic functions. Wet samples were also exposed to pH and salt values variations at the stable room temperature. Samples were tolerant to values 3 to 10 and sometimes even to greater than 11. Tolerance to salt stress is modest, not surviving values of 30 g kg<sup>-1</sup> NaCl.

Also *in vivo*, cyanobacteria might contain photoprotective pigments, if it is exposed to UVA/UVB radiation, a larger synthesis of UV-protecting pigments (scytonemin, mycosporine amino acids, etc. (Ehling-Schulz et al., 1997, 2002; Garcia-Pichel & Castenholz, 1993)) occur.

## 2.2 Photosynthesis and Cyanobacterial Cell

Photosynthesis is a process of conversion water and CO<sub>2</sub>, to O<sub>2</sub> and sugars (glucose) with use of photon energy, while respiration is essentially opposite process (Vermaas, 2001):



This life essential process of oxygenic photosynthesis had begun about 3 billion years ago (some works suggest it even started sooner e.g. (Czaja et al., 2013)) thanks to cyanobacteria-like organisms (Shevela et al., 2013). The O<sub>2</sub> production later, about 2.45 billion years ago, caused Great Oxidation Event killing most organisms. In cyanobacteria these processes slightly differ from the algae and the higher plants.

For illustration of cyanobacterial cell structure see Figure 2.5. In a cyanobacterial cell the photosynthesis takes place in thylakoid membrane (exception is *Gloeobacter violaceus*, who lacks thylakoids; Rexorth et al., 2011). On this membrane there are the phycobylisomes, harvesting the light. Near them, tandem cooperating photosystem I and II (PSI and PSII) are integrated into the membrane. They perform

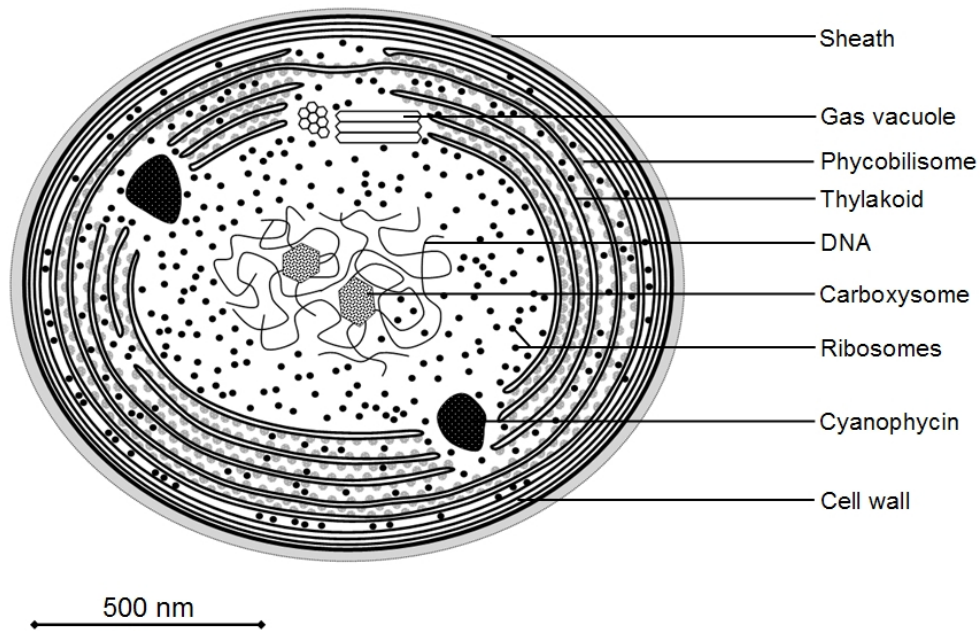


Figure 2.5: Cross-section through a cyanobacterial cell. See that thylakoid membrane exist in pairs, space between them is the lumen and around the pairs there is the cytoplasm. Modified from ([http://cronodon.com/images/cyanobacterium\\_structure\\_labeled.jpg](http://cronodon.com/images/cyanobacterium_structure_labeled.jpg)).

a conversion of light to chemical energy using in the reaction centre (RC) different chlorophyll *a*, P700 and P680. Phycobilisomes are usually connected to PSII, but can be also connected to PSI. The amount of PSI in the cyanobacteria is larger than PSII, PSI/PSII ratio vary from 3 to 5.8 (Shevela et al., 2013).

Photosynthetic reactions can be divided into two groups as light (dependent) reactions and light independent reactions, commonly named dark reactions. Light dependent reactions can start the cycle as a photon gets to phycoproteins, through them to PSII RC to the chlorophyll, Chl *a*. As result of this, Chl *a* loses its electron (in some cases it might also just re-emit the light by fluorescence or dissipate the energy to heat). An electron is transported by an electron transport chain (through other protein complexes like cytochrom, Cyt  $b_6f$ , and plastoquinone pool, PQ) to PSI, while causing transport of  $H^+$  (proton) from cytoplasm to lumen. Chl *a* without electron,  $P680^+$  has so high oxidizing potential (potential to make molecule lose an electron) that it is able to acquire an electron from water, producing  $O_2$  and  $H^+$ . PSII function is illustrated in the Figure 2.6.

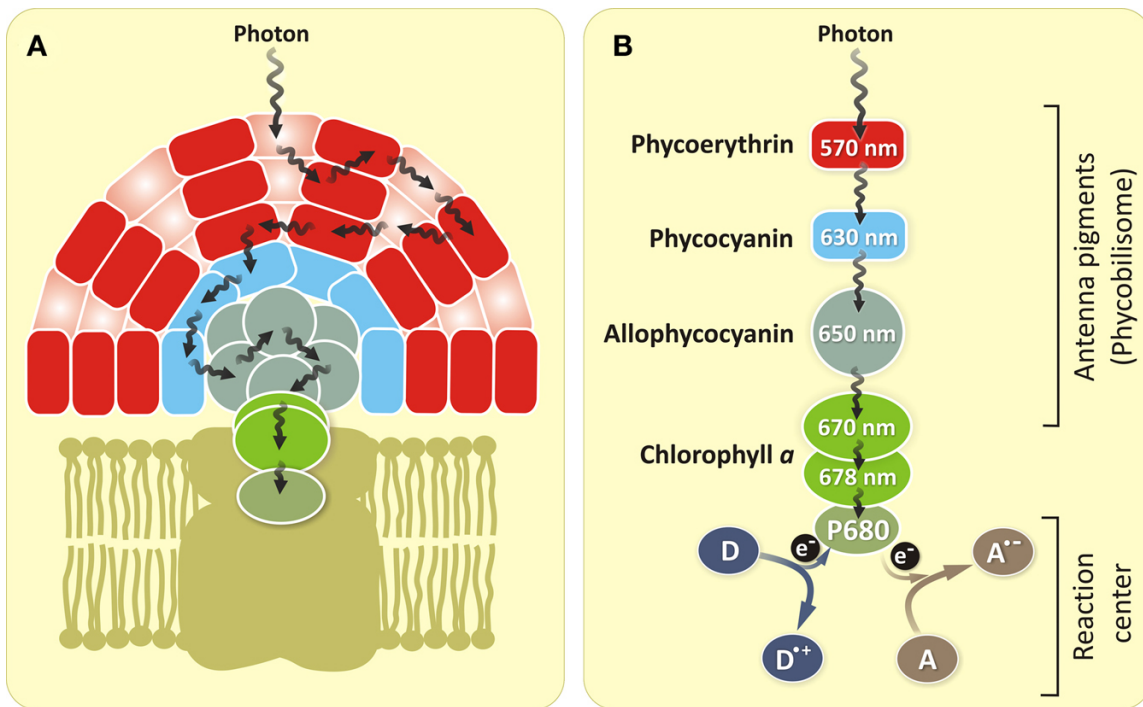


Figure 2.6: Structural organization of the antenna system of PSII for red algae and cyanobacteria (A) and energy transfer steps including charge separation (photochemical reaction) at the PSII RC (B) for cyanobacteria. The energy of absorbed photons is passed through a number of antenna molecules [phycoerythrin (absent in most cyanobacteria) - phycocyanin - allophycocyanin] until it reaches the RC Chl  $a$  (P680) [chlorophyll  $a$ , denoted as P for pigment and 680 for the wavelength of the maximum absorption]. The excited P680 donates its electron to an electron acceptor (A). The electron vacancy of the Chl  $a$  is filled by the electron from an electron donor (D) [ $H_2O$  molecule]. The wavelength inside the cartouches represent long wavelength absorption maxima of these pigments. Adapted from (Govindjee, 2011).

In PSI photon is expected to arrive, nearly in the same time as to PSII, and the result is again an electron loss of pigment. Its electron is passed to  $NADP^+$  and creates NADPH (nicotinamide adenine dinucleotide phosphate) molecule. chlorophyll gets a new electron from PSII. In the whole process a gradient of  $H^+$  is created and this runs the conversion of ADP (adenosine diphosphate) to ATP (adenosine triphosphate) by ATP synthase enzyme, a protein complex integrated in the mem-

brane. ATP is a chemical organism's use for energy storage; if energy is needed, ATP can be converted to ADP and energy is released in this process.

The results of this phase are therefore ATP, NADPH and  $O_2$ . The dark reactions fix  $CO_2$  in Calvin cycle (also known as Calvin-Benson-Bassham (CBB) cycle) with the contribution of ATP and NADPH, with use of RuBisCO (ribulose-1,5-bisphosphate carboxylase/oxygenase) enzyme, which produces sugars-glucose. For illustration of thylakoid membrane structure see Figure 2.7.

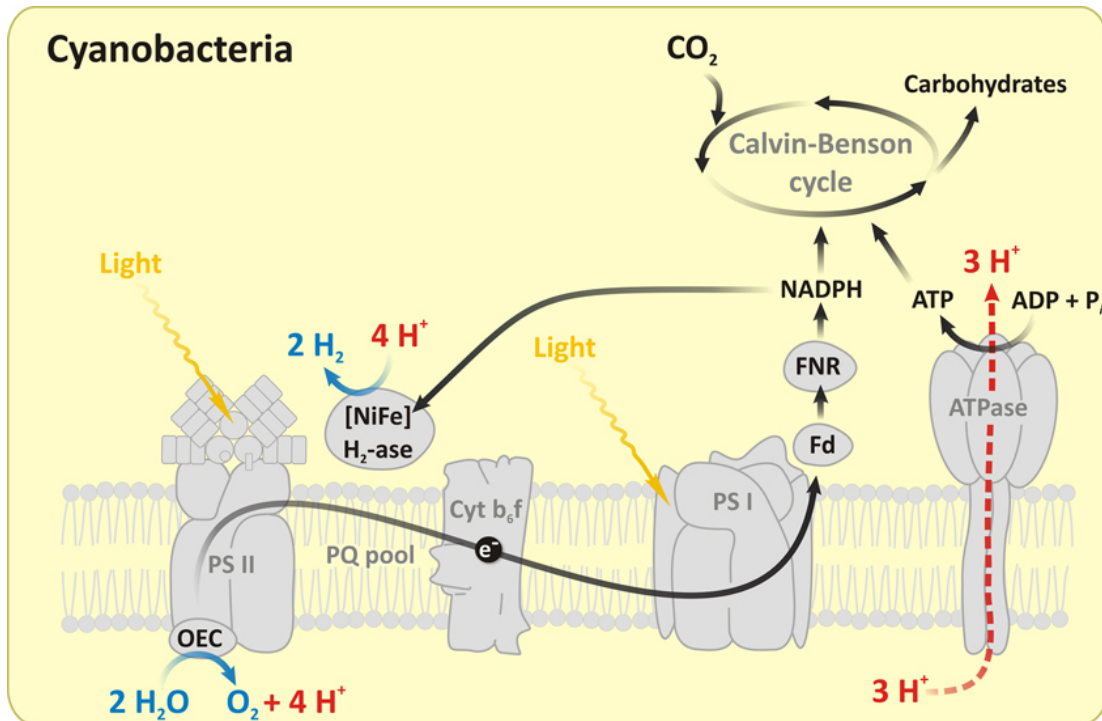


Figure 2.7: Structure of thylakoid membrane complex.

Parts important for photosynthesis and the relevant processes are indicated. Complexes not mentioned in text (e.g. Fd, ferredoxin; FNR, ferredoxin–NADP reductase and ATP synthase as ATPase).

Adapted from (Govindjee, 2011).

Cyanobacteria are able to perform photosynthesis and respiration simultaneously, sharing part of electron transport pathways (Vermaas, 2001). The best understood is the system of *Synechocystis* sp. PCC 6803 or PCC 7002. The first step of respiration is the process of glycolysis. A molecule of glucose is converted into a pyruvate. These

pyruvates, if oxygen is present, then turn to acetyl coenzyme A (AcCoA) and enter the Krebs cycle (in literature also named tricarboxylic acid, TCA, cycle or citric acid cycle). If oxygen is not present, fermentation starts. The cycle is different from the one occurring in higher plants as cyanobacteria lack one of the substances (2-oxoglutarate dehydrogenase) (Zhang & Bryant, 2011), so the cycle goes through different bypasses (Knoop, 2013). The cycle produces ATP and coenzymes, like NADH (nicotinamide adenine dinucleotide) and also carbon dioxide. NADH is then converted to  $\text{NAD}^+$ , causing proton gradient; this proton gradient is used by ATP synthase to make ATP, some of the protons reacts with oxygen to make water.

Both processes of photosynthesis and respiration are in fact very complex. More details can be found in (Shevela et al., 2013); (Nagarajan & Pakrasi, 2016) or (Borowitzka, 2016) and references there in.

## 2.3 Mechanisms of Stress Response

Although it is well known, that *Nostoc commune* can withstand many stress conditions, the mechanisms of the stress tolerance are not well understood yet and are subject of many researches. Concentrations of chemicals, proteins etc. before and after stress treatment is usually estimated to hint the processes of the stress response. The *Nostoc commune* is highly desiccation-tolerant, as was mentioned in section 2.1, i.e. water stress response mechanisms of this cyanobacteria are explored the most. Since this thesis deals with dessicated samples, it is good to have at least a clue about how it works.

During desiccation of *Nostoc* gene expression remains active for some time. In *Nostoc* sp. HK-01 gene expression was increased until it reached certain low values of water content, in dessication-sensitive cyanobacteria *Anabaena* sp. PCC 1720 was only transient (Yoshimura et al., 2006)). From both laboratory grown and field samples of *Nostoc commune* were isolated very stable proteins, so-called water stress proteins (Wsp). These Wsp are believed to have important role for cells, since they require "considerable metabolic investment". Wsp are accumulated in extra-cellular glycan along with UV-absorbing pigments, beside UV absorbing compounds also protects cell superoxide dismutase (SodF) from reactive oxygen species. Large amount of cyanophycin polypeptide is accumulated during dessication, disappearing soon after rehydration. Also stability of enzymes is interesting questions, it might be that enymes can remain active even in dead cells (in *E.coli*, dessication sensitive bacterium, enymes necessary for infection were active in dried dead cell (Webb, 1965)). And it is known phycobilisomes undrengo structural changes after short time of drying. Membranes are stabilized by trehalose and sucrose in so-called water re-

placement strategy (more in (Potts, 2001)). Cell is repairing damages during and after rehydration - (Potts 1999, 2001); (Potts & Scherer, 1989); (Billi & Potts 2002); (Shirkey et al., 2000).

There are still a lot of questions that need to be answered to fully understand the mechanisms of stress response (and combined stress response), whether it is about preventing cell damage, repairing it or for example if and how does the proteins differ in particular stress sensitive and tolerant organisms.

## 2.4 Damage Expected Due to Experiment

Aim of the thesis is to simulate the extraterrestrial conditions on desiccated, anhydrobiotic *Nostoc* samples in the apparatus described in the section 3.1. These conditions will be the low pressure and the hydrogen CCP as the solar wind-like environment.

As was mentioned in the subsections above, damage due to low pressure is not expected, but it has to be verified by our measurements.

During the plasma discharge the electrodes will be heated, so the damage due to high temperature might occur, as the samples are placed on one of the electrodes (the samples will be heated by plasma, but not as much as by the electrode). To avoid damage by high temperature during the experiments, the electrode water cooling system will be used. Therefore, only an influence of plasma will be tested. Lethal damage due to UV radiation produced by discharge is not expected. Damage due to ionised particles and free electrons, which is relatively little studied, is expected. Also the results are expected to differ for Antarctic and Brno *Nostoc commune*, since they were collected in very different places and exposed to different influences.

# Chapter 3

## Experimental Methodology

### 3.1 Experimental Apparatus

For the purpose of the experiment, we built a specialized apparatus. As a goal of this work is to simulate the solar wind, the set up was designed to fulfil several roles: maintain low pressure, contain hydrogen, excite hydrogen to ions and to produce UV radiation. The obvious choice was an electrical plasma device based on capacitively coupled plasma (CCP) operating at low pressure and excited using industrial RF frequency of 13.56 MHz. The gas pressure in the interplanetary environment is so low that it cannot be achieved in any lab on Earth. Moreover, to excite electric discharge, pressure higher by several orders of magnitude is needed. And since the cyanobacteria have extreme endurance to low pressure (see chapter 2), it is not expected that the samples will behave differently in high vacuum and in the pressure of our apparatus. Also ion and electron fluxes are so low, they cannot be simulated in the apparatus, but it can be assumed that plasma represents a certain cumulative dose. Electrodes are heated during discharge, therefore a simple water cooling system was made to cool down the electrode where the samples are placed to exclude the damage due to high temperature. The detailed description of apparatus in Figure 3.1, schema of apparatus in Figure 3.2.

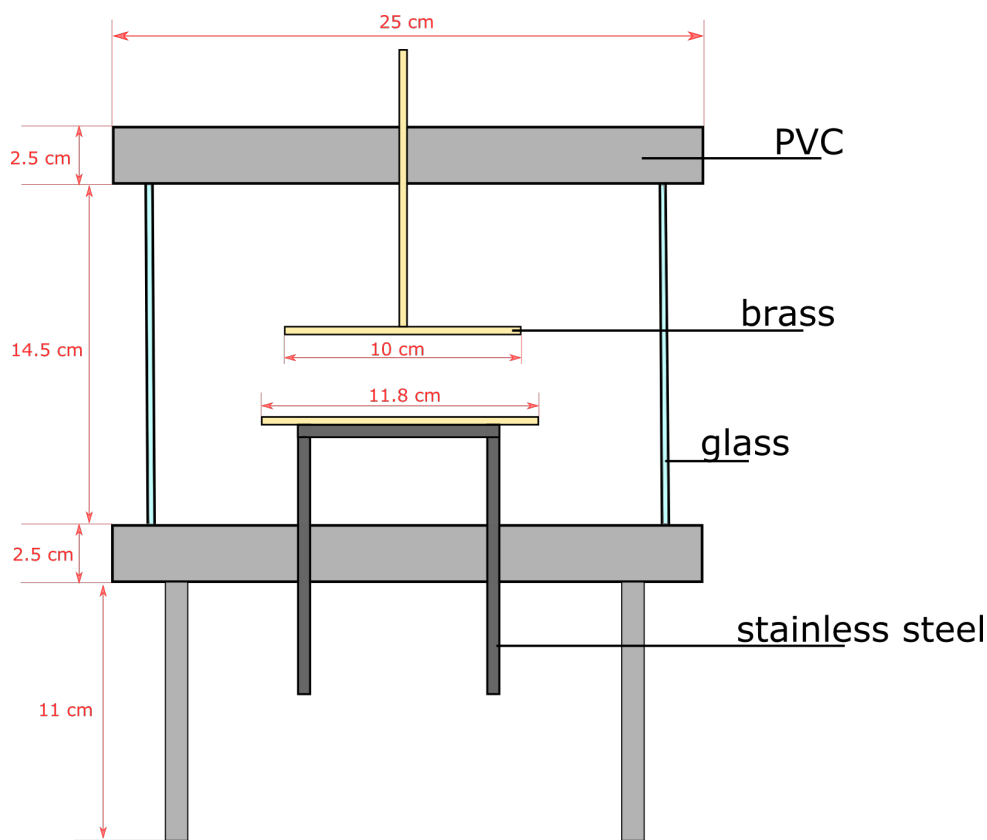


Figure 3.1: Detailed description of the apparatus.

Same materials are depicted with the same colour. The samples in Petri dishes were placed on the lower, rectangular electrode with dimensions 11.8x6.7 cm, upper electrode is circular, with diameter described in the Figure. The pipe made of stainless steel was soldered to the rectangular electrode for water cooling.

To be able to compare the properties of solar wind and our laboratory plasma, parameters of our plasma were estimated. For this estimation we used only simple measurements, like measure of currents and voltages during discharge. From these measurements, with help of dr. Pavel Dvořák, the plasma diagnostic was done. With use of dr. Dvořák's program (see (Dvořák, 2013)), electron density order was estimated as  $n_e \approx 10^{14} \text{ m}^{-3}$  and the electron temperature as (1-2) eV (this is a typical value for this type of plasma). From estimation of these values it is possible

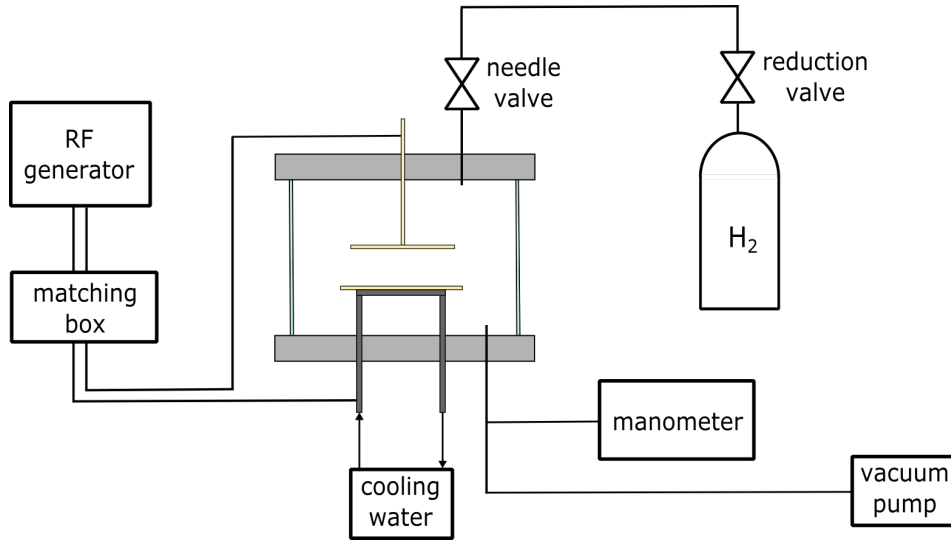


Figure 3.2: Schematic arrangement of our apparatus.

to calculate the ion current density

$$j = ne\sqrt{\frac{kT_e}{m_i}}, \quad (3.1)$$

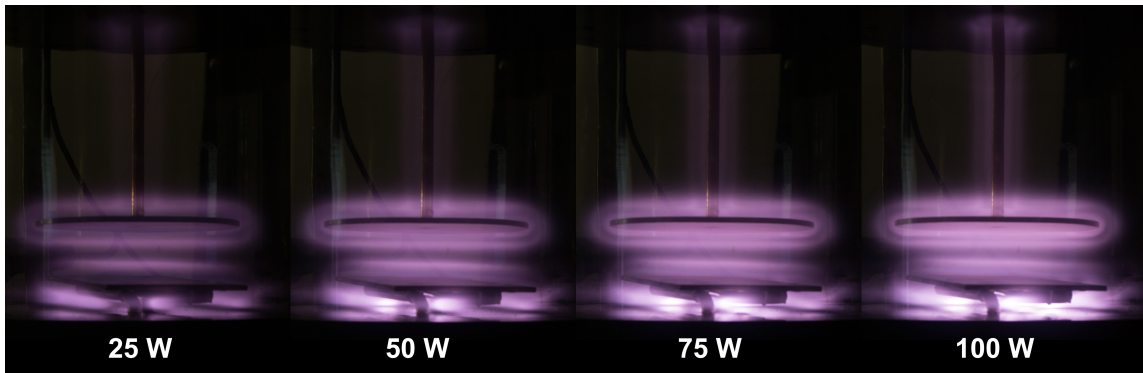
where  $e$  is elementary charge,  $k$  is Boltzmann constant and  $m_i$  is ion mass. The ion current density is in order of magnitude  $j \approx 10^{-1} \text{ A m}^{-2}$ . Mean energy of ions impinging the sample,  $\overline{E_{ion}}$ , was estimated as  $\approx 40 \text{ eV}$ . The particle density of our CCP is higher than in the outer space. The electron and proton temperatures are roughly in the same order of magnitude as in an interplanetary environment around Earth's orbit.

## 3.2 Measuring Equipment

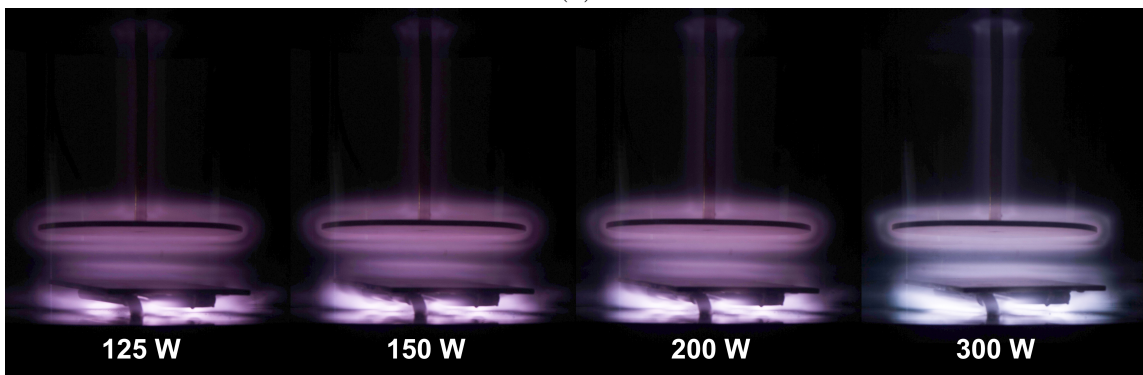
### 3.2.1 Fluorometer

Fluorometer OS1-FL was used to establish a state of samples, thanks to dr. Peter Vaczi from the Department of Experimental Biology, Masaryk University.

The fluorometer device was used to measure photosynthetic activity of samples, to determine the activity or inactivity of a sample and to compare the state of the sample before and after the experiment. Term "active" means that the sample lives,



(a)



(b)

Figure 3.3: Plasma around the electrodes at different power levels of RF generator. Taken by Nikon D5200, 18-55 mm f/3.5-3.6 objective. a) exposure time 1/30 s, f/10 aperture, ISO 1000 b) exposure time 1/60s, f/100 aperture, ISO 100, EV3.

"inactive" that sample died. The device works on the principle of induced chlorophyll fluorescence in PSII. Sample, adapted to dark, is illuminated by pulses of light and the chlorophyll response is measured. The chlorophyll fluorescence is not static and time evolution of sample response can be observed.

For the measurements the Fluorometer OS1-FL was used. It measures the sample minimal fluorescence intensity  $F_0$ , in dark adapted sample this is a state, when all PS are opened (and most of the incoming energy is used for photochemistry processes and not to fluoresce) and the maximal fluorescence intensity  $F_M$ , when all PS are closed by pulses of saturation light and the most of energy is used in fluorescence. From these values the fluorometer can estimate the maximal variable fluorescence

$F_V$  as  $F_V = F_M - F_0$  and the parameter  $F_V/F_M$ . This last parameter is important in studies as stress indicator.  $F_V/F_M$  represents the maximum efficiency of PSII (opened) centres. The more stressed samples is, the less PSII centres are available.

At first, ap 100 Fluorometer AquaPen was used for the measurements, the samples were measured mainly by OJIP protocol. The OJIP protocol is for chlorophyll fluorescence induction kinetic analysis (i.e. for the analysis of processes occurring after a light gets to a PSII light-harvesting antenna). Result of measurement is a curve of intensity dependent on time, see Figure 3.4. The curve has four characteristic parts O, J, I and P. O stands for origin, when dark-adapted sample (all PS are open) is illuminated by measuring light and  $F_0$  is estimated. J and I correspond to electron transport phase from PSII to PSI and P is a peak of function in maximal irradiation intensity,  $F_M$ . Also  $F_V$  and  $F_V/F_M$  can be estimated from these values. Transition from  $F_0$  to  $F_M$  is called fast phase (duration up to 1 s). The samples were

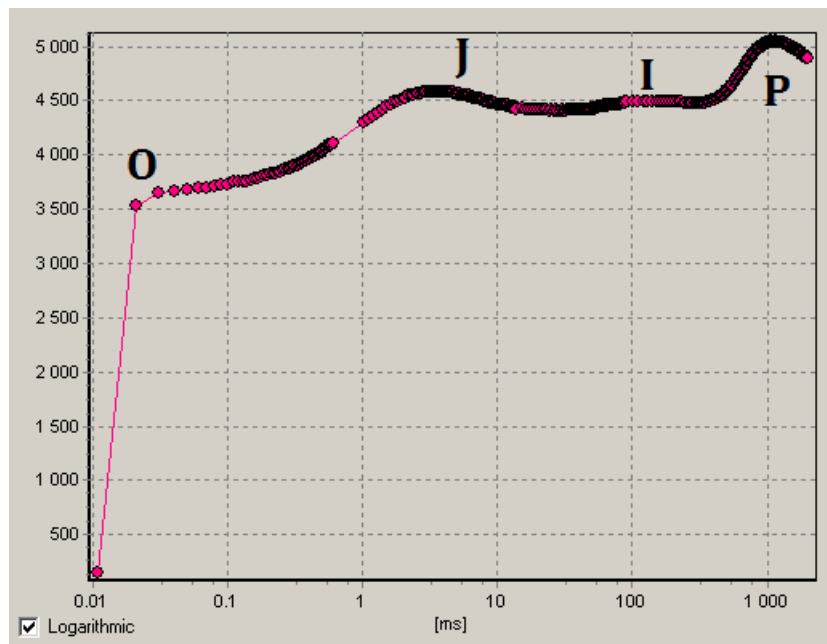


Figure 3.4: OJIP curve of *Nostoc commune*.

Illustrative OJIP curve of one of our Brno samples as measured by AquaPen, x axis shows time in a milliseconds in logarithmic scale, y axis shows intensity in a.u.

measured by AquaPen in several ways, because they showed suspiciously low and divergent values of  $F_V/F_M$  (just rarely exceeding 0.2). Therefore, groups of samples were measured one by one for 1-3 days by OJIP protocol in room temperature, dark

adapted 10 minutes before measurement. They were also measured by OJIP at room temperature in dark for 3 days, then at stable temperature (20°C) under LED light for a day, then 5 days in dark at the same temperature. The last test showed little improvement, but the values were still too low (around 0.3). It was probably due to AquaPen's use of blue light (which is the best light for green algae samples). The Fluorometer OS1-FL using the red light pulses, better for cyanobacteria, was tested and the difference was substantial and therefore was used for further measurements.

Based on the device manual and (Maxwell & Johnson, 2000).

### 3.2.2 Atomic Force Microscope

Equipment used to determine mechanical properties of samples at nano-scale was the Atomic Force Microscope (AFM), JPK NanoWizard 3, thanks to dr. Jan Přebyl, from CEITEC (Central European Institute of Technology).

AFM uses a probe to determine the topography and physical properties of the samples. The probe is a cantilever with a tip, in this case a V-shape cantilever with a four-sided pyramidal tip. The cantilever can scan the sample surface in contact, tapping or non-contact mode. In contact mode the cantilever is dragged across sample surface. In tapping mode the cantilever oscillates and at certain frequency touches the sample, from the changes in the frequency the surface properties are determined. In non-contact mode cantilever oscillates above the sample and from the changes in its frequency (caused by van der Waals interaction with sample) the surface is mapped. Using laser beam reflected from the cantilever, the device is able to measure deflection of cantilever with high precision. Also piezoelectric scanner is able to move and measure the position of the tip above sample with atomic precision.

For this work, quantitative imaging and force mapping was used. The force between the tip and sample depends on the distance between them. Force mapping mode measures these force curves and by fitting the curves by model it estimates the elastic modulus,  $E$ , (Young's modulus). Force curves are measured for each point, like it is illustrated in Figure 3.5.

The quantitative imaging is a compromise between force mapping and tapping mode, as it taps the sample it is quicker than force mapping and gives a certain information about sample's stiffness (it is proportional to slope of the force curve), adhesion forces and about the height of the set point.

The original idea was to measure the samples before and after exposure to simulated extraterrestrial conditions. But the measurements revealed large variance in elastic modulus values even before any treatment. Because of these large differences in  $E$ , even on small spatial scale, it was decided to make scan of only a few specially

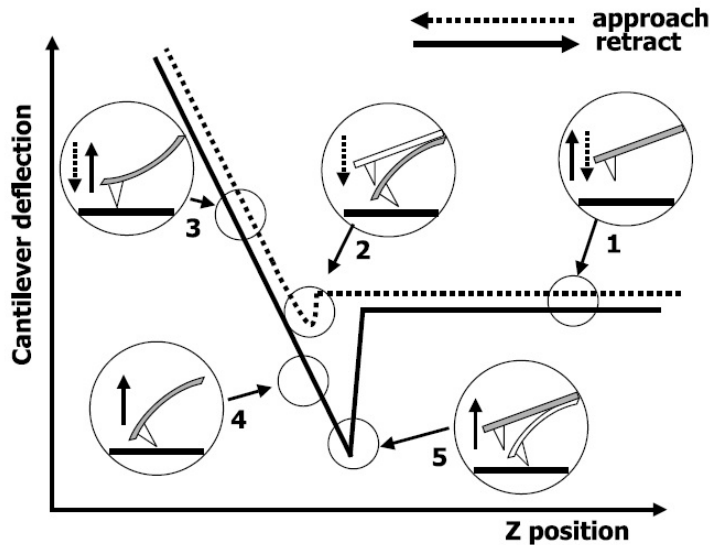


Figure 3.5: Force-distance curve formation.

In step 1 cantilever is approaching the sample, in step 2 the tip jumps to contact with sample, in step 3 the cantilever deflects more due to increasing force to the certain set point and then the motion is reversed. Due to adhesion the tip stays in contact longer than in approach part, step 4. In step 5 cantilever detaches itself from sample and goes back to position 1. Taken from Jandt (2001).

selected parts of Brno and Antarctic samples, to show the *Nostoc commune* surface and its properties.

### 3.2.2.1 Sample attachment

For AFM measurement, it is crucial to have a sample attached firmly and as horizontally as possible. Because the sample should not be moving and should be without large jumps in its horizontal profile that would cause cantilever detachment during the measurement. Also as the measurement takes quite a while, it is important that the sample does not desiccate during the process. For that reason, it was decided to make a measurement in liquid - in this case in distilled water. Several attachment types were tried.

When the attachment by low melting temperature agarose was tested, there was a problem of not creating sufficiently flat layer to hold a sample. Thus there was problem of finding a good measuring area. But more importantly if the distilled

water was added, samples started to float.

Another attachment test was performed using adhesive tapes. At first the measurements looked good, but after a short time most samples unstuck and started to float again.

Then tried epoxy glue was used, which has proven itself useful in some other biological sample measurements. This has proven as very good in both holding the sample in place and being sufficiently flat. But if sample was glued too soon (1-3 minutes after application of glue to Petri dish), it turned brown. So it was decided not to risk a degradation of samples due reaction with epoxy glue.

Finally a transparent nail polish was chosen to hold the samples, see Figure 3.6. This medium hold the samples quite well and was able to create a sufficiently flat layer. Also it did not visibly affected the samples, which were left attached on it overnight.

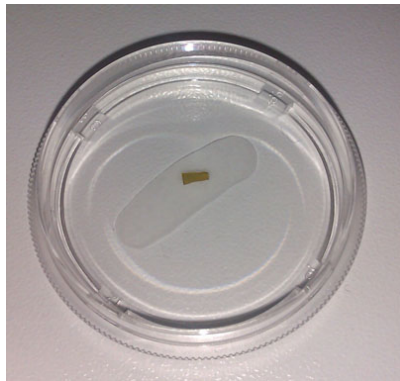


Figure 3.6: Sample prepared for AFM.  
Small piece of sample held by nail polish in Petri dish with 4 cm diameter.

### 3.3 Sample Preparation and Storage

When collected, both Antarctic and Brno samples were cleaned (by distilled water), dried on air (at ambient temperature) and stored in freezer ( $-18^{\circ}\text{C}$ ). The procedure for AFM measurement and for measurement in apparatus differs, samples was prepared separately and individually. For experiments in apparatus the samples were prepared according to following scheme:

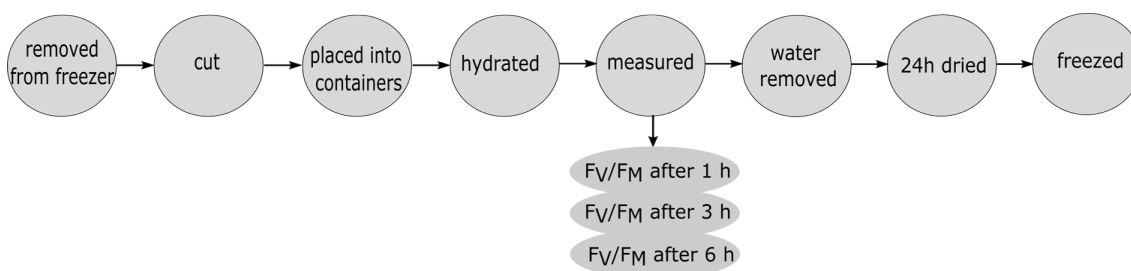


Figure 3.7: Scheme of sample preparation treatment.

For experiments the collected samples were taken out of freezer, cut to small pieces (approximately 1x1 cm) and placed into sample container (to see sample container look at Figure 3.8). Samples were hydrated by 1.5 ml of distilled water and their photosynthetic activity was measured by fluorometer after 1, 3 and 6 hours of hydration. Then the water was removed from containers by pipette and the samples were dried on air in laboratory at constant temperature of 17° C for approximately 24 hours. Wet and dry weight of samples was measured to be sure that time for desiccation is estimated correctly and the weight of sample is not changing any more, i.e. the samples are dry. Then the samples were placed into freezer again. The first set of samples was dried at the desiccator, this drying turned out to be not sufficient - after 24 hours of desiccation the samples were still very wet. The samples were measured by fluorometer and dried in laboratory at constant temperature of 17° C, the cutting of the mats was done at laboratory in constant temperature of 20° C.

### 3.3.1 Visual Characterisation of Samples

For the first experiments samples were put out and cut to pieces randomly, see Figure 3.8. This randomness was thought to cause large differences in the data, especially for the Antarctic samples. Antarctic samples were noticeably different from the Brno samples, they were more colourful (from light green to dark brown), the Brno samples were much less diverse (nearly all mats were dark green). To eliminate the large diversity due to unknown number of differently coloured samples it was decided to choose the samples with more care. The samples were put out from the freezer and the mats were examined carefully. Then the samples were cut to pieces and sorted by colour. To achieve at least some control over samples variability the samples were set in a certain scheme. To see the example of unsorted samples see Figure 3.8, to see example of sorted samples see 3.9.

For AFM measurement no special pre-treatment was necessary, but the obtained data were also very variable. We chose samples most similar to each other.



Figure 3.8: Randomly selected samples.  
On the left are the Brno samples, on the right the Antarctic samples. Sample container dimensions: 10x10 cm.

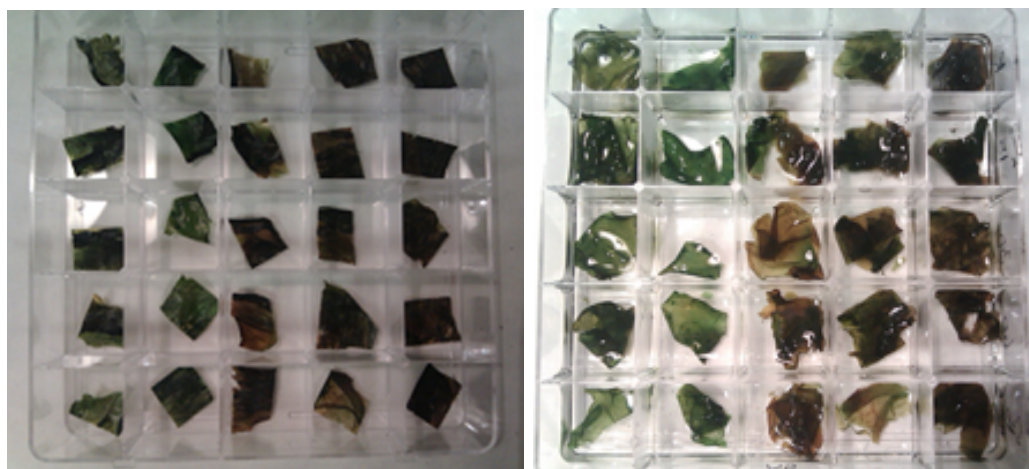


Figure 3.9: Sorted Antarctic samples.  
On the left dried samples, on the right wet samples. Sample container dimensions: 10x10 cm.

## 3.4 Measuring Protocols

### 3.4.1 Measuring with the Fluorometer

The photosynthetic activity measurement was always done as follows:

1. After 50, 170 and 350 minutes of hydration the sample container was placed into dark room, to adapt to dark and left there for 10 minutes.
2. In the dark room, one sample was put out from the sample container with tweezers and placed on the Petri dish with wet cotton.
3. Sample in the Petri dish was placed under the fluorometer and measured. Values were written down.
4. Sample was placed back to the sample container with tweezers.
5. Next sample from the container was picked.

### 3.4.2 Experiments in Apparatus

Each experiment was done on 5 representative samples from Brno and 5 from Antarctica at once. Also for every experiment series there were 5 control (i.e. not affected) samples. Measurements were done according to this scheme:

1. Sample containers were taken out of the freezer and transported in cold box (maintaining the freezer-like temperature) to the apparatus.
2. Sample containers were taken out of the box, put beside the apparatus and left there for 1.5 hour to acclimate to room temperature.
3. The apparatus was cleaned by 96% ethanol.
4. Samples were placed into two autoclave-sterilized Petri dishes, one for Brno samples, the other one for Antarctic samples. Position of the sample on the Petri dish was marked.

From this point the scheme differs for each type of test.

#### **3.4.2.1 Low pressure**

5. Apparatus with the Petri dishes inside was closed, depressurization by a vacuum pump begun and:
  - (a) continued until the desired pressure level was reached and pump turned off,
  - (b) was left to reach the lowest pressure the apparatus capable of.
6. Samples were left in the apparatus for a certain amount of time, depending on the experimental settings.
7. Pressure was increased by slowly opening the needle valve (if the needle valve is opened too quickly samples may get blown off from the Petri dish) and the apparatus opened.
8. Samples were removed from the container and placed into the cold box.
9. Samples were placed into freezer.

#### **3.4.2.2 Plasma**

5. The apparatus was closed, needle valve was closed.
6. Pump valve was opened and the vacuum pump turned on.
7. Water cooling was turned on.
8. To prevent RF damage of the manometer, it was turned off and plugged out.
9. The RF generator was turned on and the power set.
10. Samples were left in plasma for a predetermined amount of time, depending on the experimental settings.
11. RF generator was turned off.
12. Manometer was plugged in and the pressure was checked.
13. Needle valve and pump valve were closed, vacuum pump was turned off.
14. Supply of hydrogen was closed and plugged out of the apparatus.
15. Pressure was slowly increased by needle valve and the apparatus was opened.

16. Temperature of electrode was measured.
17. Samples were removed from the apparatus.

Tested samples were left in room temperature, until all samples from the sample container were tested and transported in the cold box to the freezer.

The samples waited in the freezer for the final photosynthetic activity measurement. This measurement was done according to the scheme in this way:

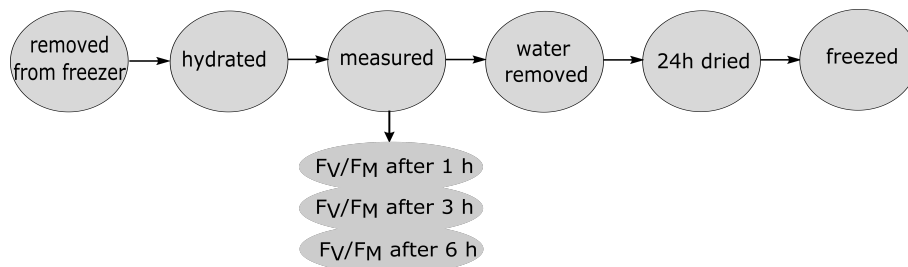


Figure 3.10: Scheme of the final sample treatment.

### 3.4.3 AFM

In AFM the samples were tested one by one at constant room temperature ( $\approx 20^{\circ}\text{C}$ ). Samples for AFM scanning were prepared in the following way:

1. Sample was removed from the freezer, left to acclimate in room temperature.
2. Sample was hydrated by distilled water. The sample was either hydrated before or after transportation (in the cold box) to the microscope. The duration of the hydration was at least half an hour before cutting.
3. Cutting of the sample. The hydrated sample was cut to 2 or 3 little pieces (approximately  $2 \times 4$  mm), to have a backup in the case that the sample would detach during testing.
4. Nail polish was applied to Petri dish and sample was carefully place into it. The medium dried for maximum of 10 minutes.
5. Petri dish was filled by distilled water, in the way that the whole sample is under the water.

Then the sample was either put into AFM immediately, or after a short period of time (no longer than 24 hours). This was due to limited access to the AFM, which meant the exact time, when the samples would be scanned, was determined on the day.

After that, samples were neither stored nor used in any other way.

# Chapter 4

## Results

### 4.1 AFM Surface Mapping

Force mapping mode and/or quantitative imaging mode were used for the surface mapping of our samples. Set point value for force mapping was 10 nN, for quantitative imaging 3 nN. Results for each mode are in separate subsections, but they are linked together. It was chosen randomly, which areas to map. Several different morphological types of surface were found. They were classified into 3 categories: "grainy", "smooth" and "unspecified" (if the surface couldn't be unambiguously assigned to neither of the former two). Examples are shown in the following subsections. Values of Young's modulus estimated by force mapping are in the tables below. In quantitative imaging mode the stiffness parameter was measured and its values are also in tables in corresponding subsections.

#### 4.1.1 Force mapping

##### 4.1.1.1 Antarctic Samples

Illustrative examples of the sample surface force map of various types of surface are shown below, as well as values of the Young's modulus ( $E$ ).

The "smooth" area scanned in Figure 4.1, was also imaged by quantitative imaging (see Figure 4.6). In this Figure, there is a map of Young's modulus and a map of the contact point height. The average value of the Young's modulus  $E = (20 \pm 5)$  MPa, average height of contact point is  $(69 \pm 38)$  nm.

The "grainy" area scanned in Figure 4.2, was also imaged by quantitative imaging (see Figure 4.7). The average value of the Young's modulus  $E = (497 \pm 147)$  MPa, average height of contact point is  $(630 \pm 70)$  nm.

In the third Figure, 4.3, there can be found an interesting group of oval shaped objects with diameter around  $1.5 \mu\text{m}$ . For this area  $E = (9 \pm 13) \text{ MPa}$ , the value of the estimated error is too large, because the mapped surface was too divergent. Results of quantitative imaging can be seen in Figure 4.8).

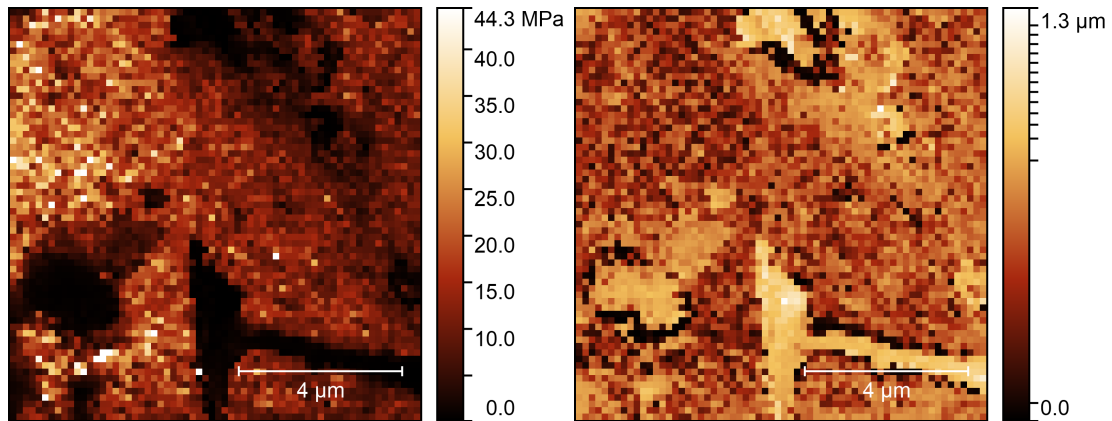


Figure 4.1: Results of force mapping for the "smooth" part of the Antarctic sample. In the left part of the figure Young's modulus map can be seen, while in the right part of the figure there is a map of the contact point height.

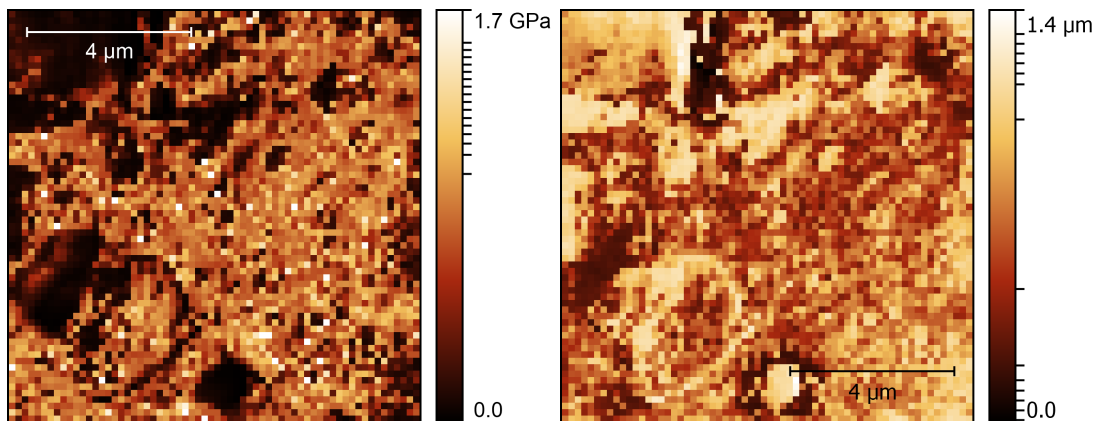


Figure 4.2: Results of force mapping for the "grainy" part of the Antarctic sample. In the left part of the figure Young's modulus map can be seen, while in the right part of the figure there is a map of the contact point height.

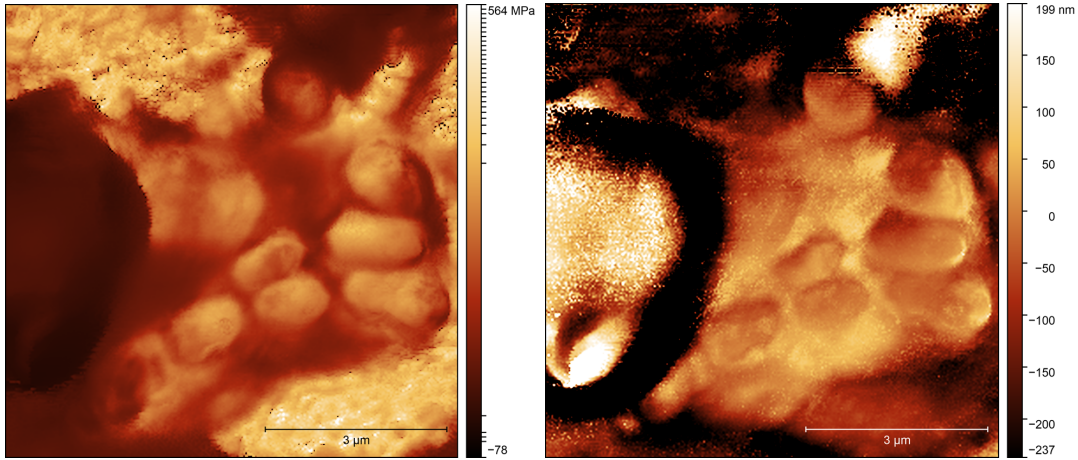


Figure 4.3: Results of force mapping for the "unspecified" part of the Antarctic sample.

In the left part of the figure Young's modulus map can be seen, while in the right part of the figure there is a map of the contact point height.

In following table 4.1, the measured values of  $E$  are listed alongside with measurement uncertainty. In many cases the uncertainty is higher than the averaged value, this is caused by large distribution of measured values. Since the uncertainties are large and there is just a small number of values, the averaged values for each morphology type are not provided.

Table 4.1: Table of Young's modulus of the Antarctic samples

E [MPa]	type
$49.7 \pm 64.8$	"grainy"
$8.0 \pm 11.0$	
$19.7 \pm 5.1$	"smooth"
$38.0 \pm 23.9$	
$219.2 \pm 94.9$	"unspecified"
$0.0004 \pm 0.0001$	

#### 4.1.1.2 Brno Samples

The "smooth" area of the sample from Brno is mapped in Figure 4.4, where  $E = (3.3 \pm 1.7)$  MPa and the average height of contact point is  $(153 \pm 40)$  nm. Results of quantitative imaging of this area can be seen in Figure 4.9.

The "grainy" area mapped in Figure 4.5 has  $E = (62 \pm 34)$  MPa and the average height of contact point is  $(14 \pm 11)$  nm. Results of quantitative imaging are shown in Figure 4.10.

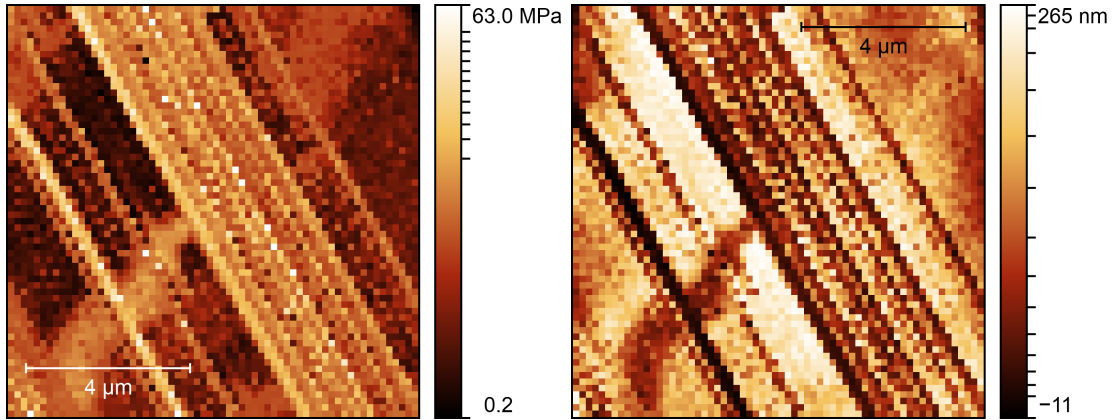


Figure 4.4: Results of force mapping for "smooth" part of Brno sample. In the left part of the figure Young's modulus map can be seen, while in the right part of the figure there is a map of the contact point height.

Table 4.2 shows the values of  $E$  for every scanned sample. Also, the category of the sample is displayed. Since there are more measurements for the Brno samples than for the Antarctic samples, the average value of modulus,  $\bar{E}$ , was computed for each type.

Table 4.2: Table of Young's modulus of the Brno samples

E [MPa]	type	$\bar{E}$ [MPa]
$11.4 \pm 1.6$	"grainy"	$33.4 \pm 19.1$
$62.5 \pm 34.2$		
$0.38 \pm 0.03$		
$4.7 \pm 3.6$		
$87.8 \pm 55.9$		
$5.8 \pm 4.2$	"smooth"	$2.4 \pm 1.5$
$0.019 \pm 0.004$		
$0.38 \pm 0.01$		
$3.3 \pm 1.7$		

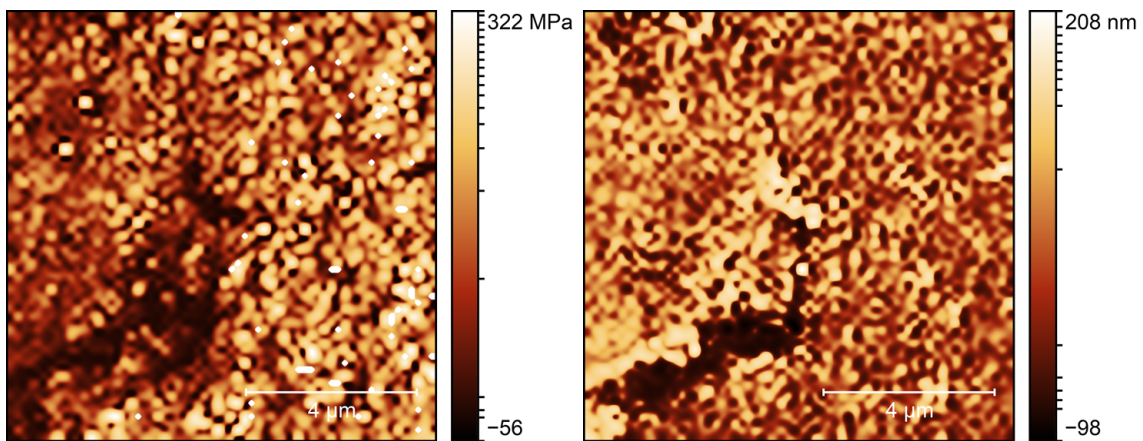


Figure 4.5: Results of force mapping for "grainy" part Brno sample. In the left part of the figure Young's modulus map can be seen, while in the right part of the figure there is a map of the contact point height.

## 4.1.2 Quantitative imaging

### 4.1.2.1 Antarctic Samples

Illustrative results of the quantitative imaging are shown in figures below. In every figure, there are three graphs. The first one shows the height of set point in  $\mu\text{m}$  or nm, the second one shows the adhesion force of every measured point and the last one shows the stiffness of the sample (it is proportional to the slope).

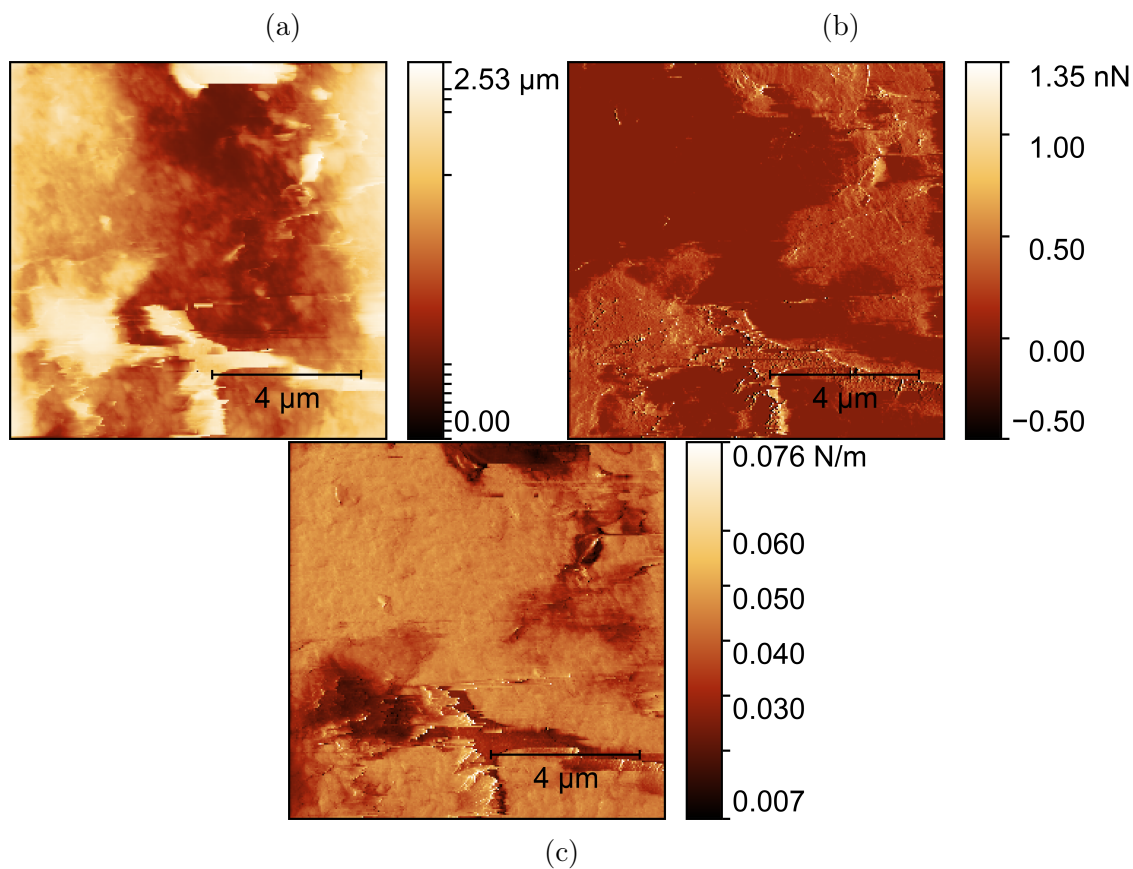


Figure 4.6: Results of quantitative imaging of the "smooth" part of the Antarctic sample.

(a) Set point height map. (b) Map of adhesion. (c) Slope map.

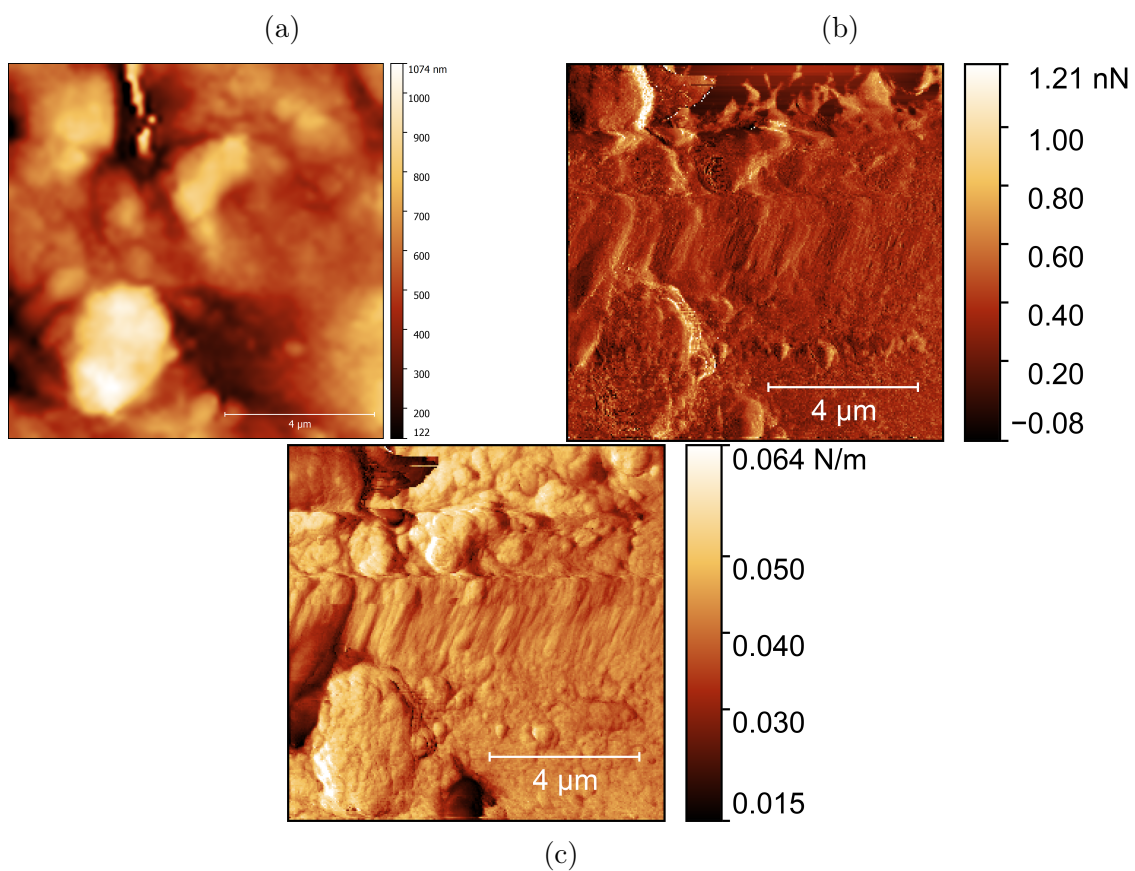


Figure 4.7: Results of quantitative imaging of the "grainy" part of the Antarctic sample.

(a) Set point height map. (b) Map of adhesion. (c) Slope map.

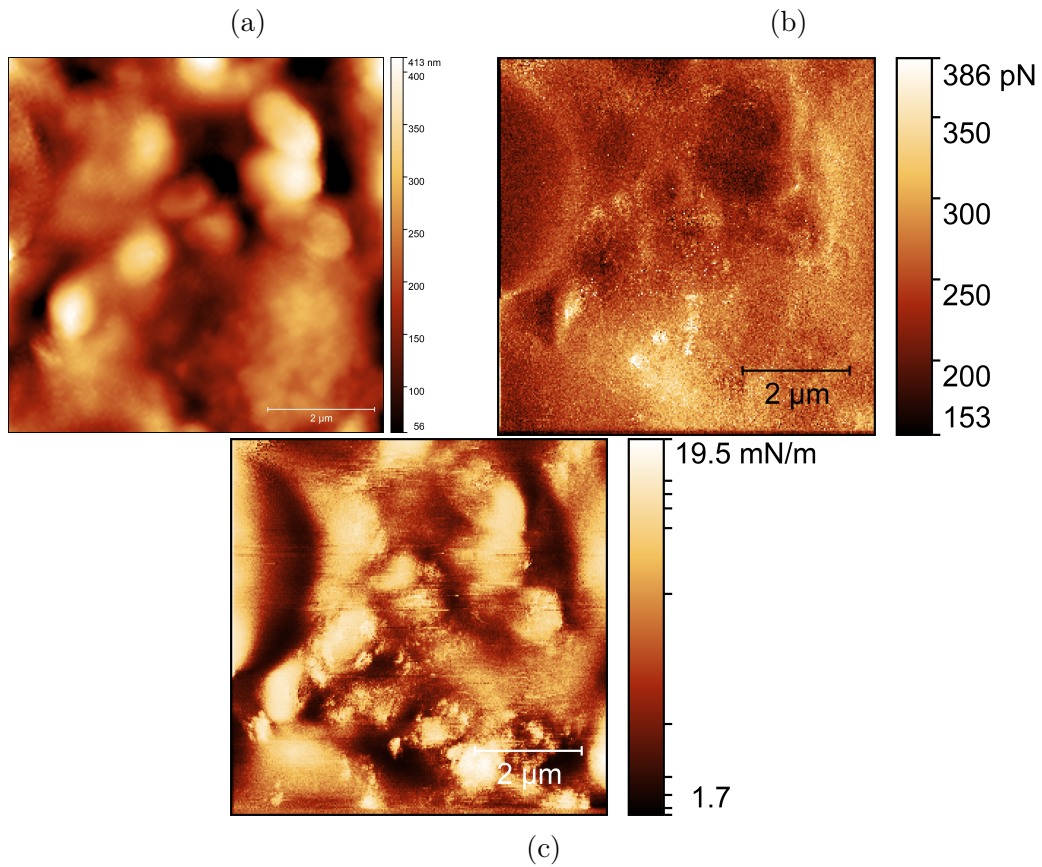


Figure 4.8: Results of quantitative imaging of the "unspecified" part of the Antarctic sample.

(a) Set point height map. (b) Map of adhesion. (c) Slope map.

Table 4.3: Stiffness of the Antarctic samples.

stiffness [mN/m]		
"smooth"	"grainy"	"unspecified"
$39.5 \pm 6.5$	$40.6 \pm 6.0$	$49.0 \pm 8.7$
$33.1 \pm 9.9$	$30.2 \pm 14.9$	$7.8 \pm 3.4$
$4.6 \pm 4.8$	$41.2 \pm 4.4$	$28.4 \pm 6.1$

### 4.1.2.2 Brno Samples

In the following part, results obtained by scanning in quantitative imaging mode can be found. In Figure 4.9 the "smooth" surface scan is shown. In Figure 4.10 is the "grain" surface scan is shown. The "grain" structure can be seen in more detail is in Figure 4.11.

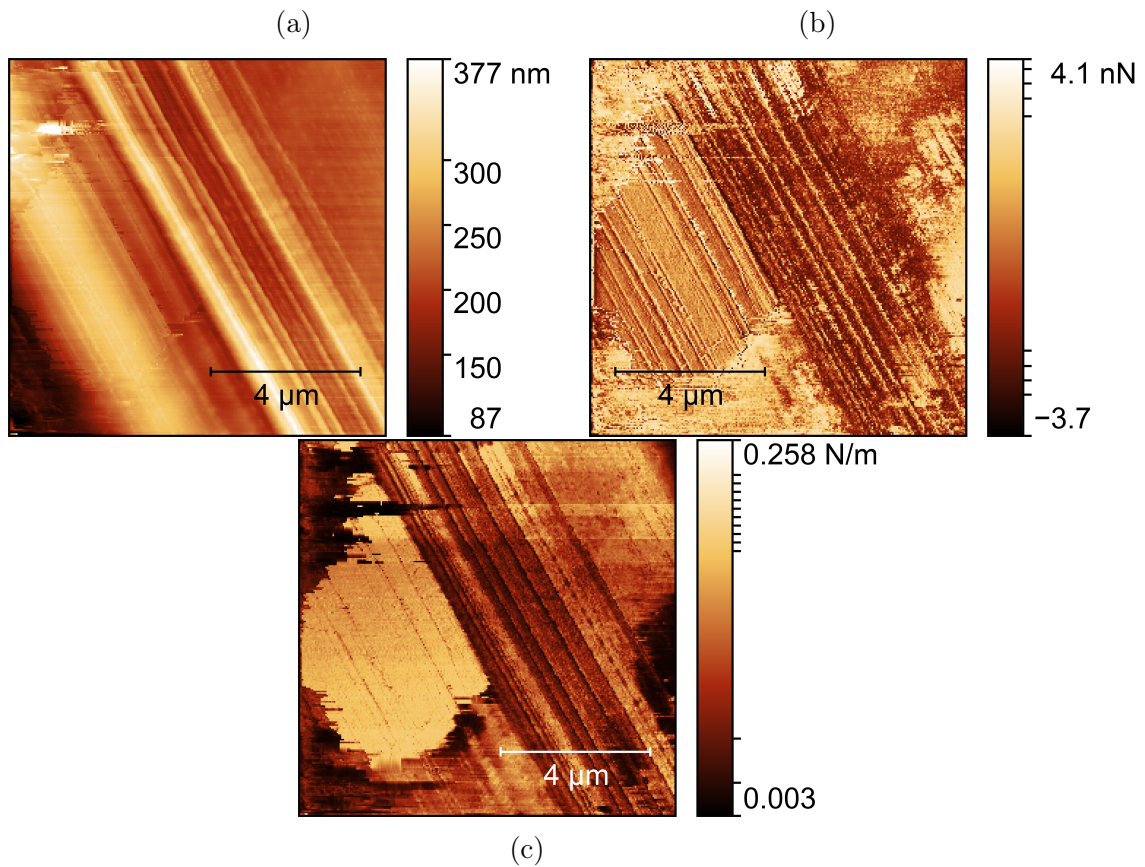


Figure 4.9: Results of quantitative imaging of the "smooth" part of the Brno sample. (a) Set point height map. (b) Map of adhesion. (c) Slope map.

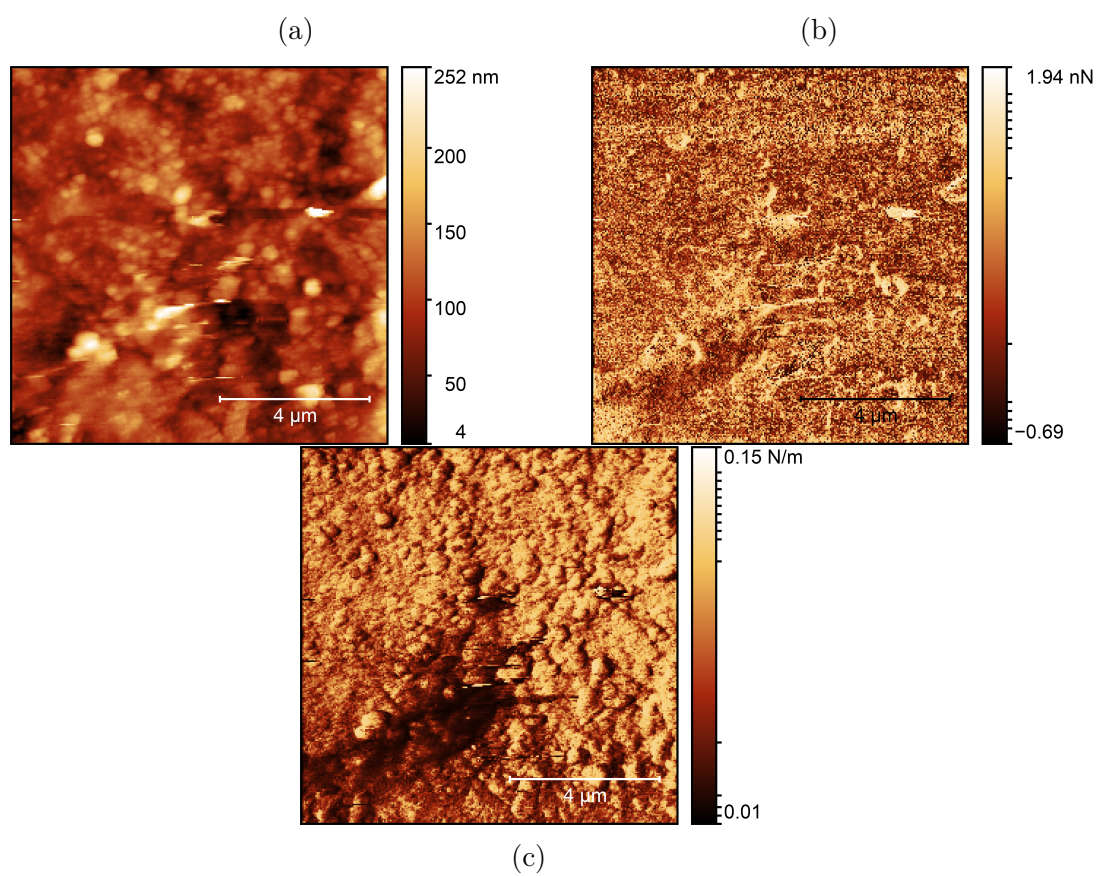


Figure 4.10: Results of quantitative imaging of the "grainy" part of the Brno sample. (a) Set point height map. (b) Map of adhesion. (c) Slope map.

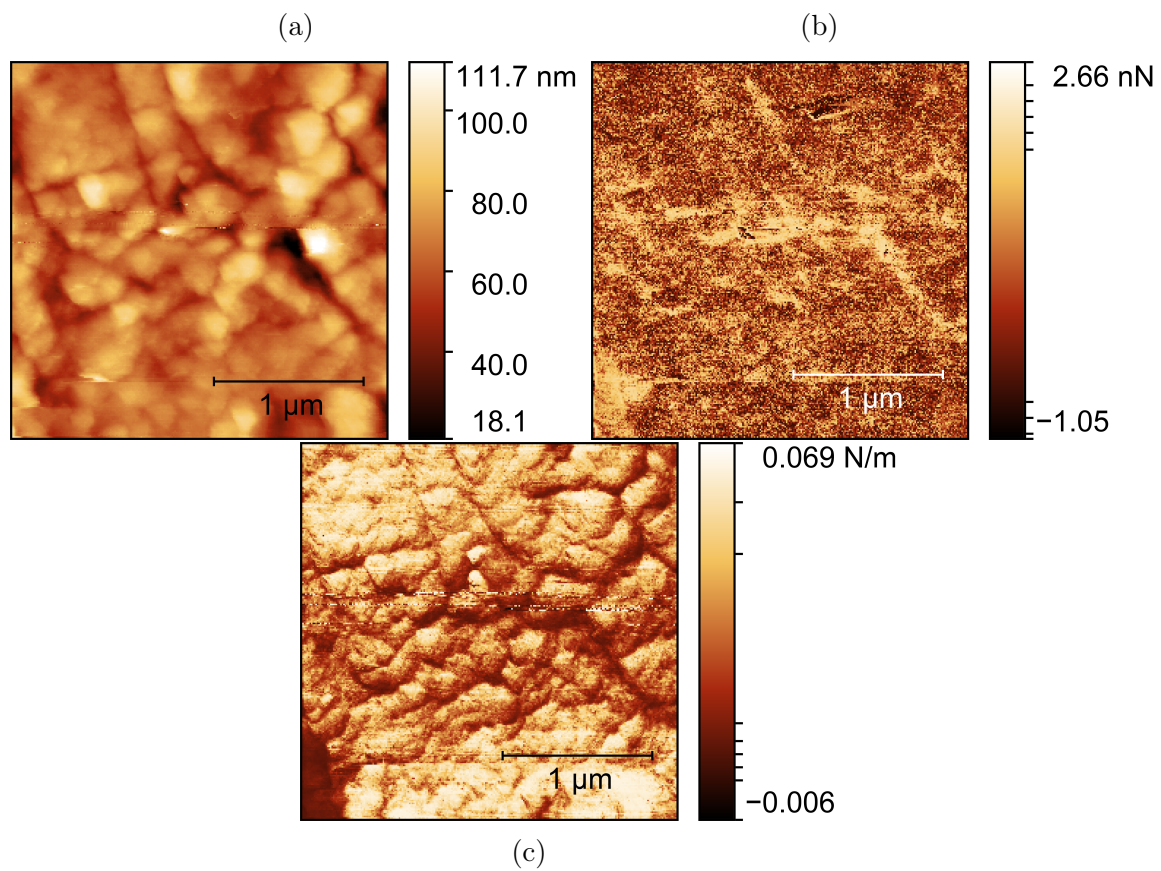


Figure 4.11: The "grainy" structure of the Brno sample displayed in detail. Detail of Figure 4.11. (a) Set point height map. (b) Map of adhesion. (c) Slope map.

Table 4.4: Stiffness values for the Brno samples

stiffness [mN/m]		
"smooth"	"grainy"	" unspecified"
$40.6 \pm 12.4$	$41.6 \pm 0.8$	$50.3 \pm 4.5$
$40.7 \pm 12.3$	$41.4 \pm 0.6$	$31.9 \pm 2.6$
$71.4 \pm 1.6$	$43.6 \pm 3.9$	$41.1 \pm 3.6$
$62.5 \pm 4.0$	$58.1 \pm 0.7$	
$43.8 \pm 3.0$	$58.1 \pm 0.9$	
$54.1 \pm 17.5$	$43.8 \pm 3.3$	
	$47.4 \pm 3.2$	
	$38.9 \pm 7.5$	

## 4.2 Low Pressure Tolerance

The results of the low pressure sample treatment are shown here, measured data are shown in a graphic form as an arithmetic mean with one standard deviation error bars.

### 4.2.1 20 Pa

Two groups of 5 samples (Antarctic and Brno), were left in the apparatus in the pressure of 20 Pa for 25 hours. Results for Antarctic are in Figure 4.12, for Brno in Figure 4.13. As can be seen in Figure 4.12, the difference between values of  $F_V/F_M$  ratio of the control samples and the samples placed in the apparatus is minor. Figure 4.13 shows larger difference, but the error bars still match.

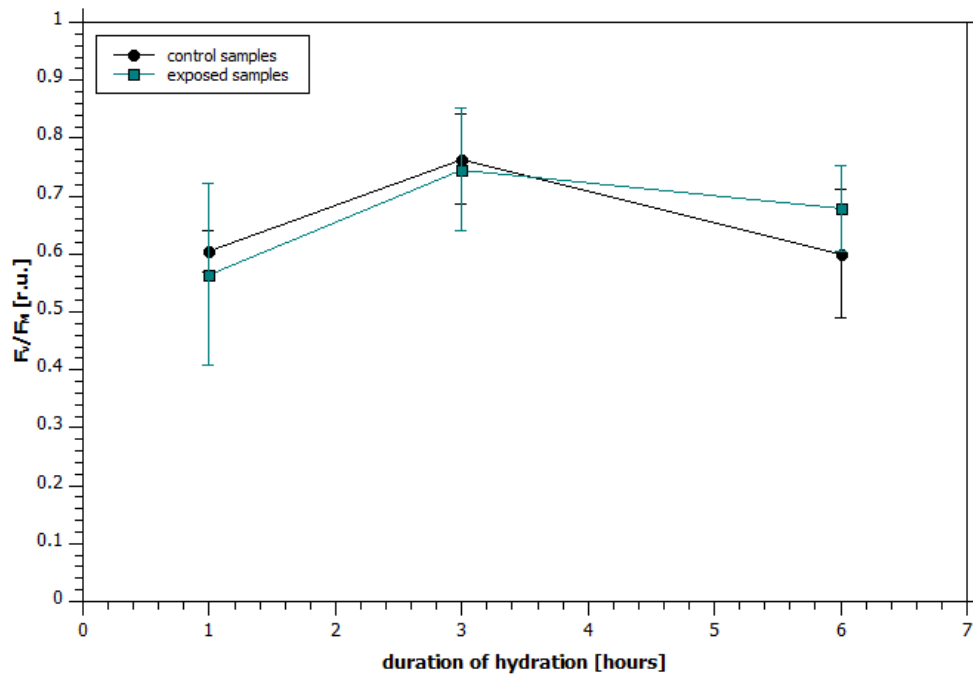


Figure 4.12: Visualization of the  $F_V/F_M$  time evolution for Antarctic samples - control samples and samples exposed to low pressure (20 Pa).

The x-axis represents duration of hydration in distilled water, y-axis denotes  $F_V/F_M$  ratio. Standard deviation error bars are displayed for every mean value.

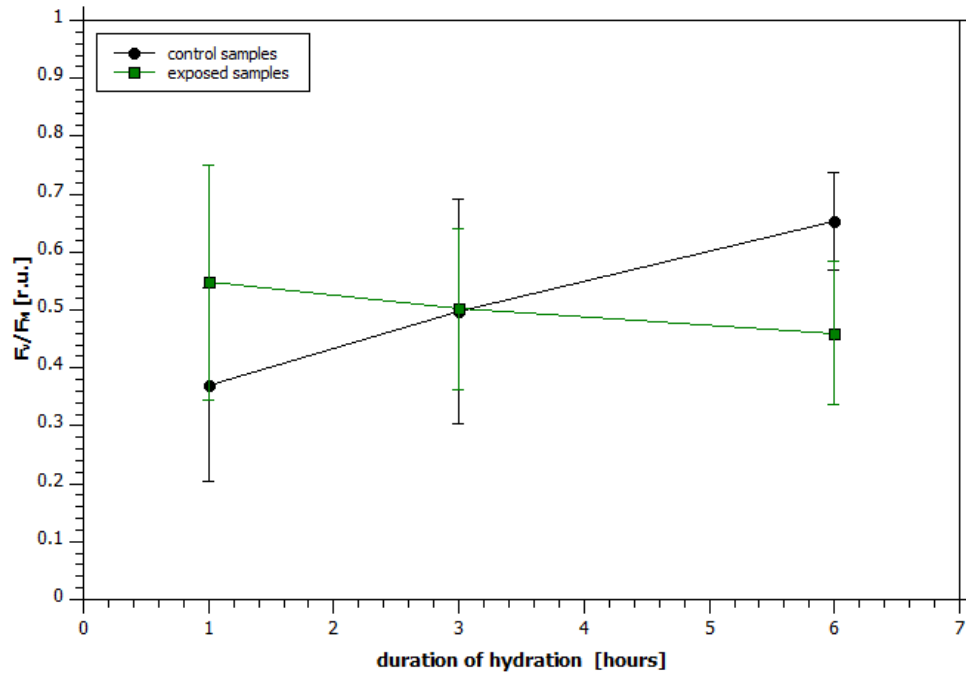


Figure 4.13: Visualization of the  $F_V/F_M$  time evolution, for Brno samples - control samples and samples exposed to low pressure (20 Pa).

The x-axis represents duration of hydration in distilled water, y-axis denotes  $F_V/F_M$  ratio. Standard deviation error bars are displayed for every mean value.

## 4.2.2 100 Pa

Brno and Antarctic samples were left in the apparatus at 100 Pa for 90 hours. Results for Antarctic samples are shown in Figure 4.14, for Brno samples in Figure 4.15. It is apparent from Figure 4.14, that the difference between the control samples and the samples left in 100 Pa is negligible. Also the difference between the control samples and the Brno samples is minimal as can be seen in Figure 4.15.

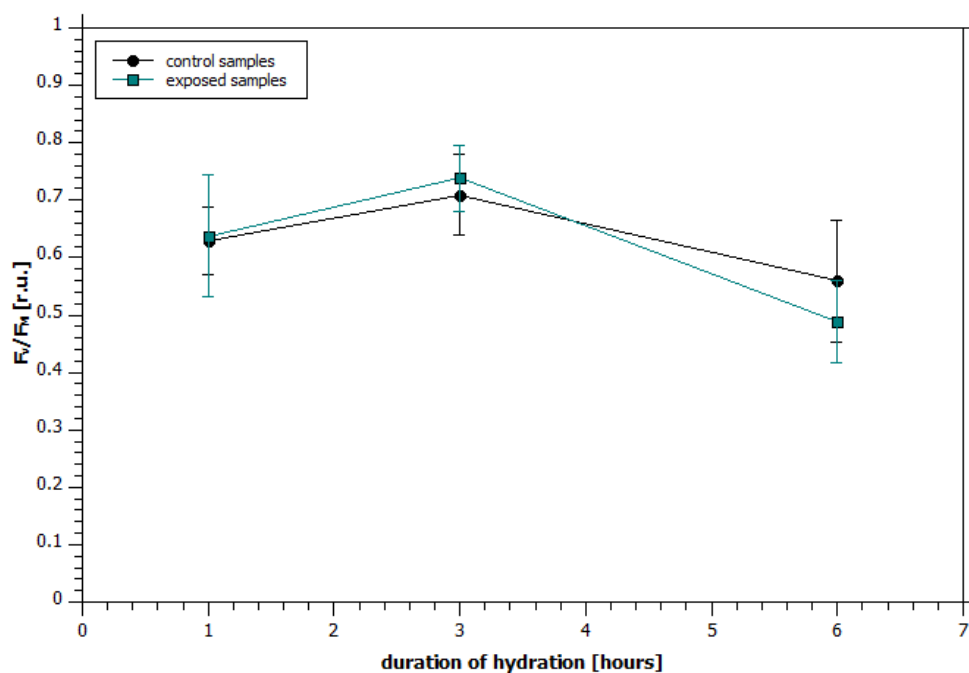


Figure 4.14: Visualization of the  $F_V/F_M$  time evolution, for Antarctic samples - control samples and samples exposed to low pressure (100 Pa).

The x-axis represents duration of hydration in distilled water, y-axis denotes  $F_V/F_M$  ratio. Standard deviation error bars are displayed for every mean value.

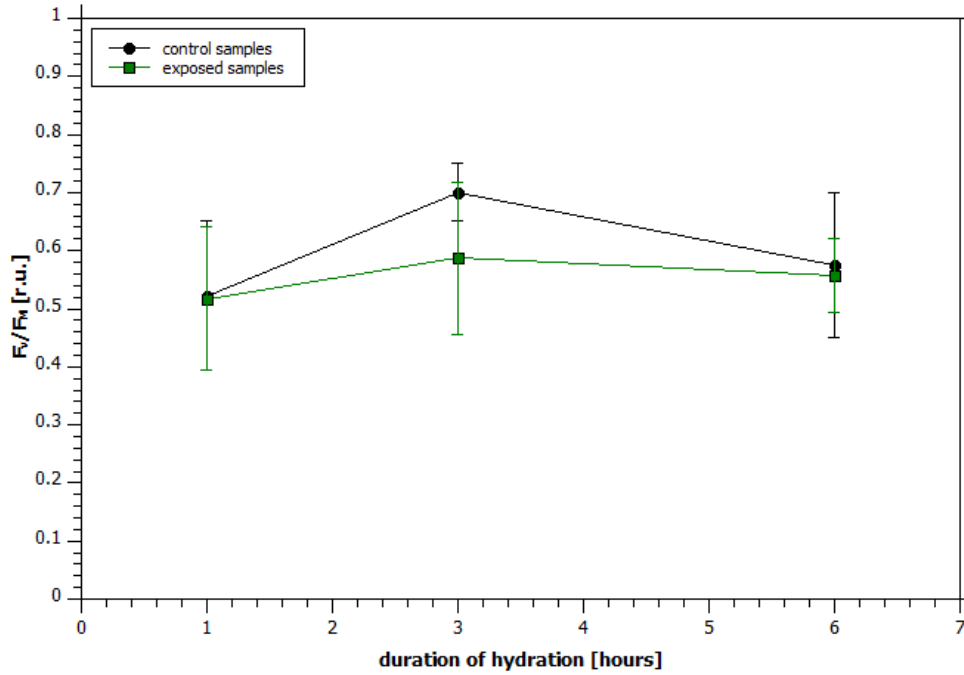


Figure 4.15: Visualization of the  $F_V/F_M$  time evolution, for Brno samples - control samples and samples exposed to low pressure (100 Pa).

The x-axis represents duration of hydration in distilled water, y-axis denotes  $F_V/F_M$  ratio. Standard deviation error bars are displayed for every mean value.

### 4.3 Plasma Tolerance

The results of our plasma sample treatment are shown in below sections, sorted with respect to power levels set on RF generator. The pressure during the experiment was  $\approx 100$  Pa, distance between the electrodes was 1.5 cm. Data measured by fluorometer are shown in graphs in form of mean values (and their standard deviations) and normalized data are shown in tables. The data in tables are normalized with respect to initial values (activity before exposure to plasma), i.e.  $F_V/F_M$  before and after exposure to experimental conditions was measured and the normalized value was obtained by dividing the value after by value before exposure. Normalized values of  $F_V/F_M$  ratios were estimated for each sample and their mean values were computed, along with one standard deviation. To see individual values of  $F_V/F_M$

and normalized values for each sample, see Appendices and the tables therein.

### 4.3.1 150 W

#### 4.3.1.1 Antarctic Samples

Groups of Antarctic samples were left in plasma three different times. The non-normalized results are shown in Figure 4.16 for 15 min treatment, in Figure 4.17 for 30 min treatment, in Figure 4.18 for 60 min treatment.

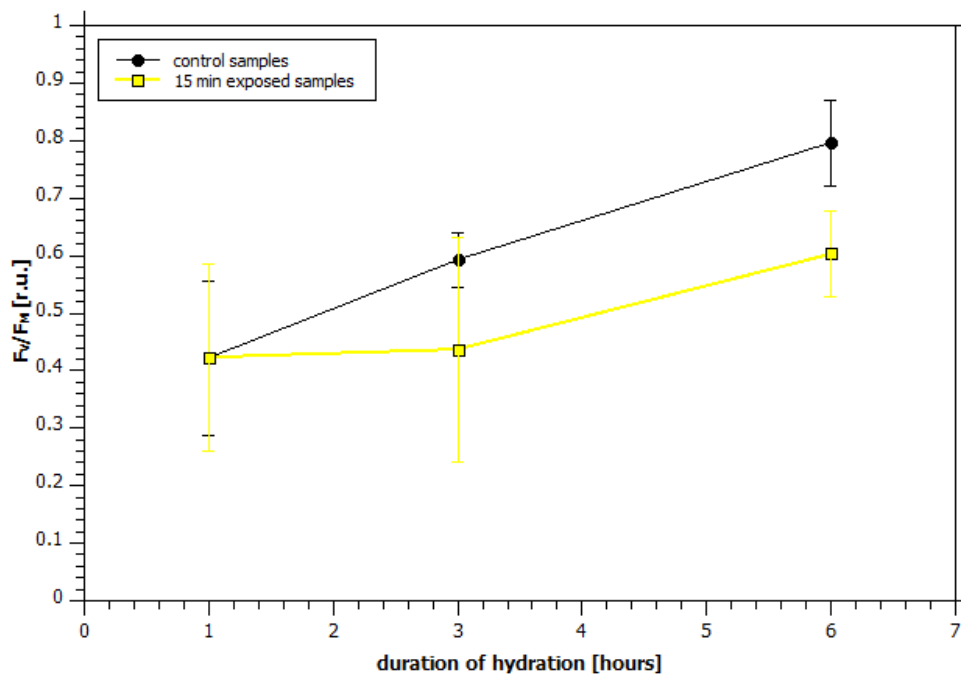


Figure 4.16: Visualization of the  $F_V/F_M$  time evolution, for Antarctic samples - control samples and samples exposed to plasma (15 min).

The x-axis represents duration of hydration in distilled water, y-axis denotes  $F_V/F_M$  ratio. Standard deviation error bars are displayed for every mean value.

As can be seen in Figure 4.16, activity of both control samples and plasma-exposed samples grows with the time of the hydration. The  $F_V/F_M$  values of both sample groups were the same in the first measurement and the difference between the samples becomes visible after 6 hours of hydration.

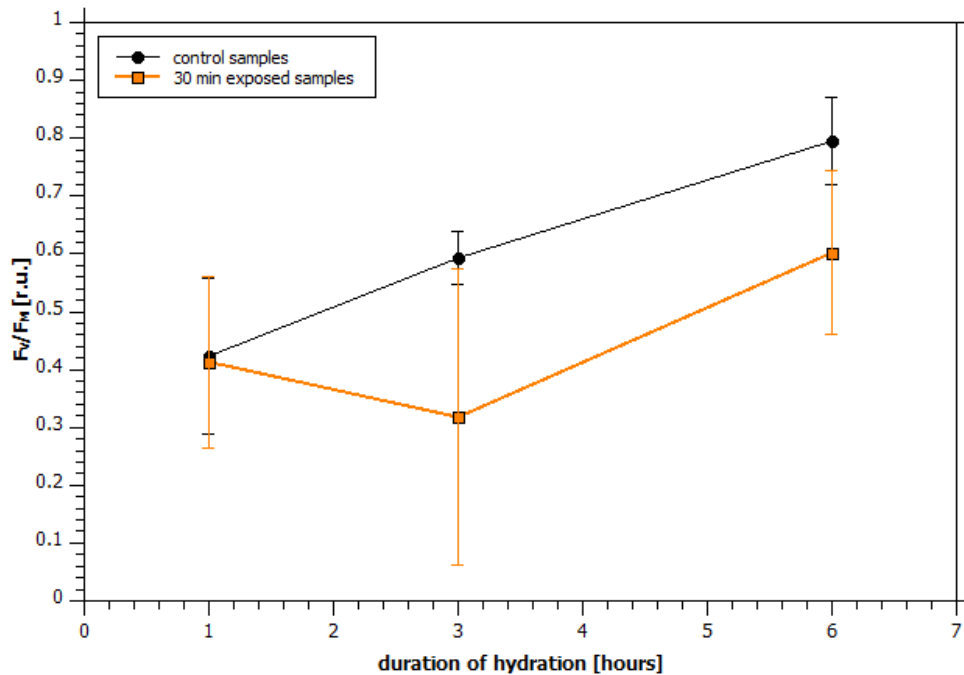


Figure 4.17: Visualization of the  $F_V/F_M$  time evolution, for Antarctic samples - control samples and samples exposed to plasma (30 min).

The x-axis represents duration of hydration in distilled water, y-axis denotes  $F_V/F_M$  ratio. Standard deviation error bars are displayed for every mean value.

Figure 4.17 shows graph for Antarctic samples, exposed to plasma for 30 minutes. Activity of control samples grows continuously. However, although exposed samples have same level of activity at first, they show a certain drop, when measured 3 hours after hydration. After this point, their activity starts to grow again.

In Figure 4.18 can be seen evolution of activity of both control samples and samples exposed to plasma for 60 minutes. The control samples grow continuously, the exposed samples do not show this trend. The activity of both groups of samples differs after 1 hour of hydration more than in previous two graphs and also the activity after 6 hours is still low and nearly not changed from the activity after 3 hours.

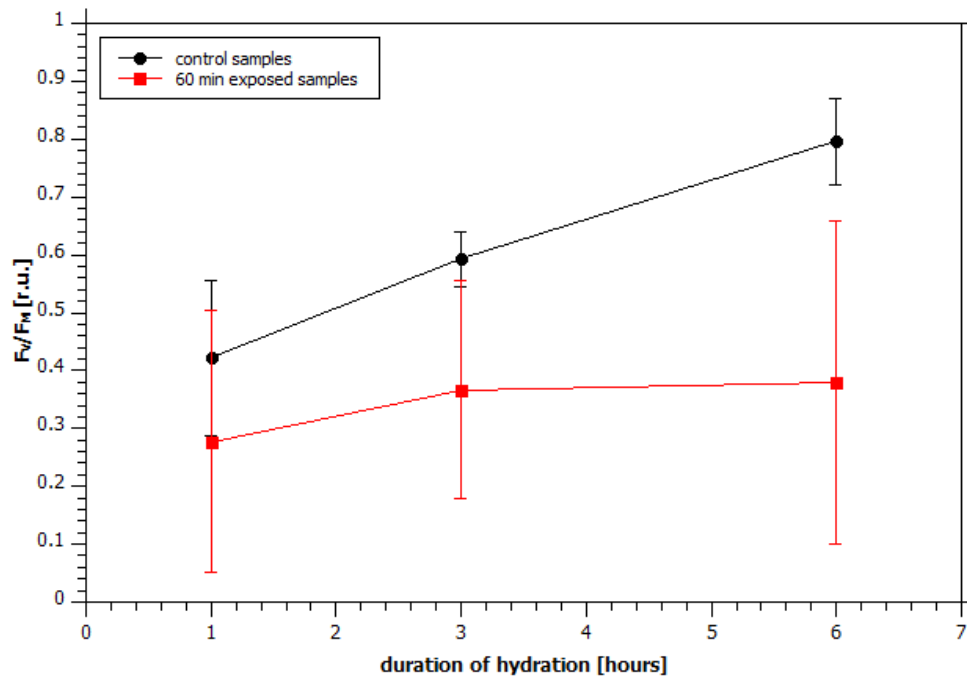


Figure 4.18: Visualization of the  $F_V/F_M$  time evolution, for Antarctic samples - control samples and samples exposed to plasma (60 min).

The x-axis represents duration of hydration in distilled water, y-axis denotes  $F_V/F_M$  ratio. Standard deviation error bars are displayed for every mean value.

Normalized values of  $F_V/F_M$  are shown in the table 4.5. The activity of control samples was increased. And the highest value of normalized  $F_V/F_M$  was accomplished after the first hour, after that the activity was slightly lower. The samples exposed to plasma for 15 minutes reached its maximum value after 1 hour of hydration, then the activity decreased and after 6 hours increased a bit. The samples exposed 30 minutes to plasma showed lower activity after 1 hour of hydration, than samples exposed to plasma for 15 minutes. Then their activity decreased and after 6 hours of hydration returned to its initial value. The lowest activity after 1 hour was measured on samples exposed to plasma for 60 minutes. Then their activity increased after 6 hour of hydration values returned near the initial value.

Table 4.5: Table of mean normalized values of  $F_V/F_M$  for Antarctic samples, 150 W.

$F_V/F_M$			
	1 hour	3 hours	6 hours
control samples	$1.36 \pm 0.65$	$1.13 \pm 0.21$	$1.10 \pm 0.15$
samples exposed 15 min.	$1.05 \pm 0.57$	$0.71 \pm 0.31$	$0.85 \pm 0.07$
samples exposed 30 min.	$0.86 \pm 0.38$	$0.66 \pm 0.62$	$0.86 \pm 0.19$
samples exposed 60 min.	$0.56 \pm 0.49$	$0.90 \pm 0.57$	$0.59 \pm 0.47$

### 4.3.1.2 Brno Samples

The control samples for this set of samples do not show continuous growth, but the maximum value of the  $F_V/F_M$  is reached after 3 hours of hydration, then the activity returns near the initial value.

In the Figure 4.19 can be seen time evolution of the samples exposed to plasma for 15 minutes. For whole duration of hydration the activity is less than the value for control samples, but the trend showed by the data is the same as for the control samples (maximum after 3 hours).

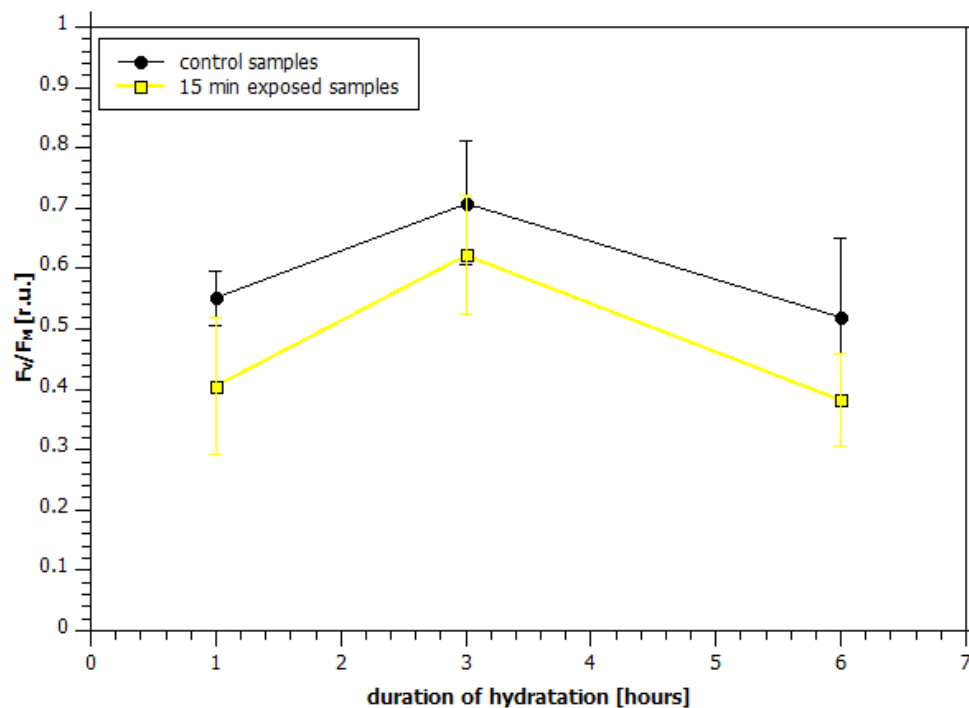


Figure 4.19: Visualization of the  $F_V/F_M$  time evolution, for Brno samples - control samples and samples exposed to plasma (15 min).

The x-axis represents duration of hydration in distilled water, y-axis denotes  $F_V/F_M$  ratio. Standard deviation error bars are displayed for every mean value.

In the Figure 4.20 the trend showed by samples exposed 30 minutes to plasma do not follow the trend of the control samples. Initial value of the exposed samples is near the initial value of the control samples, but then they show continuous decrease of their  $F_V/F_M$  ratio.

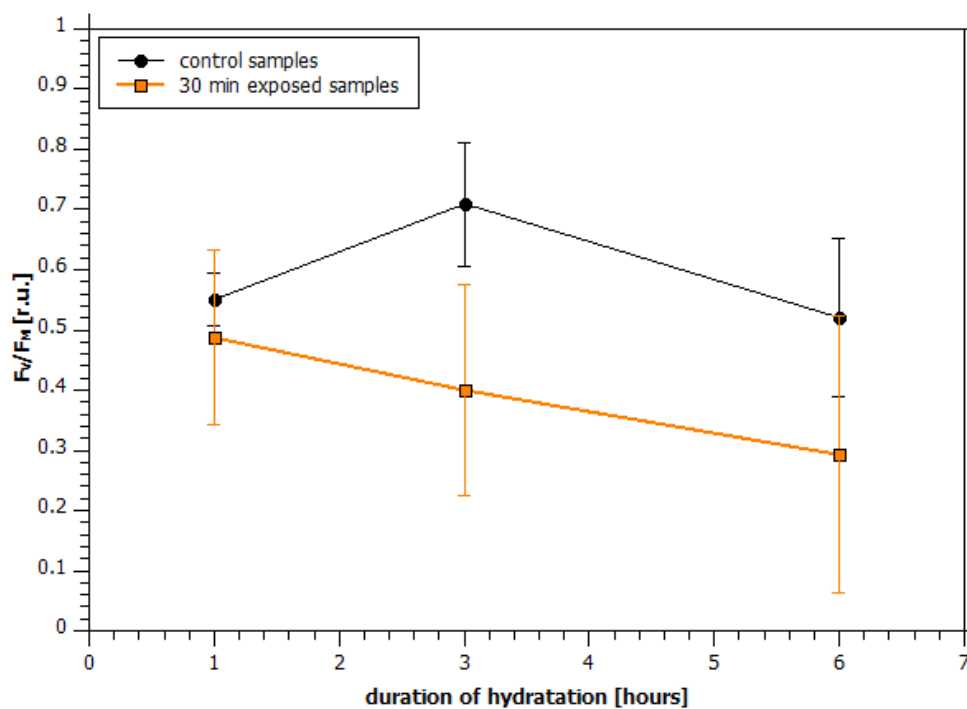


Figure 4.20: Visualization of the  $F_V/F_M$  time evolution, for Brno samples - control samples and samples exposed to plasma (30 min).

The x-axis represents duration of hydration in distilled water, y-axis denotes  $F_V/F_M$  ratio. Standard deviation error bars are displayed for every mean value.

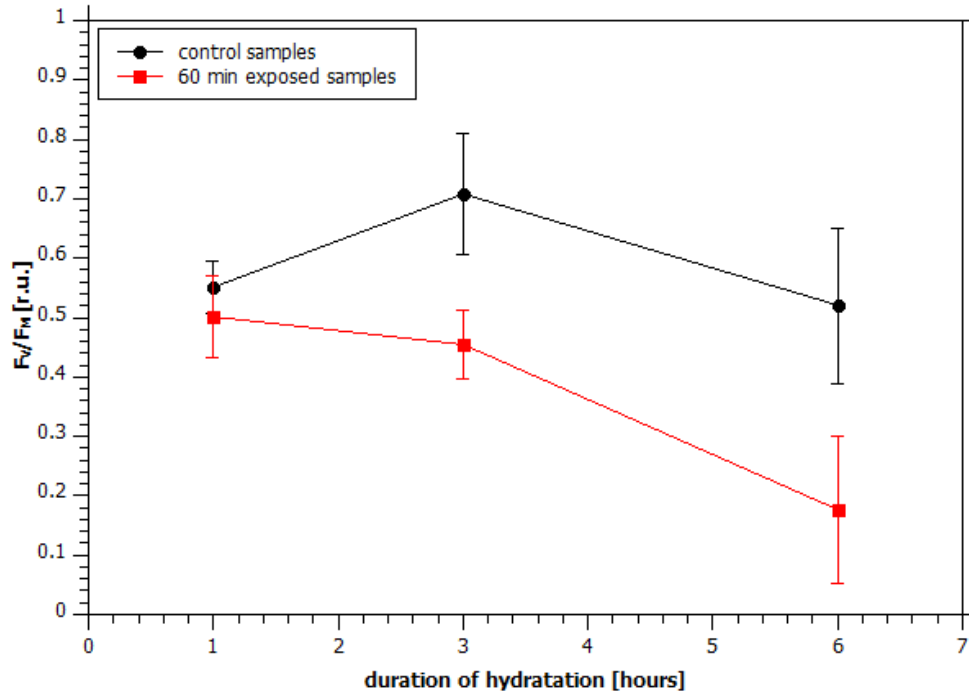


Figure 4.21: Visualization of the  $F_V/F_M$  time evolution, for Brno samples - control samples and samples exposed to plasma (60 min).

The x-axis represents duration of hydration in distilled water, y-axis denotes  $F_V/F_M$  ratio. Standard deviation error bars are displayed for every mean value.

The Figure 4.21 shows the time evolution of the  $F_V/F_M$  value for samples left in plasma for 60 minutes as well as the values of the control samples. There the  $F_V/F_M$  values of exposed samples start near the control samples value, but decrease continuously over the duration of hydration.

Table 4.6 shows the normalized values of  $F_V/F_M$ . The control samples  $F_V/F_M$  shows similar values after 1 and 3 hours of hydration and decrease after 6 hours. For the samples exposed to plasma for 15 minutes, there is decreased activity after 1 hour, increase after 3 hours and decrease again after 6 hours. The samples exposed to plasma for 30 minutes shows the increase after 1 hour, then decrease after 3 hours and even larger decrease after 6 hours. The samples exposed 60 minutes to plasma shows the decrease after 1 hour. After 3 hours values seems to be neither increased nor decreased and after the 6 hours the activity significantly decreased.

Table 4.6: Table of mean normalized values of  $F_V/F_M$  for Brno samples, 150 W.

$F_V/F_M$			
	1 hour	3 hours	6 hours
control samples	$1.33 \pm 0.35$	$1.35 \pm 0.31$	$0.93 \pm 0.22$
samples exposed 15 min.	$0.92 \pm 0.51$	$1.26 \pm 0.26$	$0.80 \pm 0.22$
samples exposed 30 min.	$1.19 \pm 0.42$	$0.73 \pm 0.27$	$0.46 \pm 0.29$
samples exposed 60 min.	$0.92 \pm 0.23$	$1.01 \pm 0.24$	$0.33 \pm 0.20$

### 4.3.2 250 W

All of the samples were not measured at once (they did not belong to the same set of samples). Instead, they were measured in batches, based on their time of exposure to plasma. Each batch was measured on different day - that is why we have used different control samples in each experiment.

#### 4.3.2.1 Antarctic Samples

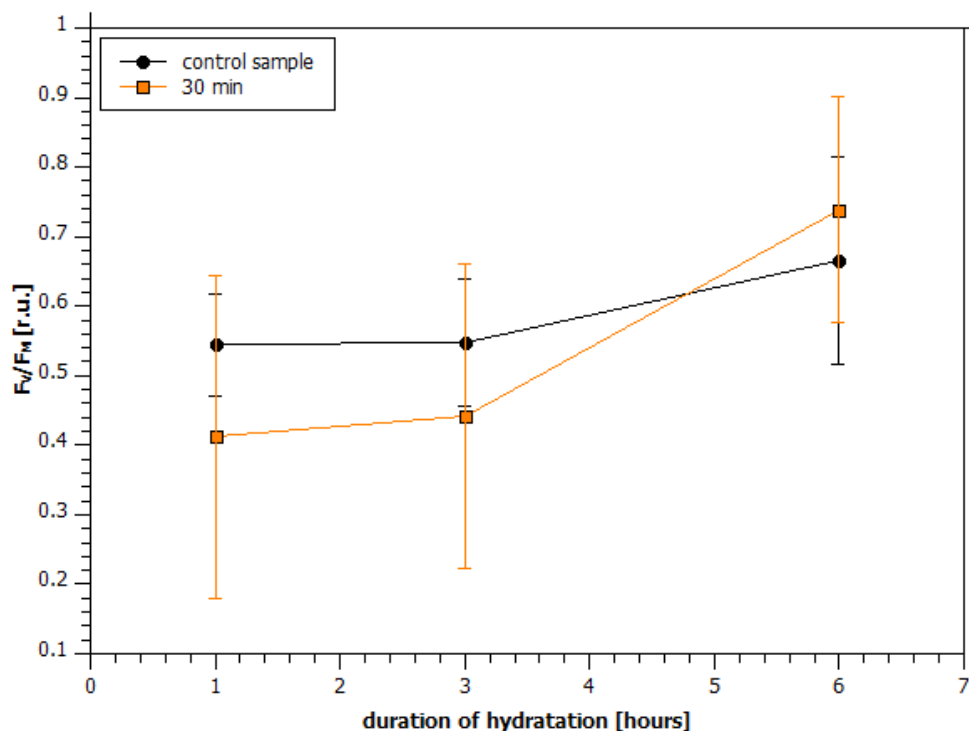


Figure 4.22: Visualization of the  $F_V/F_M$  time evolution, for Antarctic samples - control samples and samples exposed to plasma (30 min, 250 W).

The x-axis represents duration of hydration in distilled water, y-axis denotes  $F_V/F_M$  ratio. Standard deviation error bars are displayed for every mean value.

In the graph 4.22 is shown the evolution of the  $F_V/F_M$  values in time. The control samples activity remains constant for 1 and 3 hours and then it is slightly increased.

The samples exposed to plasma for 30 minutes shows at first values lesser and after 6 hours of hydration the values are increased, higher than those of control samples. The large error bars are due to inactivity (or very low activity) of a few samples.

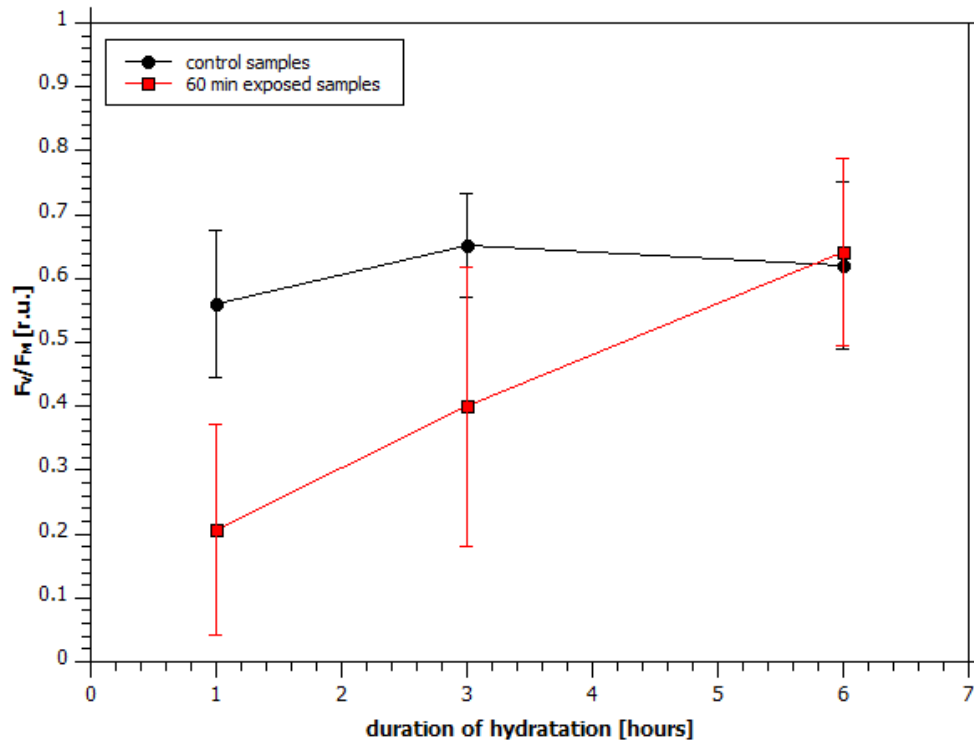


Figure 4.23: Visualization of the  $F_V/F_M$  time evolution, for Antarctic samples - control samples and samples exposed to plasma (60 min, 250 W).

The x-axis represents duration of hydration in distilled water, y-axis denotes  $F_V/F_M$  ratio. Standard deviation error bars are displayed for every mean value.

In the Figure 4.23 are shown the samples exposed to plasma for 60 minutes and their control samples. The control samples exhibit nearly constant values of  $F_V/F_M$  throughout the duration of hydration. The exposed samples, show low values, measured 1 hour after hydration and their activity is increasing, until after the 6 hour of hydration their activity is the same as the activity of the control samples.

At the table 4.7 are shown the normalized values of  $F_V/F_M$ . It can be seen from the table that the control samples have increased activity after 1 hour of hydration

and after 6 hours their activity is nearly identical. The 30 minutes to plasma exposed samples showed only a little decrease in their activity after 1 hour, then after 3 hours their activity decreased and after 6 hours the activity was the same as at the 1 hour. The samples left 60 minutes in plasma exhibit a large decrease in activity after 1 hour and their activity grew during the hydration, after 6 hours the values were very near to the values of control samples.

Table 4.7: Table of mean normalized values of  $F_V/F_M$  for Antarctic samples, 250 W.

Fv/Fm			
	1 hour	3 hours	6 hours
control samples (30 min.)	$1.39 \pm 0.77$	$0.87 \pm 0.19$	$0.87 \pm 0.19$
30 min. exposed samples	$0.96 \pm 0.67$	$0.64 \pm 0.28$	$0.95 \pm 0.31$
control samples (60 min.)	$1.32 \pm 0.49$	$1.37 \pm 0.32$	$0.85 \pm 0.18$
60 min. exposed samples	$0.47 \pm 0.38$	$0.56 \pm 0.27$	$0.78 \pm 0.15$

### 4.3.2.2 Brno Samples

The results of the 30 minutes exposure to the plasma are in Figure 4.24. The control samples there exhibit slight increase of activity during hydration. The samples exposed to plasma at 1 hour of hydration had the values of  $F_V/F_M$  lower than the control samples, after the 3 hours samples are again less active than control ones and after 6 hours of hydration the activity of the exposed samples drops significantly.

The results of the 60 minutes exposure to the plasma are in Figure 4.25. There the activity of the control samples remains nearly constant for through the hydration duration. The exposed samples are significantly less active than the control samples and exhibit a small decrease after 3 hours of hydration.

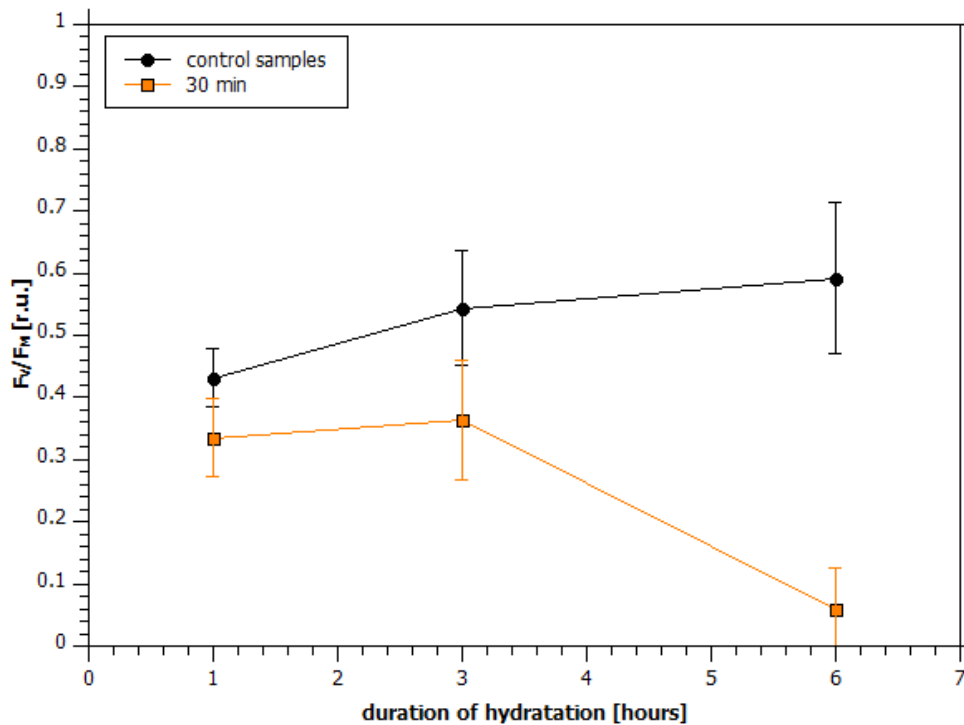


Figure 4.24: Visualization of the  $F_V/F_M$  time evolution, for Brno samples - control samples and samples exposed to plasma (30 min, 250 W).

The x-axis represents duration of hydration in distilled water, y-axis denotes  $F_V/F_M$  ratio. Standard deviation error bars are displayed for every mean value.

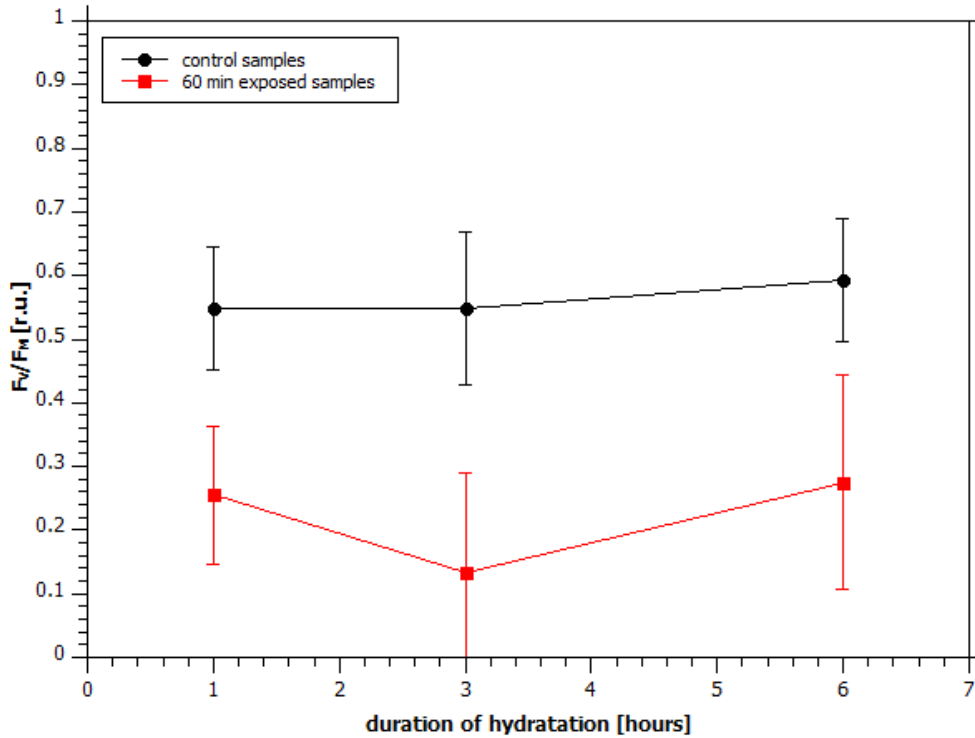


Figure 4.25: Visualization of the  $F_V/F_M$  time evolution, for Brno samples - control samples and samples exposed to plasma (60 min, 250 W).

The x-axis represents duration of hydration in distilled water, y-axis denotes  $F_V/F_M$  ratio. Standard deviation error bars are displayed for every mean value.

The normalized values of  $F_V/F_M$  are given in the table 4.7. The control samples for 30 minutes exposure have constant not significantly increased or decreased activity, the activity of the control samples for 60 minutes exposure increased slightly after the first two measurements, after 6 hours it does not seem to have changed. The samples exposed 30 minutes to plasma show after 1 hour of hydration increased activity, but after 3 and 6 hours the activity steeply decreased. The samples exposed to plasma for 60 minutes show the decrease in activity after 1 hour of hydration. It decreased even more after 3 hours of hydration and after 6 hours of hydration the activity was similar to the value after 1 hour of hydration.

Table 4.8: Table of mean normalized values of  $F_V/F_M$  for Brno samples, 250 W.

$F_V/F_M$			
	1 hour	3 hours	6 hours
control samples (30 min.)	$0.99 \pm 0.17$	$1.06 \pm 0.24$	$1.04 \pm 0.28$
30 min. exposed samples	$0.62 \pm 0.17$	$0.68 \pm 0.20$	$0.12 \pm 0.13$
control samples (60 min.)	$1.19 \pm 0.20$	$1.18 \pm 0.26$	$0.99 \pm 0.15$
60 min. exposed samples	$0.59 \pm 0.27$	$0.34 \pm 0.54$	$0.51 \pm 0.27$

# Chapter 5

## Discussion

### 5.1 AFM

Besides transmission electron microscopy and scanning electron microscopy, the AFM is also used for biological measurements for some time, see e.g. (Hernández et al., 2004). Although there were not many AFM studies of cyanobacterial surface (Stukalov et al., 2008), topographic study of cyanobacterial interior was done on the cyanobacteria *Gloeothece* sp. (Tiribilli et al., 2012). Cyanobacterial PSI was also imaged (Niroomand et al. 2017), etc.

At least two different morphological types of surface were found in our samples, we have characterized one of them as "grainy" (see Figure 4.9), the other one as "smooth" (see Figure 4.10). Their Young's modulus was estimated (see tables 4.1 and 4.2) and in quantitative imaging mode also their stiffness (see tables 4.3 and 4.4). It can be seen that the stiffness of the samples is roughly in the same interval, but their values of  $E$  are not. This might be caused by the large adhesion of samples, which could caused problems during the fitting of the force curve to the Hertz model.

Fibre of cyanobacteria *Nostoc* sp. PCC 6720, was studied in depth in the work of (Dhahri et al., 2013) in quantitative imaging mode. In this work the values of stiffness for extracellular matrix of the sample is stated as  $(90 \pm 30)$  mN/m. They have also estimated Young's modulus for the cyanobacterium in their work - they stated that  $E = (20 \pm 3)$  MPa and for extracellular matrix it is  $(4-15 \pm 3)$  MPa. Our data are in tables 4.1 and 4.2, some of our values lie in this interval, but the rest of them does not. This might be caused by the problematic fitting of force curves due to large adhesion, as was mentioned above. Or it might be the glycan surface structure of both our Brno and Antarctic *Nostoc* is considerably more heterogeneous.

In one of the scans of the Antarctic samples (in Figure 4.3), the small oval-shaped

objects with size of  $\approx 1.5 \mu\text{m}$  can be seen. If these ovals are scanned without other surroundings, their  $E$  equals to  $(2.01 \pm 1.6)$  MPa. According to available literature, this size seems to be too small for *Nostoc* cells (Potts, 2000). When hydrated Antarctic mats were examined under optical microscope, a pair of *Chroococcus* cells were found in one case, but such little oval cannot be mistaken for it.

## 5.2 Low Pressure

The measurement of low pressure tolerance was chosen to make sure that low pressure treatment does not significantly affect the desiccated organism if it is left in low pressure for a relatively short time and that the organism will behave the similar way as those treated in other works e.g. (Arai et al., 2008). In the work of (Arai et al., 2008), *Nostoc* survived the pressure of  $10^{-5}$  Pa. Our studied samples were exposed to two distinct levels of pressure: 20 Pa for 25 hours, to test the limits of the experimental apparatus, and to the usual experimental pressure 100 Pa, for 90 hours. The pressure of 20 Pa was kept constant for the whole duration of the experiment. However it was not able to retain the 100 Pa pressure on the constant level throughout an entire duration of the experiment and at the end of the measurement the pressure was nearly atmospheric. The results indicate that the initial hypothesis was correct - none of the tested sample groups have shown any significant decline in activity with respect to the control samples. The low pressure damage could have possibly occurred to wet samples, if the water vaporization would be too fast, but since we placed samples into the apparatus already in an desiccated state, significant damage did not seem to occur.

## 5.3 Plasma

The results of our solar wind-like plasma treatment will be discussed below. It can be clearly seen from graphs, that samples from Antarctica and Brno behaved differently (compare e.g. Figures 4.22 and 4.24). In all cases Antarctic samples showed growth of their activity in the interval between 3 and 6 hours of hydration. The values after 6 hours of hydration were near to those of the control samples. The initial values of the Antarctic samples (after 1 hour of hydration) differed from the control samples. The longer the duration of exposition to plasma was the lower values were measured. This effect can be seen the best in 250 W measurements. Measurement of the samples exposed to plasma excited by 150 W does not have such effect - only the 60 minutes exposure had caused a decline in initial activity. The Brno samples

exhibit the opposite effect, after the 6 hour of hydration the activity has declined (except the 60 minutes 250 W treatment, where a considerable number of samples exhibited either low or no activity after 3 hours of hydration).

It seems that after 1 hour of hydration the damage done to the photochemical apparatus of the samples is minimal or it is quite efficiently repaired in all samples (Antarctic and Brno) exposed to 150 W and in samples exposed to the plasma for 30 minutes at 250 W. The 250 W CCP had the most significant effect to the photochemical apparatus for both groups of samples.

Brno samples seem to be less able to withstand the exposure to plasma. At first, it seems that the photochemical apparatus was not influenced by any damage that might have occurred to the sample. However, due to some later activated process or perhaps due to some product of the reparation processes the activity of PSII was reduced.

An analysis of the available literature has not yielded any other work for comparison with the results of this study. Only freshwater cyanobacteria were previously exposed to plasma in order to get rid of a cyanobacterial bloom e.g. in (Sekugawa et al., 2014). Also among the studies of Antarctic samples, the activity was examined only during dehydration e.g. in (Barták et al., 2016) or (Trnková & Barták, 2016). Some studies of *Nostoc* hydration examined different types of influencing factors e.g. high illumination in work of (Raanan et al., 2016).

The difference between the Antarctic and Brno samples could be in the composition of the EPS. It is possible that the Antarctic and Brno samples have a different composition of their EPS envelope - the natural environmental conditions in Antarctica are much harsher than those in Brno and the samples are probably adapted to them (Ehling-Schulz, 1997). Since DNA analysis nor any chemical analysis of the samples were not performed, it is difficult to ascertain if the difference was due to different EPS composition and/or the different *Nostoc commune* studied strain.

The experimental pressure was roughly the same during each measurement. As was said earlier, the UV radiation was not expected to significantly affect the samples during the measurement, since e.g. UVC was used for cleaning of the cultures (Mehta & Hawxby, 2017). A water cooling system was used to prevent an influence of high temperature on the measurements. Additionally, temperatures exceeding 100°C were tested during the preliminary measurements, and no significant effects of such high temperatures were observed, compared to the measurements in 20°C. This is in agreement with findings of (Sand-Jensen & Jespersen, 2012). They observed only minor changes in the activity of samples exposed to temperature of 105°C for 36 hours.

The large error bars (one standard deviation) in graphs with measured  $F_V/F_M$

values were due to the inactivity or low activity of one or more samples. This effect could be minimized if a larger number of samples were tested. The effect of the large variability of the activity is probably mainly caused by a large variability of the mats. This effect was attempted to be kept under control by sorting the samples by colour. Every set of samples had a fixed number of the samples with a certain visual characterisation. To minimize this effect even further, the values of  $F_V/F_M$  were normalized. Nevertheless, the variability was still significant and the testing of larger set of samples is still needed to eliminate such large variability.

# Chapter 6

## Conclusions

### 6.1 Synthesis

Terrestrial cyanobacteria *Nostoc commune* from two different locations (Antarctica and Brno) were collected and used for several different tests in this work. The AFM scans of *Nostoc commune* surface were done in force mapping and quantitative imaging modes. Illustrative images of the surface were obtained as well. At least two different morphological types of the surface were identified both in the Brno and Antarctic samples. Also the Young's modulus and the stiffness values of samples were estimated. The accurate values of modulus showed a large divergence, the values of the stiffness were more consistent (but there also seemed to be some stiffer and softer areas). It can be concluded that the surfaces of the samples were heterogeneous.

The ability of *Nostoc commune* to survive in special conditions, similar to the solar wind and the low pressure was tested. For this purpose, a new special experimental apparatus was successfully built. Samples were exposed to two different levels of low pressure, but as expected, it did not have any noticeable effect on them. However, the differences were observed between Antarctic and Brno samples during the measurement of activity of PSII (i.e. measuring parameter  $F_V/F_M$ ), when the samples were exposed to plasma. The difference can be seen especially after 6 hours of hydration. The activity of the Antarctic samples after this time of hydration seemed to be the same as the activity of the control samples, but the activity of the Brno samples drops. This could be caused by the better adaptation of Antarctic samples to extreme conditions. Initial photosynthetic activity (after 1 hour of hydration) seemed to be more affected, the longer the samples were exposed to the plasma and higher the power level of the RF generator was. In general, the samples have survived all of the tests. This, along with other studies of this cyanobacteria

suggest that the endurance of the *Nostoc* is considerable. This could have interesting consequences for the theories of life propagation in space, regardless of whether we are talking about the panspermia theory or the risk of the unwanted contamination of celestial bodies. Or for the possible colonization of other planetary objects, since the *Nostoc* was already considered as possible "space food".

## 6.2 Future Work

A larger set of samples and more repeated measurements would be beneficial to minimize the diversity of the samples due to e.g. various ages of different parts of the samples, in both the measurements in simulated extraterrestrial conditions and AFM measurements. Also DNA analysis would be required - to precisely identify the strain of the *Nostoc commune*. Moreover, to estimate the differences in samples composition, which could be important (since the Brno and Antarctic samples are naturally adapted to different climate), it might be worth to perform their chemical analysis before and after testing.

# Bibliography

Arai, M. et al. (2008). Growth of terrestrial cyanobacterium, *Nostoc* sp., on Martian Regolith Simulant and its vacuum tolerance. *Biological Sciences in Space*. 22, 1 (2008), 8-17.

Aschwanden, M. (2005). *Physics of the Solar Corona: An Introduction With Problems and Solutions* (Springer-Praxis books in geophysical sciences). Springer Verlag.

Asplund, M. et al. (2009). The Chemical Composition of the Sun. *Annual Review of Astronomy and Astrophysics*. 47, 1 (2009), 481-522.

Bagenal, F. et al. (2015). Solar wind at 33 AU: Setting bounds on the Pluto interaction for New Horizons. *Journal of Geophysical Research: Planets*, 102(9), pp.1497-1511.

Bagenal, F. et al. (2016). Plutos interaction with its space environment: Solar wind, energetic particles, and dust. *Science*. 351. aad9045-aad9045.

Barcza, S. (2016). Greenhouse effect from the point of view of radiative transfer. *Acta Geodaetica et Geophysica*, 52(4), pp.581-592.

Barták, M. et al. (2016). Dehydration-induced responses of primary photosynthetic processes and spectral reflectance indices in Antarctic *Nostoc commune*. *Czech Polar Reports*, 6(1), 87-95.

Billi, D. et al. (2008). *Desert Cyanobacteria under simulated space and Martian conditions*. European Planetary Science Congress.

Billi, D., & Potts, M. (2002). Life and death of dried prokaryotes. *Research in Microbiology*, 153(1), pp.7-12.

- Bittencourt, J.A. (2004). Fundamentals of plasma physics. Springer-Verlag New York.
- Bochsler, P. Solar Wind Composition. In Murdin, ed. The Encyclopedia of Astronomy and Astrophysics. IOP Publishing, 2001.
- Borowitzka, M. et al. (2016). The Physiology of Microalgae. Cham: Springer.
- Bottke, F. et al. (2006). The Yarkovsky and YORP Effects: Implications for Asteroid Dynamics. Annual Review of Earth and Planetary Science, 34. 157-91.
- Brož, M., & Šolc, M. (2013). Fyzika sluneční soustavy. Vyd. 1. Praha: Matfyzpress.
- Capria, M. et al. (2014). Vesta surface thermal properties map. Geophysical Research Letters, 41(5), 1438-1443.
- Carroll, B., & Ostlie, D. (2007). An introduction to modern astrophysics. San Francisco: Pearson Addison-Wesley.
- Chen, F. (1984). Uvod do fyziky plazmatu. Praha: Academia.
- Czaja, A. et al. (2013). Biological Fe oxidation controlled deposition of banded iron formation in the ca. 3770Ma Isua Supracrustal Belt (West Greenland). Earth And Planetary Science Letters, 363, 192-203.
- DeVincenzi, D. (1998). Planetary protection, sample return missions and Mars exploration: History, status, and future needs. Journal Of Geophysical Research: Planets, 103(E12), 28577-28585.
- Deblo, M. (2004). The nature of near-earth asteroids from the study of their thermal infrared emission. Doctoral thesis. Freie Universität Berlin.
- Delbo, M., & Harris, A. (2002). Physical properties of near-Earth asteroids from thermal infrared observations and thermal modeling. Meteoritics & Planetary Science, 37(12), 1929-1936.
- Deblo, M. et al. (2015). Asteroid thermophysical modeling. arXiv:1508.05575.

Dhahri, S. et al. (2013). In-Situ Determination of the Mechanical Properties of Gliding or Non-Motile Bacteria by Atomic Force Microscopy under Physiological Conditions without Immobilization. *Plos ONE*, 8(4), e61663.

Di Pippo, F. et al. (2013). Characterization of exopolysaccharides produced by seven biofilm-forming cyanobacterial strains for biotechnological applications. *Journal Of Applied Phycology*, 25(6), 1697-1708.

Dvořák, P. (2013). Modelling of electric characteristics of capacitively coupled discharges including nonlinear effects of sheaths. *Plasma Sources Science And Technology*, 22(4), 045016.

Ehling-Schulz, M. et al. (1997). UV-B-induced synthesis of photoprotective pigments and extracellular polysaccharides in the terrestrial cyanobacterium *Nostoc commune*. *Journal Of Bacteriology*, 179(6), 1940-1945.

Ehling-Schulz, M. et al. (2002). The UV-B stimulon of the terrestrial cyanobacterium *Nostoc commune* comprises early shock proteins and late acclimation proteins. *Molecular Microbiology*, 46(3), 827-843.

Elliott, H. et al. (2016). The new horizons solar wind around Pluto (SWAP) observations of the solar wind from 11-33 AU. *The Astrophysical Journal Supplement Series*, 223(2), 19.

Frick, A. F. et al. (2014). Overview of Current Capabilities and Research and Technology Developments for Planetary Protection. *Advances in Space Research*. 54, 221-240.

Garcia-Pichel, F., & Castenholz, R. W. (1993). Occurrence of UV-Absorbing, Mycosporine-Like Compounds among Cyanobacterial Isolates and an Estimate of Their Screening Capacity. *Applied and environmental microbiology*, Jan., p. 163-169.

Gao, K., & Ye, C. (2007). Photosynthetic insensitivity of the terrestrial cyanobacterium *Nostoc flagelliforme* to solar UV radiation while rehydrated or desiccated. *Journal Of Phycology*, 43(4), 628-635.

Gargaud, M. ed. (2011). *Encyclopedia of Astrobiology*. Berlin: Springer.

- Govindjee. (2011). Adventures with cyanobacteria: a personal perspective. *Frontiers In Plant Science*, 2.
- Gundlach, B., & Blum, J. (2013). A new method to determine the grain size of planetary regolith. *Icarus*, 223(1), 479-492.
- Harris, A. (1998). A Thermal Model for Near-Earth Asteroids. *Icarus*, 131(2), 291-301.
- Harris, A., & Lagerros, J. Asteroids in the Thermal Infrared. In: *Asteroids III*, Bottke, W., Tucson: University of Arizona Press (2002).
- Hernández, M. et al. (2004). Microscopy methods applied to research on cyanobacteria. *Limnetica*. 23. 179-186.
- Jandt, K. (2001). Atomic force microscopy of biomaterials surfaces and interfaces. *Surface Science*, 491(3), 303-332.
- Kalina, T., & Váňa, J. (2005). *Sinice, řasy, houby, mechorosty a podobné organismy v současné biologii*. Praha: Karolinum.
- Kaltenegger, L., & Sasselov, D. (2011). Exploring the habitable zone for kepler planetary candidates. *The Astrophysical Journal*, 736(2), L25.
- Kehr, J., & Dittmann, E. (2015). Biosynthesis and Function of Extracellular Glycans in Cyanobacteria. *Life*, 5(1), 164-180.
- Kim, T. K. et al. (2016). Modeling the Solar Wind at the Ulysses, Voyager, and New Horizons Spacecraft. *The Astrophysical Journal*, 832, 1.
- Kimura, Y. et al. (2014). Utilization of a cyanobacterium, *Nostoc sp.* HK-01, under the space environment. 44th International Conference on Environmental Systems, 13-17 July, Tucson, Arizona.
- Kimura, Y. et al. (2016). Space environmental tolerance of a terrestrial cyanobacterium, *Nostoc sp.* HK-01, under the space environment. 46th International Conference on Environmental Systems, 10-14 July 2016, Vienna, Austria.

- Kirk, J. G. et al. (1994). *Plasma astrophysics*. Springer-Verlag New York.
- Knoop, H. et al. (2013). Flux Balance Analysis of Cyanobacterial Metabolism: The Metabolic Network of *Synechocystis* sp. PCC 6803. *Plos Computational Biology*, 9(6), e1003081.
- Komárek, J. et al. (2014). Taxonomic classification of cyanoprokaryotes (cyanobacterial genera) 2014, using a polyphasic approach. *Preslia* 86: 295–335.
- Lebofsky, L. et al. (1986). A refined “standard” thermal model for asteroids based on observations of 1 Ceres and 2 Pallas. *Icarus*, 68(2), 239-251.
- Lebofsky, L. & Spencer, J. (1989). Radiometry and a thermal modeling of asteroids. In: *Asteroids II*, pp. 128–147. University of Arizona Press, Tucson, AZ.
- Leyrat, C. et al. (2012). Thermal properties of (4) Vesta derived from Herschel measurements. *Astronomy & Astrophysics*, 539, A154.
- Li, J. et al. (2013). Global photometric properties of Asteroid (4) Vesta observed with Dawn Framing Camera. *Icarus*, 226(2), 1252-1274.
- Lieberman, M., & Lichtenberg, A. (1994). *Principles of plasma discharges and materials processing*. New York: Wiley.
- Lin, H., & Loeb, A. (2015). Statistical signatures of panspermia in exoplanet surveys. *The Astrophysical Journal*, 810(1), L3.
- Maxwell, K., & Johnson, G. (2000). Chlorophyll fluorescence—a practical guide. *Journal Of Experimental Botany*, 51(345), 659-668.
- Mehta, R. & Hawxby, K. (2017). Use of ultraviolet radiation to achieve bacteria-free algal culture. ([http://digital.library.okstate.edu/oAs/oas\\_pdf/v57/p54\\_60.pdf](http://digital.library.okstate.edu/oAs/oas_pdf/v57/p54_60.pdf)).
- Méndez, A., & Rivera-Valentín, E. (2017). The Equilibrium Temperature of Planets in Elliptical Orbits. *The Astrophysical Journal*, 837(1), L1.
- Mueller, M. (2007). *Surface Properties of Asteroids from Mid-Infrared Observations*

*and Thermophysical Modeling*. Doctoral thesis. Freie Universität Berlin.

Nagarajan, A. & Pakrasi, H. (2016). Membrane-Bound Protein Complexes for Photosynthesis and Respiration in Cyanobacteria. In: eLS. John Wiley & Sons, Ltd: Chichester.

Newbury, J. et al. (1998). Electron temperature in the ambient solar wind: Typical properties and a lower bound at 1 AU. *Journal Of Geophysical Research: Space Physics*, 103(A5), 9553-9566.

Niroomand, H. et al. (2017). Tuning the photoexcitation response of cyanobacterial Photosystem I via reconstitution into Proteoliposomes. *Scientific Reports*, 7(1).

Paerl, H. et al. (2000). Cyanobacterial-bacterial mat consortia: examining the functional unit of microbial survival and growth in extreme environments. *Environmental Microbiology*, 2(1), 11-26.

De Pater, I., & Lissauer, J. (2015). *Planetary sciences*. Cambridge: Cambridge University Press.

Potts, M. (1997), Etymology of the Genus Name *Nostoc* (Cyanobacteria). *International Journal Of Systematic Bacteriology*, 47(2), 584-584.

Potts, M. (1999). Mechanisms of desiccation tolerance in cyanobacteria. *European Journal Of Phycology*, 34(4), 319-328.

Potts, M. (2000). *Nostoc*. In: Whitton B.A., Potts M. (eds) *The Ecology of Cyanobacteria*. Springer, Dordrecht, 470.

Potts, M. (2001). Desiccation tolerance: a simple process?. *Trends In Microbiology*, 9(11), 553-559.

Potts, M., & Scherer, S. (1989). Novel water stress protein from a desiccation-tolerant cyanobacterium. Purification and partial characterization. *The Journal of Biological Chemistry*, 264, 21, 25, pp. 12546-12553.

Pravec, P. et al., Asteroid Rotations. In: *Asteroids III*, Bottke et. al., Tucson: University of Arizona Press (2002).

- Pravec, P. et al. (2006). NEA rotations and binaries. *Proceedings Of The International Astronomical Union*, 2(S236), 167.
- Pereyra, D., & Ferrari, S. (2016). Extracellular Polymeric Substance (EPS) Production by *Nostoc minutum* under Different Laboratory Conditions. *Advances In Microbiology*, 06(05), 374-380.
- Priest, E. (2000). *Solar magneto-hydrodynamics*. Dordrecht, Holland: D. Reidel Pub. Co.
- Richardson, J. et al. (1995). Radial evolution of the solar wind from IMP 8 to Voyager 2. *Geophysical Research Letters*, 22(4), 325-328.
- Sakugawa, T. et al. (2014). A Method of Cyanobacteria Treatment Using Underwater Pulsed Streamer-Like Discharge. *IEEE Transactions On Plasma Science*, 42(3), 794-798.
- Sand-Jensen, K. & Jespersen, T. (2012). Tolerance of the widespread cyanobacterium *Nostoc commune* to extreme temperature variations (-269 to 105 C), pH and salt stress. *Oecologia*, 169(2), 331-339.
- Slade, M. et al. (1992). Mercury Radar Imaging: Evidence for Polar Ice. *Science*, 258(5082), 635-640.
- McKay, C. et al. (1999). Analytic Solutions for the Antigreenhouse Effect: Titan and the Early Earth. *Icarus*, 137(1), 56-61.
- Raanan, H. et al. (2016). Towards clarifying what distinguishes cyanobacteria able to resurrect after desiccation from those that cannot: The photosynthetic aspect. *Biochimica Et Biophysica Acta (BBA) - Bioenergetics*, 1857(6), 715-722.
- Rozitis, B., & Green, S. (2011). Directional characteristics of thermal-infrared beaming from atmosphereless planetary surfaces - a new thermophysical model. *Monthly Notices Of The Royal Astronomical Society*, 415(3), 2042-2062.
- Secker, J. et al. (1996). Astrophysical and Biological Constraints on Radiopanspermia. Available from (<https://arxiv.org/pdf/astro-ph/9607139.pdf>).

- Selsis, F. et al. (2007). Habitable planets around the star Gliese 581?. *Astronomy & Astrophysics*, 476(3), 1373-1387.
- Sharov, A. & Gordon, R. (2013). Life before Earth. Available from (<https://arxiv.org/ftp/arxiv/papers/1304/1304.3381.pdf>).
- Shevela, D. et al., Oxygenic Photosynthesis of Cyanobacteria. In : Stress biology of cyanobacteria: molecular mechanisms to cellular responses, Srivastava, A. K. et al., Boca Raton: Taylor & Francis, (2013).
- Shirkey, B. et al. (2000). Active Fe-Containing Superoxide Dismutase and Abundant sodF mRNA in *Nostoc commune* (Cyanobacteria) after Years of Desiccation. *Journal Of Bacteriology*, 182(1), 189-197.
- Schwartz, S. J. et al. (2004). Astrophysical plasmas. Astronomy Unit, Queen Mary, University of London.
- Stukalov, O. et al. (2008). Use of Atomic Force Microscopy and Transmission Electron Microscopy for Correlative Studies of Bacterial Capsules. *Applied And Environmental Microbiology*, 74(17), 5457-5465.
- Taiz, L., & Zeiger, E. (2002). Plant physiology. New York: W.H. Freeman.
- Tamaru, Y. et al. (2005). Crucial Role of Extracellular Polysaccharides in Desiccation and Freezing Tolerance in the Terrestrial Cyanobacterium *Nostoc commune*. *Applied And Environmental Microbiology*, 71(11), 7327-7333.
- Tandeau de Marsac, N. (1977). Occurrence and Nature of Chromatic Adaptation in Cyanobacteria. *Journal of Bacteriology*, 130(1), 82-91.
- Thomas, D. et al (2005). Common Freshwater Cyanobacteria Grow in 100% CO<sub>2</sub>. *Astrobiology*, 5(1), 66-74.
- Tosi, F. et al. (2014). Thermal measurements of dark and bright surface features on Vesta as derived from Dawn/VIR. *Icarus*, 240, 36-57.
- Tiribilli, B. et al. (2012). AFM imaging on embedded sections of cyanobacteria reveals their inner structures. Conference paper. 4th International Meeting on Atomic

Force Microscopy (AFM) in Life Sciences and Medicine.

Trnková, K., & Barták, M. (2016). Desiccation-induced changes in photochemical processes of photosynthesis and spectral reflectance in *Nostoc commune* (Cyanobacteria, Nostocales) colonies from polar regions. *Phycological Research*, 65(1), 44-50.

Verseux, C. et al. (2015). Sustainable life support on Mars – the potential roles of cyanobacteria. *International Journal Of Astrobiology*, 15(01), 65-92.

Vermaas, W. F. (2001). *Photosynthesis and Respiration in Cyanobacteria*. eLS.

Webb, S. (1965). *Bound water in biological integrity*. Springfield, Ill.: C.C. Thomas.

Williams, D., & Pollard, D. (2002). Earth-like worlds on eccentric orbits: excursions beyond the habitable zone. *International Journal Of Astrobiology*, 1(01).

Winter, D., & Krupp, J. (1971). Directional characteristics of infrared emission from the moon. *The Moon*, 2(3), 279-292. <http://dx.doi.org/10.1007/bf00561881>

Wolters, S., & Green, S. (2009). Investigation of systematic bias in radiometric diameter determination of near-Earth asteroids: the night emission simulated thermal model (NESTM). *Monthly Notices Of The Royal Astronomical Society*, 400(1), 204-218.

Worth, R. et al. (2013). Seeding Life on the Moons of the Outer Planets via Lithopanspermia. *Astrobiology*, 13(12), 1155-1165.

Yoshimura, H. et al. (2006). Up-regulated Gene Expression during Dehydration in a Terrestrial Cyanobacterium, *Nostoc* sp. Strain HK-01. *Microbes And Environments*, 21(2), 129-133.

Zhang, S., & Bryant, D. (2011). The Tricarboxylic Acid Cycle in Cyanobacteria. *Science*, 334(6062), 1551-1553.

## Electronic Sources

NASA Exoplanet Archive. (2017). [Exoplanetarchive.ipac.caltech.edu](http://exoplanetarchive.ipac.caltech.edu). Retrieved 10 May 2017, from <https://exoplanetarchive.ipac.caltech.edu/>

Asteroid Fact Sheet. (2017). Nssdc.gsfc.nasa.gov. Retrieved 10 May, from <https://nssdc.gsfc.nasa.gov/planetary/factsheet/asteroidfact.html>

Sun Fact Sheet. (2017). Nssdc.gsfc.nasa.gov. Retrieved 13 May 2017, from <https://nssdc.gsfc.nasa.gov/planetary/factsheet/sunfact.html>

Stars and Nebulae. (2017). Skyserver.sdss.org. Retrieved 25 May 2017, from <http://skyserver.sdss.org/dr1/en/astro/stars/stars.asp>

The Very Latest SOHO Images. (2017). Sohonascom.nasa.gov. Retrieved 25 May 2017, from <https://sohowww.nascom.nasa.gov/data/realtime-images.html>

Photosynthesis Lab Manual. (2014). Yorku.ca. Retrieved 1 June 2017, from [http://www.yorku.ca/planters/photosynthesis/2014\\_08\\_15\\_lab\\_manual\\_static\\_html/index.html](http://www.yorku.ca/planters/photosynthesis/2014_08_15_lab_manual_static_html/index.html)

<http://ns.umich.edu/Releases/2013/Mar13/algae.html>. (2013).

[http://cronodon.com/images/cyanobacterium\\_structure\\_labeled.jpg](http://cronodon.com/images/cyanobacterium_structure_labeled.jpg).

Solar spectrum. (2017). Retrieved 3 June 2017 from [https://commons.wikimedia.org/w/index.php?title=File:Solar\\_spectrum\\_ita.svg&oldid=261911890](https://commons.wikimedia.org/w/index.php?title=File:Solar_spectrum_ita.svg&oldid=261911890)

# Appendices

## A Data for Antarctic samples plasma treatment

Table 1: Table of values of  $F_V/F_M$  measured by fluorometer before and after exposure to experimental conditions (RF generator power 150 W) and their normalized values

Antarctica	$F_V/F_M$ [r.u.]											
	1 hour of hydration			3 hours of hydration			6 hours of hydration			6 hours of hydration		
	before	after	normalized	before	after	normalized	before	after	normalized	before	after	normalized
control samples	0.305	0.277	0.908	0.514	0.550	1.070	0.762	0.865	1.135			
	0.202	0.530	2.624	0.565	0.563	0.996	0.714	0.789	1.105			
	0.289	0.267	0.924	0.611	0.551	0.902	0.682	0.879	1.289			
	0.421	0.431	1.024	0.431	0.647	1.501	0.817	0.669	0.819			
	0.459	0.606	1.320	0.557	0.652	1.171	0.684	0.778	1.137			
15 minutes	0.289	0.51	1.765	0.636	0.526	0.827	0.68	0.563	0.828			
	0.43	0.361	0.840	0.503	0.383	0.761	0.61	0.544	0.892			
	0.579	0.403	0.696	0.506	0.088	0.174	0.823	0.75	0.911			
	0.402	0.668	1.662	0.586	0.658	1.123	0.643	0.567	0.882			
	0.573	0.176	0.307	0.800	0.532	0.665	0.81	0.592	0.731			
30 minutes	0.485	0.347	0.715	0.657	0.243	0.370	0.735	0.717	0.976			
	0.761	0.411	0.540	0.595	0.115	0.193	0.715	0.353	0.494			
	0.413	0.652	1.579	0.524	0.57	1.088	0.613	0.593	0.967			
	0.343	0.197	0.574	0.398	0.661	1.661	0.665	0.592	0.890			
	0.508	0.459	0.904	0.315	0	0.000	0.772	0.755	0.978			
60 minutes	0.477	0.624	1.308	0.446	0.26	0.583	0.629	0.086	0.137			
	0.371	0	0	0.524	0.34	0.649	0.556	0.759	1.365			
	0.601	0.288	0.479	0.615	0.084	0.137	0.702	0.369	0.526			
	0.579	0.071	0.123	0.413	0.585	1.416	0.651	0.061	0.094			
	0.451	0.405	0.898	0.334	0.565	1.692	0.753	0.624	0.829			

Table 2: Table of values of  $F_V/F_M$  measured by fluorometer before and after exposure to experimental conditions (RF generator power of 250 W) and their normalized values

Antarctica	$F_V/F_M$ [r.u.]								
	1 hour of hydration			3 hours of hydration			6 hours of hydration		
	before	after	normalized	before	after	normalized	before	after	normalized
control samples (for 30 min)	0.435	0.567	1.303	0.539	0.537	0.996	0.739	0.414	0.560
	0.202	0.586	2.901	0.725	0.405	0.559	0.79	0.688	0.871
	0.700	0.631	0.901	0.633	0.575	0.908	0.794	0.756	0.952
30 minutes	0.512	0.488	0.953	0.836	0.656	0.785	0.688	0.795	1.156
	0.490	0.452	0.922	0.505	0.564	1.117	0.826	0.671	0.812
	0.351	0.668	1.903	0.732	0.728	0.995	0.893	0.879	0.984
60 minutes	0.676	0.303	0.448	0.656	0.427	0.651	0.601	0.918	1.527
	0.642	0.323	0.503	0.768	0.122	0.159	0.862	0.744	0.863
	0.381	0.636	1.669	0.615	0.516	0.839	0.838	0.579	0.691
control samples (for 60 min)	0.440	0.130	0.295	0.728	0.413	0.567	0.84	0.571	0.680
	0.287	0.631	2.199	0.445	0.546	1.227	0.617	0.448	0.427
	0.378	0.464	1.228	0.443	0.686	1.549	0.678	0.737	0.726
60 minutes	0.656	0.623	0.950	0.357	0.627	1.756	0.78	0.572	1.087
	0.452	0.412	0.912	0.507	0.767	1.513	0.725	0.767	0.733
	0.745	0.674	0.905	0.763	0.631	0.827	0.888	0.575	1.058
60 minutes	0.72	0.323	0.449	0.588	0.332	0.565	0.814	0.398	0.648
	0.369	0.379	1.027	0.682	0.673	0.987	0.836	0.722	0.489
	0.35	0.264	0.754	0.79	0.182	0.230	0.869	0.705	0.864
60 minutes	0.502	0.07	0.139	0.661	0.225	0.340	0.753	0.621	0.811
	0.457	0	0.000	0.855	0.587	0.687	0.832	0.765	0.825

## B Data for Brno samples plasma treatment

Table 3: Table of values of  $F_V/F_M$  measured by fluorometer before and after exposure to experimental conditions (RF generator power of 150 W) and their normalized values.

Brno	$F_V/F_M$ [r.u.]								
	1 hour of hydration		3 hours of hydration		6 hours of hydration				
	before	after	normalized	before	after	normalized			
control samples	0.357	0.591	1.655	0.549	0.775	1.412	0.615	0.473	0.769
	0.301	0.532	1.767	0.582	0.558	0.959	0.672	0.419	0.624
	0.427	0.580	1.358	0.628	0.693	1.104	0.56	0.69	1.232
	0.611	0.567	0.928	0.446	0.827	1.854	0.441	0.393	0.891
	0.505	0.483	0.956	0.48	0.691	1.440	0.564	0.625	1.108
15 minutes	0.563	0.300	0.533	0.465	0.463	0.996	0.561	0.25	0.446
	0.316	0.595	1.883	0.500	0.709	1.418	0.518	0.406	0.784
	0.562	0.345	0.614	0.414	0.700	1.691	0.403	0.384	0.953
	0.432	0.421	0.975	0.564	0.612	1.085	0.411	0.447	1.088
	0.617	0.367	0.595	0.572	0.626	1.094	0.562	0.423	0.753
30 minutes	0.366	0.732	2.000	0.572	0.406	0.710	0.621	0.265	0.427
	0.359	0.412	1.148	0.414	0.196	0.473	0.537	0	0.000
	0.546	0.502	0.919	0.654	0.554	0.847	0.57	0.192	0.337
	0.466	0.371	0.796	0.563	0.256	0.455	0.534	0.39	0.730
	0.392	0.419	1.069	0.496	0.588	1.185	0.747	0.616	0.825
60 minutes	0.495	0.615	1.242	0.628	0.435	0.693	0.689	0	0.000
	0.439	0.441	1.005	0.563	0.500	0.888	0.615	0.212	0.345
	0.741	0.507	0.684	0.377	0.528	1.401	0.507	0.186	0.367
	0.450	0.463	1.029	0.367	0.407	1.109	0.427	0.136	0.319
	0.765	0.478	0.625	0.419	0.398	0.950	0.542	0.342	0.631

Table 4: Table of values of  $F_V/F_M$  measured by fluorometer before and after exposure to experimental conditions (RF generator power of 250 W) and their normalized values

Brno	$F_V/F_M$ [r.u.]											
	1 hour of hydration			3 hours of hydration			6 hours of hydration			6 hours of hydration		
	before	after	normalized	before	after	normalized	before	after	normalized	before	after	normalized
control samples (for 30 min)	0.361	0.401	1.111	0.486	0.445	0.916	0.574	0.633	1.103	0.574	0.633	1.103
	0.378	0.404	1.069	0.542	0.549	1.013	0.515	0.550	1.068	0.515	0.550	1.068
	0.515	0.446	0.866	0.636	0.497	0.781	0.548	0.728	1.328	0.548	0.728	1.328
	0.555	0.398	0.717	0.465	0.695	1.495	0.789	0.406	0.515	0.789	0.406	0.515
	0.429	0.507	1.182	0.489	0.534	1.092	0.530	0.640	1.208	0.530	0.640	1.208
	0.478	0.376	0.787	0.470	0.398	0.847	0.502	0.006	0.012	0.502	0.006	0.012
30 minutes	0.479	0.249	0.520	0.747	0.411	0.550	0.870	0.001	0.001	0.870	0.001	0.001
	0.543	0.204	0.376	0.487	0.48	0.986	0.456	0.066	0.145	0.456	0.066	0.145
	0.517	0.292	0.565	0.557	0.281	0.504	0.665	0.054	0.081	0.665	0.054	0.081
	0.421	0.355	0.843	0.492	0.248	0.504	0.463	0.169	0.365	0.463	0.169	0.365
	0.477	0.629	1.319	0.482	0.558	1.158	0.781	0.709	0.908	0.781	0.709	0.908
	0.507	0.600	1.183	0.410	0.404	0.985	0.425	0.546	1.285	0.425	0.546	1.285
control samples (for 60 min)	0.502	0.504	1.004	0.457	0.735	1.608	0.553	0.476	0.861	0.553	0.476	0.861
	0.400	0.609	1.523	0.630	0.541	0.859	0.733	0.676	0.922	0.733	0.676	0.922
	0.417	0.398	0.954	0.388	0.503	1.296	0.572	0.558	0.976	0.572	0.558	0.976
	0.593	0.113	0.191	0.45	0.06	0.133	0.630	0.434	0.689	0.630	0.434	0.689
	0.374	0.294	0.786	0.565	0.053	0.094	0.39	0.285	0.731	0.39	0.285	0.731
	0.397	0.345	0.869	0.324	0.396	1.222	0.599	0.384	0.641	0.599	0.384	0.641
60 minutes	0.465	0.354	0.761	0.655	0.154	0.235	0.584	0.273	0.467	0.584	0.273	0.467
	0.478	0.168	0.351	0.356	0.003	0.008	0.575	0	0	0.575	0	0